Bundesamt für Energie BFE

# EMPIRISCHE VALIDIERUNG VON GEBÄUDESIMULATIONSPROGRAMMEN

## SCHWEIZER BEITRAG ZU IEA Task 34 / Annex 43

## Schlussbericht

Ausgearbeitet durch

P. Loutzenhiser und H. Manz, Empa, Building Technologies Ueberlandstrasse 129, CH-8600 Duebendorf, peter.loutzenhiser@empa.ch, heinrich.manz@empa.ch, www.empa.ch

unter Verwendung von Beiträgen von

- S. Carl, T. Frank und R. Bundi, Empa, Building Technologies Ueberlandstrasse 129, CH-8600 Duebendorf
- S. Moosberger und G. Zweifel Hochschule für Technik+Architektur Luzern, Technikumstrasse 21, CH-6048 Horw
- P. Oelhafen, G. Reber und R. Steiner Institut für Physik, Universität Basel, Klingelbergstr. 82, CH-4056 Basel
- M. Camenzind, K. Meyer und M. Amberg, Empa St Gallen Lerchenfeldstrasse 5, CH-9014 St. Gallen

## **Impressum**

Datum: 15. November 2006

## Im Auftrag des Bundesamt für Energie

Forschungsprogramm Rationelle Energienutzung in Gebäuden

Mühlestrasse 4, CH-3063 Ittigen

Postadresse: CH-3003 Bern

Tel. +41 31 322 56 11, Fax +41 31 323 25 00

www.bfe.admin.ch

BFE-Projektleiter: Andreas Eckmanns, andreas.eckmanns@bfe.admin.ch

Projektnummer: 100'765

Bezugsort der Publikation: www.energieforschung.ch

Für den Inhalt und die Schlussfolgerungen ist ausschliesslich der Autor dieses Berichts verantwortlich.

ii

# TABLE OF CONTENTS

List of Figures	<b>v</b> i
List of Tables	ix
Acknowledgements	<b>xi</b> i
Abstract	<b>xii</b> i
Chapter 1: Introduction	1
Chapter 2: Experiments, Validation Exercises, Methodology, and Participants	2
2.1. Experiments	2
2.2. Validations Exercises	
2.3. Empirical Validation Methodology	
2.4. Participating Organizations and Simulation Tools	5
Chapter 3: Facility Description	6
3.1. Test Cell Location and Dimensions	6
3.2. Thermal Bridge Quantification	
3.3. Thermal Mass and Air-tightness	
3.4. Thermophysical and Optical Properties	
3.5. Sensors	
3.7. Explanation of Experimental Data	
•	
Chapter 4: Transient Characterization Experiment (Exercise 1)	
4.1. Test Cell	
4.2. Thermophysical Properties.	
4.3. Experimental Setup	
Chapter 5: Evaluation of Irradiation Models on Tilted Facades (Exercise 2)	
Chapter 6: Glazing Unit Only (Exercise 3)	
6.1. Description of the Experiment	
6.1.1. Glazing Unit Properties	
6.1.3. Thermophysical Properties of the Test Cell Envelope	
6.2. Results	
Chapter 7: Glazing Unit with Exterior Shading Screen (Exercise 4)	
7.1. Description of the Experiment	
7.1.1. Geometry and Optical Properties of the Exterior Shade Screen	
7.1.2. Thermophysical Properties of the Test Cell Envelope	
7.2. Results	
Chapter 8: Glazing Unit with an Interior Shading Screen (Exercise 5)	42
8.1. Description of the Experiment	
8.1.1. Geometry and Optical Properties of the Interior Shade Screen	
8.1.2. Thermophysical Properties of the Test Cell Envelope	43
8.2. Results	44

Chapter 9: Glazing Unit with Exterior Venetian Blind (Exercise 6)	49
9.1. Description of the Experiment	
9.1.1. Geometry and Optical Properties of the Exterior Venetian Blind Assembly	
9.1.2. Thermophysical Properties of the Test Cell Envelope	
9.2. Results	
9.2.1. Horizontally Positioned Venetian Blind Slat Position	51
9.2.2. Tilted 45° Downward Venetian Blind Slat Position	
Chapter 10: Glazing Unit with Interior Mini-blind (Exercise 7)	58
10.1. Description of the Experiment	58
10.1.1. Geometry of Interior Mini-blind Assembly and Blind Slat Optical Properties	
10.1.2. Thermophysical Properties of the Test Cell Envelope	
10.2. Results	
10.2.1. Horizontally Positioned Mini-Blind Slat Position	
10.2.2. Tilted 45° Downward Mini-Blind Slat Position	63
Chapter 11: Window (Exercise 8)	66
11.1. Description of the Experiment	66
11.1.1. Window Properties	
11.1.2. Thermal Transmittances and Bridges	67
11.1.2.1. Linear Thermal Transmittance of the Spacer	69
11.1.2.2. Thermal Conductance of the Window Frame	
11.1.2.3. Linear Thermal Transmittance Due to Mounting	
11.1.2.4. Quantities Used for the Calculations	
11.1.3. Thermophysical Properties of the Test Cell Envelope	
11.2. Results	74
Chapter 12: Modeler's Reports	78
12.1. HELIOS.	78
12.1.1. General Information	
12.1.2. Transient Experiment Modeling (Exercise 1)	78
12.1.3. Evaluation of Irradiation Models on Tilted Surfaces (Exercise 2)	78
12.1.4. Glazing Only Experiment (Exercise 3)	
12.1.5. Exterior and Interior Shading Screens (Exercises 4 and 5)	
12.1.6. Exterior Venetian Blind and Internal Mini-Blind Assemblies (Exercises 6 and 7	)79
12.1.7. Window (Exercise 8)	
12.1.8. Discussion of Results	
12.1.9. Validation Impact	
12.2. EnergyPlus	80
12.2.1. General Information	
12.2.2. Transient Experiment Modeling (Exercise 1)	
12.2.3. Evaluation of Irradiation Models on Tilted Facades (Exercise 2)	
12.2.4. Glazing Only Experiment (Exercise 3)	
12.2.5. Exterior and Interior Shading Screen (Exercises 4 and 5)	
12.2.6. Exterior Venetian Blind and Interior Mini-Blind Assemblies (Exercises 6 and 7	
12.2.7. Window (Exercise 8)	
12.2.8. Discussion of Results	
12.2.9. Validation Impact	
12.3. DOE-2.1E	
12.3.1. General Information	
12.3.2. Transient experiment Modeling (Exercise 1)	
I	04

12.3.4. Glazing Only Experiment (Exercise 3)	82
12.3.5. Exterior and Interior Shading Screen (Exercises 4 and 5)	
12.3.6. Window (Exercise 8)	83
12.3.7. Discussion of Results	83
12.4. IDA-ICE	83
12.4.1. General Information	84
12.4.2. Transient Experiment Modeling (Exercise 1)	84
12.4.3. Evaluation of Irradiation Models on Tilted Facades (Exercise 2)	84
12.4.4. Glazing Only Experiment (Exercise 3)	84
12.4.5. Exterior and Interior Shading Screens (Exercises 4 and 5)	85
12.4.6. Discussion of Results	85
12.4.7. Validation Impact	85
Chapter 13: Discussion and Conclusions	86
13.1. Experiments.	86
12.3.7. Discussion of Results  12.4. IDA-ICE  12.4.1. General Information  12.4.2. Transient Experiment Modeling (Exercise 1)  12.4.3. Evaluation of Irradiation Models on Tilted Facades (Exercise 2)  12.4.4. Glazing Only Experiment (Exercise 3)  12.4.5. Exterior and Interior Shading Screens (Exercises 4 and 5)  12.4.6. Discussion of Results  12.4.7. Validation Impact  Chapter 13: Discussion and Conclusions  13.1. Experiments  13.2. Overall Assessments  References  Appendix A: Description of Associated Files.  A.1. Exercise 1  A.2. Exercise 2  A.3. Exercise 3  A.4. Exercises 4 and 5  A.5. Exercises 6 and 7	88
Appendix A: Description of Associated Files	90
A.3. Exercise 3	93
A.4. Exercises 4 and 5	97
A.5. Exercises 6 and 7	97
A 6 Exercises 8	98

# **List of Figures**

Figure 2.1. Photograph of the test cell during the preconditioning phase	3
Figure 2.2. Methodology for empirical validation of building energy simulation programs	3
Figure 3.1. EMPA test cell schematic	6
Figure 3.2a. Computed heat fluxes at the outer surfaces of the test cell	7
Figure 3.2b. Computed heat fluxes for a horizontal cross-section of the door.	8
Figure 3.2c. Infrared picture of the test cell door	
Figure 3.3. Comparison of thermal conductances of the external wall and guarded zone as funct	ion
of temperature found by simulation and the steady-state experiment	9
Figure 4.1a. Photograph of test toom with external chamber.	13
Figure 4.1b. Outdoor test facility with removable façade element.	13
Figure 4.2. Location of temperature sensors.	
Figure 4.3. Measured pseudo-random heating power and temperatures.	
Figures 4.4a. Test cell air temperature comparisons for HELIOS.	15
Figures 4.4b. Test cell air temperature comparisons for EnergyPlus.	16
Figures 4.4c. Test cell air temperature comparisons for DOE-2.1E.	16
Figures 4.4d. Test cell air temperature comparisons for IDA-ICE.	17
Figure 4.5. Experimental uncertainty, uncertainty of simulation results due to uncertainty in inp	ut
parameters and total uncertainty.	
Figure 5.1a. Global vertical solar irradiance comparisons for HELIOS Perez 1987 averaged over	
each given hour of the day (left) and absolute maximum, mean, and minimum differences for	or a
given hour of the day (right).	20
Figure 5.1b. Global vertical solar irradiance comparisons for EnergyPlus Perez 1990 averaged of	
each given hour of the day (left) and absolute maximum, mean, and minimum differences for	
given hour of the day (right).	21
. 21	
Figure 5.1c. Global vertical solar irradiance comparisons for DOE-2.1E Perez 1990 averaged ov	
each given hour of the day (left) and absolute maximum, mean, and minimum differences for	
given hour of the day (right).	21
. 21	
Figure 5.1d. Global vertical solar irradiance comparisons for IDA-ICE Perez 1990 averaged over	
each given hour of the day (left) and absolute maximum, mean, and minimum differences for	
given hour of the day (right).	22
Figure 6.1. A photograph of the test cell.	
Figure 6.2. Position of the glazing in the exterior wall in meters seen from the inside of the test	
Figure 6.3. Dimensioned drawing of the spacer and frame in millimeters.	
Figure 6.4a. Cross-section of the glazing and frame	
Figure 6.4b. Cross-section of the aluminum spacer.	
Figure 6.5a. Isotherm illustration from the BISCO simulation.	
Figure 6.5b. Heat flow line illustration from the BISCO simulation.	
Figure 6.6a. Cooling power comparisons for HELIOS averaged over each given hour of the day	
(left) and absolute maximum, mean, and minimum differences for a given hour of the day	
(right)	31
Figure 6.6b. Cooling power comparisons for EnergyPlus averaged over each given hour of the contractions are supplied to the contraction of the con	
(left) and absolute maximum, mean, and minimum differences for a given hour of the day	
(right)	31
Figure 6.6c. Cooling power comparisons for DOE-2.1E averaged over each given hour of the data	
(left) and absolute maximum, mean, and minimum differences for a given hour of the day	J
(right)	32

(left) and absolute maximum, mean, and minimum differences for a given hour of the day (right)	.32
Figure 6.6e. Cooling power comparisons for IDA-SIA averaged over each given hour of the day (left) and absolute maximum, mean, and minimum differences for a given hour of the day	.33
Figure 6.6f. Cooling power comparisons for IDA-Detwind averaged over each given hour of the day (left) and absolute maximum, mean, and minimum differences for a given hour of the day (right)	33
	35
Figure 7.1. Photograph of the exterior shade mounted on the test cell.	
Figure 7.2. Dimensioned drawing of the external shade in meters relative to the glazing unit	36
Figure 7.3a. Cooling power comparisons for HELIOS averaged over each given hour of the day	
(left) and absolute maximum, mean, and minimum differences for a given hour of the day (right)	38
Figure 7.3b. Cooling power comparisons for EnergyPlus averaged over each given hour of the day (left) and absolute maximum, mean, and minimum differences for a given hour of the day (right)	y .38
Figure 7.3c. Cooling power comparisons for DOE-2.1E averaged over each given hour of the day (left) and absolute maximum, mean, and minimum differences for a given hour of the day	.39
Figure 7.3d. Cooling power comparisons for IDA-SIA averaged over each given hour of the day (left) and absolute maximum, mean, and minimum differences for a given hour of the day	39
Figure 7.4. Transmitted solar power averaged over each given hour of the day.	41
	42
	43
Figure 8.3a. Cooling power comparisons for HELIOS averaged over each given hour of the day	
(left) and absolute maximum, mean, and minimum differences for a given hour of the day	.44
Figure 8.3b. Cooling power comparisons for EnergyPlus averaged over each given hour of the day (left) and absolute maximum, mean, and minimum differences for a given hour of the day	y .45
Figure 8.3c. Cooling power comparisons for DOE-2.1E averaged over each given hour of the day (left) and absolute maximum, mean, and minimum differences for a given hour of the day	.45
Figure 8.3d. Cooling power comparisons for IDA-SIA averaged over each given hour of the day (left) and absolute maximum, mean, and minimum differences for a given hour of the day (right)	
Figure 8.4. Transmitted solar power averaged over each given hour of the day.	
Figure 9.1. Photograph of the exterior blind mounted in front of the test cell.	
Figure 9.2. Dimensioned drawing of the exterior Venetian blind in centimeters relative to the	.,
glazing.	49
Figure 9.3. Dimensioned blind relative to the glazing in millimeters.	50
Figure 9.4a. Cooling power comparisons for HELIOS averaged over each given hour of the day	-
(left) and absolute maximum, mean, and minimum differences for a given hour of the day	.52
Figure 9.4b. Cooling power comparisons for EnergyPlus averaged over each given hour of the day	
(left) and absolute maximum, mean, and minimum differences for a given hour of the day	j
(right)	52
Figure 9.5. Transmitted solar power averaged over each given hour of the day.	

Figure 9.6a. Cooling power comparisons for HELIOS averaged over each given hour of the day (left) and absolute maximum, mean, and minimum differences for a given hour of the day			
(right)	54		
Figure 9.6b. Cooling power comparisons for EnergyPlus averaged over each given hour of the d (left) and absolute maximum, mean, and minimum differences for a given hour of the day			
(right)	55		
Figure 9.7. Transmitted solar power averaged over each given hour of the day.	56		
Figure 10.1. Dimensioned drawing of the internal mini-blinds in centimeters relative to the glazi	ıng. 58		
Figure 10.2. Dimension internal mini-blinds relative to the glazing in centimeters.			
Figure 10.3a. Cooling power comparisons for HELIOS averaged over each given hour of the day (left) and absolute maximum, mean, and minimum differences for a given hour of the day	y		
(right)	60		
Figure 10.3b. Cooling power comparisons for EnergyPlus averaged over each given hour of the (left) and absolute maximum, mean, and minimum differences for a given hour of the day			
(right)Figure 10.4. Transmitted solar power averaged over each given hour of the day	61		
Figure 10.5a. Cooling power comparisons for HELIOS averaged over each given hour of the day			
(left) and absolute maximum, mean, and minimum differences for a given hour of the day (right)	y 63		
Figure 10.5b. Cooling power comparisons for EnergyPlus averaged over each given hour of the			
(left) and absolute maximum, mean, and minimum differences for a given hour of the day (right)	,		
Figure 10.6. Transmitted solar power averaged over each given hour of the day.			
Figure 11.1. A photograph of the test cell.	66		
Figure 11.2. Position of the glazing in the exterior wall in meters (inside view).			
Figure 11.3. Drawing of the spacer and frame in millimeters.	69		
Figure 11.4. Bitmaps for the BISCO calculation with glazing unit (left) and insulation panel (rig	ht). 70		
Figure 11.5a. Cooling power comparisons for HELIOS averaged over each given hour of the day (left) and absolute maximum, mean, and minimum differences for a given hour of the day (right)	y 74		
Figure 11.5b. Cooling power comparisons for EnergyPlus averaged over each given hour of the			
(left) and absolute maximum, mean, and minimum differences for a given hour of the day	75		
(right)Figure 11.5c. Cooling power comparisons for DOE-2.1E averaged over each given hour of the d			
(left) and absolute maximum, mean, and minimum differences for a given hour of the day	-		
(right)			
Figure 11.6. Transmitted solar power averaged over each given hour of the day	77		

## **List of Tables**

Table 2.1. List of participants, building energy simulation programs, and level of participation fo	
the EMPA experiments.	
Table 3.1. Location of the EMPA test cell.	
Table 3.2. Dimensions of the test cell.	
Table 3.3a. Heat transfer characteristics of the guarded zone	
Table 3.3b. Heat transfer characteristics of the exterior wall.	8
Table 3.4. Steady-state experiment: time-averaged values and uncertainties for thermal	
conductance calculations.	
Table 3.5. Layer properties of the ceiling, north (incl. door), east and west wall	
Table 3.6. Layer properties of the floor.	
Table 3.7. Layer properties of the external wall.	
Table 3.8. Optical properties of test cell surfaces.	
Table 3.9. Weather data parameters and equipment.	
Table 3.10. Parameters measured in the test cell, the external chamber and the guarded zone and	
approximate accuracies according to manufacturer specifications.	
Table 3.11. Ground reflectance	
Table 4.1a. Ceiling, north, east and west wall construction evaluated at $\theta = 28.38$ °C	14
Table 4.1b. Floor construction evaluated at $\theta = 28.38$ °C.	14
Table 4.1c. South wall construction evaluated at $\theta = 28.38$ °C.	14
Table 4.2. Overall uncertainty and 10 most influential parameter uncertainties that impacted the o	cell
air temperature predictions in K	
Table 4.3. Statistical analysis for the test cell air temperature.	19
Table 5.1. N-way factorial analyses to evaluate the sensitivities of outputs on input uncertainties.	.22
Table 5.2. Statistical comparisons for Exercise 2.	23
Table 6.1. Glazing unit properties.	25
Table 6.2a. Optical properties for the outer pane of glass (solar control Low-E)	
Table 6.2b. Optical properties for the inner pane of glass (clear float glass).	
Table 6.3. Transmittance and as a function of incident angle	
Table 6.4. List of materials and their respective thermal conductivities	
Table 6.5. Boundary condition properties.	
Table 6.6. Values of the variables used for the 1-D heat transfer calculation.	29
Table 6.7. Mean envelope temperatures for experiment.	
Table 6.8a. Ceiling, north, east and west wall construction evaluated at 22.78°C.	30
Table 6.8b. Floor construction evaluated at 22.72°C.	
Table 6.8c. South wall construction evaluated at 17.49°C.	30
Table 6.9. Overall uncertainty and 10 most influential input parameters from the n-way factorial	
analyses in Watts	
Table 6.10. Statistical comparisons for cooling power in Exercise 3.	
Table 7.1. Optical properties of the exterior shade.	
Table 7.2. Mean envelope temperatures for experiment.	37
Table 7.3a. Ceiling, north, east and west wall construction evaluated at 22.58°C.	
Table 7.3b. Floor construction evaluated at 22.34°C.	
Table 7.3c. South wall construction evaluated at 16.34°C.	
Table 7.4. Overall uncertainty and 10 most influential input parameters from the n-way factorial	
analyses in Watts	
Table 7.5. Statistical comparisons for cooling power in Exercise 4.	
Table 8.1. Optical properties of the interior shading screen.	
Table 8.2. Mean envelope temperatures for experiment.	43
Table 8.3a. Ceiling, north, east and west wall construction evaluated at 22.83°C.	43

Table 8.3b. Floor construction evaluated at 22.75°C.	43
Table 8.3c. South wall construction evaluated at 20.91°C.	44
Table 8.4. Overall uncertainty and 10 most influential input parameters from the n-way factoria	al
analyses in Watts	
Table 8.5. Statistical comparisons for cooling power in Exercise 5.	47
Table 9.1. Optical properties of the slat surfaces.	
Table 9.2. Mean envelope temperatures for the experiments.	50
Table 9.3a. Ceiling, north, east and west wall construction evaluated at 22.72°C.	50
Table 9.3b. Floor construction evaluated at 22.72°C.	
Table 9.3c. South wall construction evaluated at 20.82°C.	51
Table 9.4a. Ceiling, north, east and west wall construction evaluated at 22.83°C.	51
Table 9.4b. Floor construction evaluated at 22.83°C.	
Table 9.4c. South wall construction evaluated at 20.90°C.	51
Table 9.5. Overall uncertainty and 10 most influential input parameters from the n-way factoria	ıl
analyses in Watts	53
Table 9.6. Statistical comparisons for cooling power in Exercise 6 with slats horizontally	
positioned.	
Table 9.7. Overall uncertainty and 10 most influential input parameters from the n-way factoria	ıl
analyses in Watts	
Table 9.8. Statistical comparisons for cooling power in Exercise 6 with slats tilted 45° downwa	
Table 10.1. Optical properties of the slat surfaces.	
Table 10.2. Mean envelope temperatures for the experiments.	
Table 10.3a. Ceiling, north, east and west wall construction evaluated at 22.58°C.	
Table 10.3b. Floor construction evaluated at 22.72°C.	
Table 10.3c. South wall construction evaluated at 16.96°C.	
Table 10.4a. Ceiling, north, east and west wall construction evaluated at 22.94°C.	
Table 10.4b. Floor construction evaluated at 22.94°C.	
Table 10.4c. South wall construction evaluated at 15.52°C.	
Table 10.5. Overall uncertainty and 10 most influential input parameters from the n-way factor	
analyses in Watts	61
Table 10.6. Statistical comparisons for cooling power in Exercise 7 with slats horizontally	(2
positioned.	
Table 10.7. Overall uncertainty and 10 most influential input parameters from the n-way factor	
analyses in Watts.	64
Table 10.8. Statistical comparisons for cooling power in Exercise 7 with slats tilted 45° downw	ard.
T-11- 11 1 W:-1	64
Table 11.1. Window optical properties.	0/
Table 11.2a. Optical properties for the outer pane of glass (Clear Float Glass).	
Table 11.2b. Optical properties for the inner pane of glass (Low-E Pro)	
properties	60
Table 11.5a. Values used for BISCO simulation.	
Table 11.5b. Values from the hotbox measurements.	
Table 11.6. Mean envelope temperatures for experiment.	
Table 11.7a. Ceiling, north, east and west wall constructions evaluated at 22.75°C	
Table 11.7b. Floor construction evaluated at 22.98°C.	
Table 11.7c. South wall construction elements evaluated at 22.04°C.	74
Table 11.8. Overall uncertainty and 10 most influential input parameters from the n-way factor	
analyses in Watts	
Table 11.9. Statistical comparisons for cooling power in Exercise 8.	

Table A.1. Exercises and associated files.	90
Table A.2. Description of column header from the "Experiment 2.xls" workbook	91
Table A.3. Description of column header from the "Weather" worksheet.	92
Table A.4. Description of column header from the "Artificial Turf" worksheet	92
Table A.5. Description of the column headers in the "Experiment 3 Subhourly Data.xls"	workbook.
	93
Table A.6. Description of column header from the "Weather" worksheet.	94
Table A.7. Column headers for the "Temp BC and Internal Load" worksheet	95
Table A.8. Column headers for the "Glazing Measurements" worksheet.	95
Table A.9. Column headers for the "Angular Dependent Measurements" worksheet	96
Table A.10. Column headers for the "Experiment" worksheet.	97
Table A.11. Column headers for the "Uncertainties" worksheet	97
Table A.12. Column headers for the "Shade Properties" worksheet.	97
Table A.13. Column headers for the "Blind Slat Properties" worksheet.	

## Acknowledgements

We would like to gratefully acknowledge the financial support of the Swiss Federal Office of Energy (BFE) for building the test facility and funding our participation in the International Energy Agency's (IEA) Task 34/Annex 43, especially M. Zimmerman, C. Filleux, and A. Eckmanns.

During the course of this project, many companies generously donated materials, which included: Glastroesch with the glazing unit, Griesser with the exterior shading screen and Venetian blind assembly, Nysan with the interior shading screen, and 4B Bachmann with the window.

Thanks also goes to G. Maxwell from Iowa State University for overseeing the PhD dissertation that resulted from this work. Many thanks to our colleagues at EMPA, including: B. Binder, R. Blessing, M. Christenson, T. Nussbaumer, H. Simmler, and R. Vonbank, and our colleagues from IEA Task 34/Annex 43 including: J. Neymark, R. Judkoff, P. Heiselberg, P. Strachan, and C. Felsmann for their help. Finally we would like to thank S. Vardeman and M. Morris from Iowa State University for their valuable direction in the formulating the statistical and sensitivity analyses.

## **Abstract**

Buildings with highly glazed façades are becoming increasingly popular around the world. Shading devices are vital components for preventing overheating in buildings during the summer and reducing and/or eliminating the need for active cooling. Building energy simulation programs are tools which can be used to predict and optimize energy performance in buildings. The integral approach—by which all relevant energy transport paths are simultaneously processed—makes these programs essential for designing modern buildings. However, successful application of a program requires careful and thorough validations. This is especially true when assessing solar gain models. Even now, there are still very few high-quality data sets for validation of solar gain models currently available.

Therefore, the purpose of this project was to create a data set for use when evaluating the accuracies of models for glazing units and windows with and without shading devices. A series of eight experiments that subsequently increased in complexity was performed in an outdoor test cell located on the Swiss Federal Laboratories for Material Testing and Research campus in Duebendorf, Switzerland. The test cell was designed for calorimetric measurements and equipped with guarded zones. The experimental series consisted of two characterization experiments and six experiments with solar gains.

Particular emphasis was placed on accurately determining the test cell characteristics. The first two experiments were run without solar gains to specify the thermophysical properties, including the thermal bridges, of the test cell. The first experiment was a steady-state experiment that was used in conjunction with a three dimensional heat transfer simulation to quantify the thermal bridges. In the second experiment, the air temperature inside the test cell was allowed to float in response to a pseudo-random heat input. This experiment was simulated by four building energy simulation programs, and results from the programs were used to conclude that test cell specifications were very accurate for empirical validation.

Prior to the solar gain experiments, a preliminary exercise was performed to identify the most accurate tilted surface radiation model in each program. Experiments were then carried out to evaluate solar gain models in building energy simulation programs starting with the simplest case and increasing the complexity with each experiment. A solar selective glazing unit without shading, with external and internal diffuse shading screens, an external Venetian blind assembly, and internal mini-blind assembly were employed. A final experiment with a window (i.e. glazing unit with frame) was performed. Increasing the complexities of subsequent experiments allowed for careful assessments and diagnoses of the results. In these experiments, the heating/cooling powers in the test cell were adjusted to maintain a nearly constant test cell air temperature.

Robust experimental and sensitivity analyses were used to assess the impact of uncertainties of the program input and comparison measurands. A set of comprehensive statistical parameters was employed to compare results of building energy simulation programs with the experiments applying a 95% level of significance to determine whether the programs were validated or not. Up to four programs were evaluated within this Swiss Federal Office of Energy project for each experiment, including: HELIOS, EnergyPlus, DOE-2.1E, and IDA-ICE. Numerous additional simulation exercises using other codes were also performed within the scope the International Energy Agency's Task 34 / Annex 43 'Testing and Validation of Building Energy Simulation Tools'. These additional results were not included in this report because they were not yet available when this report was written. The impact of these validation exercises is already being realized. So far, several program errors and deficiencies in the programs have been identified with respect to solar radiation, glazing, shading, and surface heat transfer. These results also show that this is a high-quality data set.

This study is believed to be one of the most detailed empirical validations of solar gain models implemented in building energy simulation programs ever performed using a test cell. The authors' intention is that the data are widely used by program developers and modelers for future validation efforts.

## **Chapter 1: Introduction**

The validation of building energy simulation programs is an important component in the development and refinement of models and algorithms implemented in the software. Numerous efforts within the framework of the International Energy Agency's (IEA) Solar Heating and Cooling (SHC) Tasks and Energy Conservation in Building Community Systems Annexes (ECBCS) have dealt with many facets of program validations. Judkoff [1] discusses the three different types of validation used in building energy simulation software which include: 1) analytical validation (comparing program results to an analytical solution), 2) comparative validation (program-to-program comparisons), and 3) empirical validation (comparing results with an actual experiment). Each of these validation methodologies has its own advantages and disadvantages. For analytical comparisons, the advantages include: no input uncertainty, exact truth standard, and inexpensive to perform; however, the disadvantage is that there are limited numbers of cases for which analytical solutions can be derived. The advantages for the comparative comparisons are that there are no input uncertainties, not limited to simple cases, and quick and inexpensive to perform. The primary disadvantage to these types of comparisons is that there is no truth standard. This research focuses on the third type of validation—empirical validation. The advantages of empirical validation include: an approximate truth standard within uncertainties in the instrumentation and data acquisition system and that there are no limitations due to the complexity of the cases. The disadvantages are that measurements involve some degree of experimental uncertainty, detailed high quality measurements are very expensive and time-consuming to perform, and there are a limited number of data sites where this is economically practical.

Empirical validations can be performed at various levels including structure, systems and equipment, and whole building, which combines and integrates the first two levels of empirical validation into an additional level.

Building energy simulation programs are now being used by engineers and architects more than ever to simulate new highly glazed facades around the world. Therefore, robust empirical validations of solar gain algorithms and the associated interactions is a necessary endeavor to provide confidence that these programs simulate reality. Thus, the motivation for this study was to provide a high-quality data set and an evaluation methodology for empirical validation of solar gain algorithms in building energy simulation programs and subsidiary software. The specific focus of this research was to assess the performance of various building energy simulation programs when modeling a glazing unit with and without various shading devices, window, and the associated interactions; however, results from the experiments are now available for use in assessing the performance of future releases of current and future building energy simulation programs.

1

# Chapter 2: Experiments, Validation Exercises, Methodology, and Participants

A suit of experiments was performed in the EMPA outdoor test facility in Duebendorf, Switzerland (described more in-depth in Chapter 3). Results from the experiments were used to carry out empirical validation exercises in building energy simulation programs. To assess the performance of the various building energy simulation programs and make detailed comparisons with the experiments, a methodology that factored in experimental uncertainties in input and output parameters was designed for evaluating program performances. Descriptions of the experiments, validation exercises, methodologies, and a list of participants are described in subsequent sections of this chapter.

## 2.1. Experiments

Eight experiments were performed for empirical validations for empirical validation of building energy software in conjunction with the IEA Task 34/Annex 34 Subtask C. The experiments were designed to start very simply and subsequently increase in complexity and are listed as:

- 1. Steady-state test cell characterization
- 2. Transient test cell characterization
- 3. Glazing unit only
- 4. Glazing unit with an external shading screen
- 5. Glazing unit with an internal shading screen
- 6. Glazing unit with an external Venetian blind assembly
- 7. Glazing unit with an internal mini-blind assembly
- 8. Window (glazing unit with a frame)

#### 2.2. Validations Exercises

Eight validation exercises were performed that started simple and progressively increased in complexity and are listed below:

- 1. Test cell transient characterization (Experiment 2)
- 2. Evaluation of irradiation models on tilted facades (Experiment 3)
- 3. Glazing unit only (Experiment 3)
- 4. Glazing unit with external shading screen (Experiment 4)
- 5. Glazing unit with internal shading screen (Experiment 5)
- 6. Glazing unit with external Venetian blinds (Experiment 6)
- 7. Glazing unit with internal mini-blinds (Experiment 7)
- 8. Window (i.e. glazing unit with a window frame) (Experiment 8)

After completion of the test cell characterization experiments (Experiments 1 and 2), subsequent tests used "constant" temperatures within the test cell and the guarded zone. For all exercises except Exercise 2, measured hourly outer surface temperatures for the test cell construction element surfaces adjacent to the guarded zone and internal loads were used as boundary conditions inputs to the programs.

Additionally for the solar gain exercises (Exercises 3-8), measured weather data (both hourly and sub-hourly increments depending on the capacities of the programs) and hourly average air temperatures inside the test cell were used as program inputs. The experiments were run during periods when there was no snow on the ground in order to accurately account for ground reflectance. Before each solar gain experiment, highly reflective insulation material was fixed over the outside of the glazing unit shown in Figure 2.1. This was accounted for in the weather data by setting the irradiance values to zero for these hours. In comparisons between program predictions and experimental results of cooling power, the first 120 h were removed; so each period consisted

of 480 h (20 days). Long periods of time were chosen to run the experiment to ensure diverse atmospheric conditions (both sunny and cloudy days).



Figure 2.1. Photograph of the test cell during the preconditioning phase.

## 2.3. Empirical Validation Methodology

A consistent methodology was used to compare the performances of each building energy simulation program for all experiments. In order to carefully evaluate each program, experimental uncertainties of output parameters and detailed sensitivity studies were conducted to quantify the impact uncertainties in program input parameters propagating through the program and affecting prediction outputs. These uncertainties were evaluated at a 95% significance level and used as a measure for program validation. When the programs were within these overlapping 95% credible limits, they were considered validated. Figure 2.2 contains a flowchart diagramming the methodology.

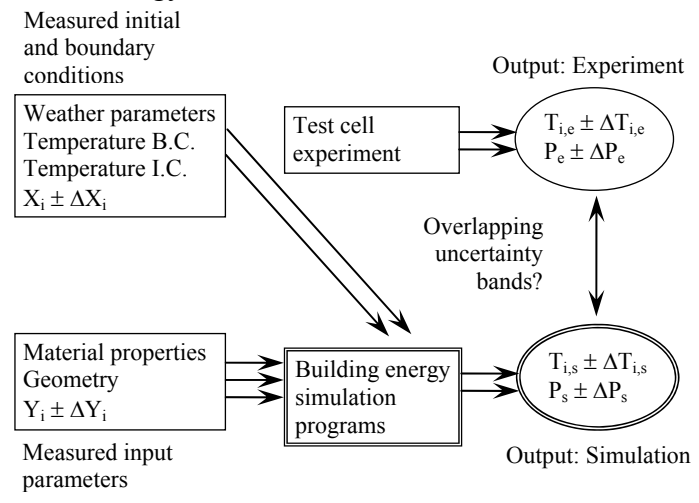


Figure 2.2. Methodology for empirical validation of building energy simulation programs.

Many simulators chose to use weather data that were in sub-hourly intervals; however all results were then provided and evaluated for 1 h time intervals to provide consistent comparisons between program outputs. A number of different measures were used to quantify the observed relationships between measured and simulated air temperatures and cooling powers. These were based on the basic statistical summary measures: the sample mean,  $\bar{x}$ , the sample maximum,  $x_{max}$ , and minimum,  $x_{min}$ , values, and sample standard deviation, s.

To compare each simulation to the experiment, differences between experimental and corresponding simulated values,  $D_i$  (where the index i hour of the experiment), were first computed. The arithmetic mean,  $\overline{D}$  and absolute maximum,  $|D_{max}|$  and minimum,  $|D_{min}|$  differences were then determined for each simulated quantity. Further, the average absolute difference,  $|\overline{D}|$ , was computed using Equation 2.1.

$$\overline{|D|} = \frac{1}{n} \sum_{i=1}^{n} |D_i| \tag{2.1}$$

This is one possible quantification of the overall magnitude of disagreement between the simulations and the experiment. Another is the root mean squared difference,  $D_{rms}$ , defined in Equation 2.2.

$$D_{rms} = \sqrt{\frac{1}{n} \sum_{i=1}^{n} D_i^2}$$
 (2.2)

It is an algebraic fact that this quantity is related to the sample mean and sample standard deviation of differences by Equation 2.3.

$$D_{rms} = \sqrt{\frac{n-1}{n}S_D^2 + \overline{D}^2}$$
 (2.3)

For additional comparisons, the 95% quantiles (the upper 5% points of the sample distributions) for the absolute differences,  $|D|_{95\%}$ , were computed for all simulations. Uncertainties associated with the average temperature calculated by summing the sample variance with the propagated error squared. The cooling power uncertainties were computed assuming Bayesian errors. Ninety-five percent credible limits were computed for all experiments at each hour,  $OU_{i,Exp}$ , and the average uncertainty,  $\overline{OU}$ , was reported in the summary tables under the experiment column. All of these calculations were performed neglecting time-series serial correlations (which could also impact the overall uncertainty).

Additional uncertainty analysis was performed in EnergyPlus, using a Monte Carlo Analyses (MCA) to quantify overall output uncertainty for the building energy simulation programs due to uncertainties in input parameters. Ninety-five percent credible limits  $OU_{i,EnergyPlus}$ , for each hour were also calculated and the mean quantity,  $\overline{OU}$ , are reported in the statistical analyses under the EnergyPlus column. N-way factorial analyses were also performed for each experiment to assess the sensitivity of all input uncertainties on the output. An in-depth description providing background information and implementation of the MCA and N-way factorial analysis in EnergyPlus is given by Loutzenhiser et al [2].

To compare the performance of the individual building energy simulation programs, uncertainty ratio,  $UR_i$ , was devised to compare hourly differences with experimental and input errors and is shown in Equation 2.4. When the quantity is less than or equal to unity, the results are considered validated within 95% credible limits.

$$UR_{i} = \frac{\left|D_{i}\right|}{OU_{i,Exp} + OU_{i,EnergyPlus}} \tag{2.4}$$

## 2.4. Participating Organizations and Simulation Tools

Numerous organizations performed the empirical validations at various levels using numerous building energy simulation programs. A list of participants in this study is given in Table 2.1. Results from additional collaborations with IEA participants from Europe and the United States.

Table 2.1. List of participants, building energy simulation programs, and level of participation for

the EMPA experiments.

Institution	Modeler(s)	<b>Building Energy</b>	<b>Header Name</b>	Level of Participation
		Simulation		
		Program		
Empa	S. Carl and T.	HELIOS	HELIOS	All exercises
	Frank			
Empa	P. Loutzenhiser	EnergyPlus	EnergyPlus	All exercises
Empa/Iowa State	P. Loutzenhiser	DOE-2.1E	DOE-2.1E	Exercises 1-5 and 8
University (ISU)				
University of Applied	S. Moosberger and	IDA-ICE	IDA-ICE	Exercises 1- 2
Science of Central	G. Zweifel			
Switzerland (HTAL)				
University of Applied	S. Moosberger and	IDA-ICE with Parasol	IDA-PAR	Exercise 3
Science of Central	G. Zweifel	for a window model		
Switzerland (HTAL)		with a 1 <sup>st</sup> parameter		
		guess		
University of Applied	S. Moosberger and	IDA-ICE with existing	IDA-SIA	Exercises 3-5
Science of Central	G. Zweifel	model and 2 <sup>nd</sup>		
Switzerland (HTAL)		parameter guess		
University of Applied	S. Moosberger and	IDA-ICE with a new	IDA-Detwind	Exercise 3
Science of Central	G. Zweifel	window model		
Switzerland (HTAL)				

## **Chapter 3: Facility Description**

The EMPA outdoor test facility is located on the EMPA campus in Duebendorf, Switzerland. The test facility is comprised of two identical test cells, where five of six faces in each test cell are adjacent to guarded zones allowing for more precise determination of boundary conditions. The test cells and guarded zones each have their own air conditioning unit. According to Strachan [3], test cells offer an economical and practical alternative between full-scale modeling of an actual building and the laboratory; test cells provide the best environment for generating high-quality data sets for whole building empirical validations.

The air in the test cell is distributed near the floor by two textile ducts and extracted near the ceiling through metal ducts. Despite large air changes in the test cell, measurements taken near the wall with a hotwire anemometer revealed very small velocities. Temperatures within the space were measured with 18 double shielding thermocouples, which divide the test cell into 18 equal parts for the solar gain experiments. An illustration of the test cell setup is shown in Figure 3.1.

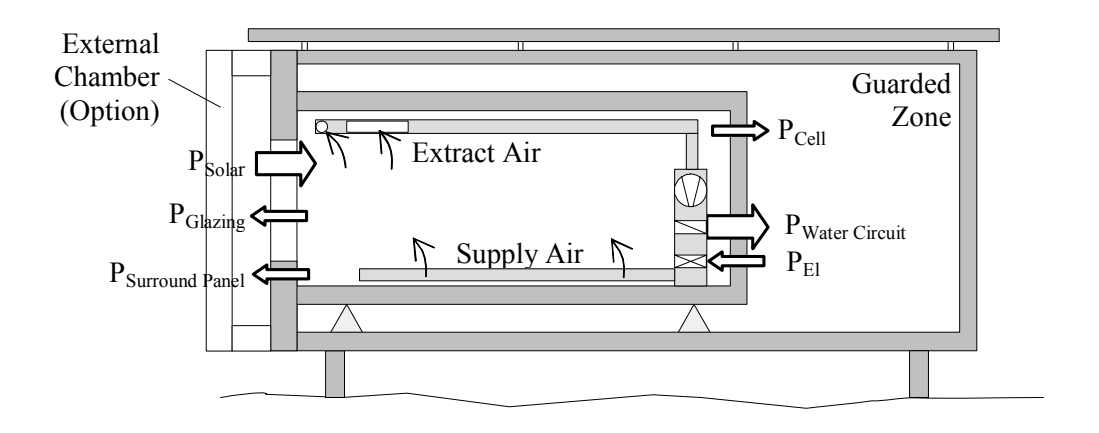


Figure 3.1. EMPA test cell schematic.

Additional characterizations of the test cell are described in this section, including:

- Test cell location and dimension
- Thermal bridge quantification
- Thermal mass and air-tightness
- Thermophysical properties
- Sensors
- Ground reflectance
- Explanation of experimental data

#### 3.1. Test Cell Location and Dimensions

The test cell is located on the EMPA campus in Duebendorf, Switzerland. Table 3.1 contains information regarding the global location, time zone, and orientation of the test cell.

Degrees of longitude	8.6° East
Degrees of latitude	47.7° North
Altitude above sea-level	430 m
Time zone	Central European Time (GMT + 1 h)
Orientation of external wall	$29^{\circ} \text{ (south = 0°, west = 90°)}$

Table 3.1. Location of the EMPA test cell.

The internal dimensions of the test cell are shown in Table 2.2.

Table 3.2. Dimensions of the test cell.

Internal height	2.360 m
Internal width	2.850 m
Internal length	4.626 m
Area of the north/south wall	$6.726 \text{ m}^2$
Area of the east/west wall	$10.917 \text{ m}^2$
Area of the floor/ceiling	$13.184 \text{ m}^2$
Internal volume	$31.114 \text{ m}^3$

### 3.2. Thermal Bridge Quantification

According to Monaird and Guyon, [4], determining the overall thermal cell characteristics is imperative for empirical validations. Thermal bridges are usually more important in test cells than in real buildings because the dimensions are smaller and conduction through the walls in the only heat loss mechanism. Therefore, the total thermal losses—including those at edges, door, sealing at external wall and intersections of pipes or flexes with the cell envelope—were computed using TRISCO software [5]. This program allowed for a three dimensional steady-state analysis of heat conduction processes. Equivalent thermal conductivities of cavities were calculated according to prEN ISO 10077-2 [6]. The final model of the test cell employed 5.6·10<sup>6</sup> nodes. The results of these simulations are shown in Figures 3.2a and 3.2b. The results in Figure 3.2a were generated for a 1 K temperature difference between the cell air and the guarded zone. High heat fluxes were seen at the sealing of the door and at the sealing between cell and removable external wall. Figure 3.2c shows an image of the test cell taken by an infrared of the thermal bridges at the door. The picture was taken for a 20 K temperature difference between the test cell air and the guarded zone.

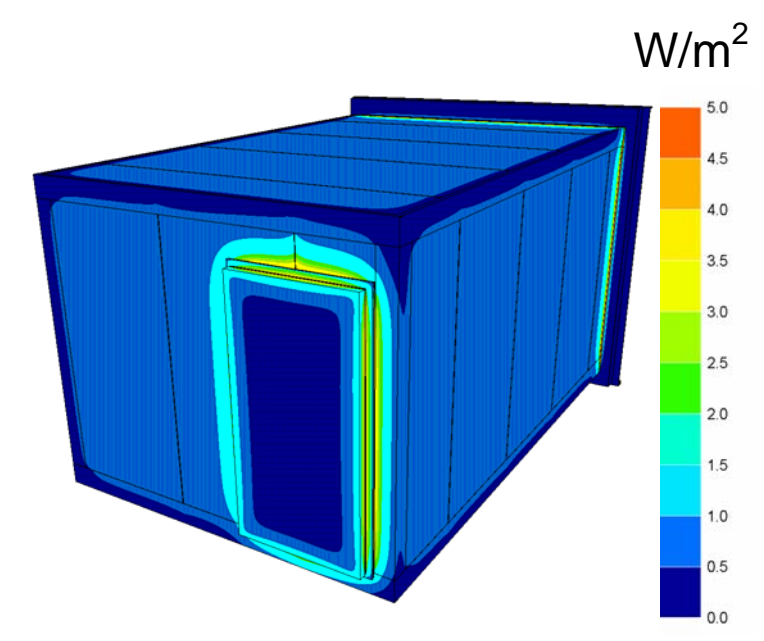


Figure 3.2a. Computed heat fluxes at the outer surfaces of the test cell.

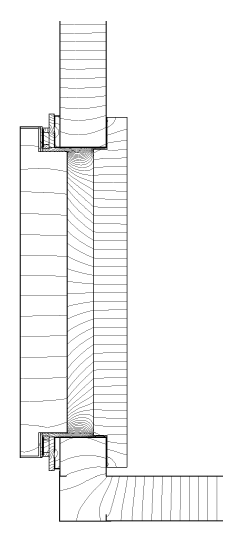


Figure 3.2b. Computed heat fluxes for a horizontal cross-section of the door.



Figure 3.2c. Infrared picture of the test cell door.

Tables 3.3a and 3.3b contain the total steady-state properties at 20°C for the thermal conductance. This parameter refers to the heat flow between the cell air and the outer surface of the cell envelope.

Table 3.3a. Heat transfer characteristics of the guarded zone.

	Area m <sup>2</sup>	Thermal conductance W/K
Ceiling, north (incl. door), east and west wall	41.745	6.478
Floor	13.184	1.941
Thermal bridges guarded zone	-	4.526
Total		12.945

Table 3.3b. Heat transfer characteristics of the exterior wall.

	Area A m <sup>2</sup>	Thermal conductance W/K
External wall	6.726	1.736
External thermal bridges	-	0.040
Total		1.776

The thermal conductance from a TRISCO software simulation of the entire cell envelope (from inside the cell to the outer surface, including thermal bridges) at 0°C and 20°C were calculated to be 13.539 W/K and 14.721 W/K, respectively.

The thermal conductance as a function of mean wall temperature for the guarded zone and the exterior wall are given in Equations 3.1 and 3.2, respectively.

Guarded zone: 
$$H_{GZ}(\theta) = 11.877 + 0.0534 \cdot \theta \text{ (W/K)}$$
 (3.1)

Exterior wall: 
$$H_{EW}(\theta) = 1.662 + 0.0057 \cdot \theta \text{ (W/K)}$$
 (3.2)

where

 $\theta$  is the mean wall temperature in °C.

A steady-state experiment (Experiment 1) was also performed and results were used to assess the computation of the thermal conductances from the 3-D simulation. An external chamber was mounted over the external facade of the test cell, and the boundary conditions were kept as close to constant values as possible. Two phases of the experiment with different sets of boundary conditions were performed. The steady-state time-averaged conditions for both phases of the experiment are giving in Table 3.4. These calculations were performed for mean wall temperatures for the exterior wall and guarded zone of  $36.6^{\circ}$ C and  $31.6^{\circ}$ C, respectively. Applying an energy balance to the test cell for each phase of the experiment and solving both equations simultaneously resulted in thermal conductances for the exterior wall and guarded zones of  $2.12 \pm 0.59$  W/K and  $12.23 \pm 0.53$  W/K, respectively. A comparison between the thermal conductance from the steady-state experiment and the conductance computed from TRISCO as a function of temperatures (Equations 2.1 and 2.2) with uncertainties is shown in Figure 3.3.

Table 3.4. Steady-state experiment: time-averaged values and uncertainties for thermal conductance calculations.

	Test Cell	Air Temperature	Temperature in the	Temperature in the
	Heat Input	in the Test Cell	Guarded Zone	External Chamber
Phase 1	282.26 ± 4 W	43.13 ± 0.5°C	$23.50 \pm 0.5$ °C	23.24 ± 0.5°C
Phase 2	145.04 ± 3 W	$36.45 \pm 0.5$ °C	$23.33 \pm 0.5$ °C	43.74 ± 0.5°C

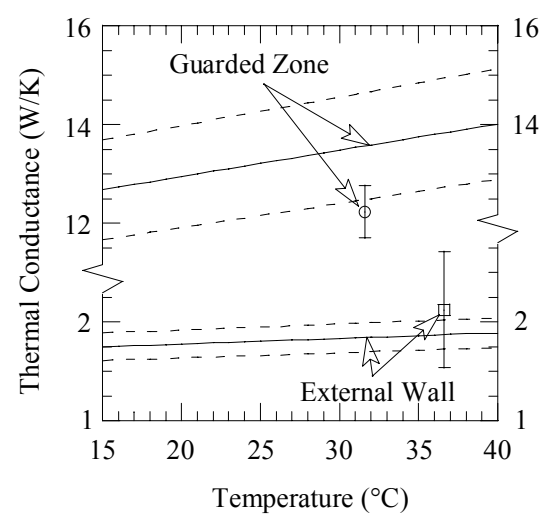


Figure 3.3. Comparison of thermal conductances of the external wall and guarded zone as function of temperature found by simulation and the steady-state experiment.

## 3.3. Thermal Mass and Air-tightness

The internal mass of the technical equipment positioned in the test cell, which consisted of metallic ducts, grills, fans, a heat exchanger apparatus inside a metal casing, an electrical cabinet, etc. was estimated to be 200 KJ/K. Because the steel sheets are a major component in the thermal

mass, the thermal response was assumed to be fast compared to the test cell envelope. The impact of this mass on the overall transient thermal behavior of the test cell was rather small.

To ensure the test cell was airtight, gaps between the steel sheets used for test cell construction were sealed with silicon. Two stage rubber seals were installed and the door and the external walls to eliminate air leaks. Test cell infiltration was tested using the blower door method. When the test cell was pressurized to 50 Pa, the air exchange rate was found to be 0.2 h<sup>-1</sup>. The assumption was then made that zone infiltration was negligible.

## 3.4. Thermophysical and Optical Properties

The thermophysical properties of the test cell were obtained from measurements, literature, product specification, a three dimensional whole test cell simulation, and a steady-state experiment used for overall thermal characterization of the test cell. Tables 3.5 to 3.7 show layer sequences, thicknesses and thermophysical properties for all layers of the test cell envelope. Layer Number 1 denotes the outside layer of the test cell. In the case of the thermal conductivity for the insulation and plywood layers, the quantities are based on a linear regression analysis calculated as a function of the average temperature in the material. Because not all building energy simulation programs can account for temperature-dependent thermophysical properties, the mean construction element temperature averaged over time was computed and, for each exercise requiring the modeling the test cell, temperature-dependent thermal conductivities were then fixed accordingly.

Table 3.5. Layer properties of the ceiling, north (incl. door), east and west wall.

			<i>D</i> <sup>2</sup>	,,	
Layer number	Material	Thickness mm	Thermal conductivity W/m-K	Density kg/m <sup>3</sup>	Specific heat J/kg-K
1	Sheet steel	0.7	53.62	7837	460.8
2	PU foam	138.6	$0.01921 + 0.000137 \cdot \theta$	30	1800
3	Sheet steel	0.7	53.62	7837	460.8

where  $\theta$  is temperature in °C.

Table 3.6. Layer properties of the floor.

Layer	Material	Thickness	Thermal conductivity	Density	Specific heat
number		mm	W/m-K	kg/m <sup>3</sup>	J/kg-K
1	Sheet steel	0.7	53.62	7837	460.8
2	PU foam	140	$0.01921 + 0.000137 \cdot \theta$	30	1800
3	PU foam (higher density)	20	0.070	45	1800
4	Sheet steel with surface structure	2.5	53.62	7837	460.8

Table 3.7 Layer properties of the external wall

Layer number	Material	Thickness Mm	Thermal conductivity W/m-K	Density kg/m³	Specific heat J/kg-K
1	Plywood	10	$0.136359 + 0.000175 \cdot 9$	850	1605
2	EPS foam	130	$0.03356 + 0.000127 \cdot \theta$	28	1460
3	Plywood	10	$0.136359 + 0.000175 \cdot \theta$	850	1605

The optical properties of the test cell surfaces were also measured and are shown in Table 3.8. The solar reflectance was computed according to European Standard EN 410 [7] using Glad Software [8] and the hemispherical emittance was measured with an emissometer based on a calorimetric method.

Table 3.8. Optical properties of test cell surfaces.

Surface Element	Solar reflectance, %	Hemispherical Emittance, %
Inner surfaces of walls and ceiling	75.7	92
Inner surface of floor	24.6	96
Outer / inner surfaces of south wall	76.6	93

#### 3.5. Sensors

The sensors used in the test facility are periodically calibrated according an EMPA quality assurance system. Nearly 150 parameters were measured every six minutes (four minutes for Experiment 1 and 2). After each full hour, averages values were computed from the last hour of data acquisition. Table 3.9 contains a list of all the metrological equipment and accuracies used at the facility. In Table 3.10, specifications for the most important parameters in the test cell and external chamber in the guarded zone are shown and accuracies.

Table 3.9. Weather data parameters and equipment.

Parameter	Unit	Type of sensor / measurement	Number of sensors	Accuracy
Solar global irradiance, façade plane	W/m <sup>2</sup>	Pyranometer (Kipp & Zonen CM 21)	1	± 2 %
Solar global horizontal irradiance	W/m <sup>2</sup>	Pyranometer (Kipp & Zonen CM 21)	1	± 2 %
Solar diffuse horizontal irradiance	W/m <sup>2</sup>	Pyranometer, mounted under the shading ball of a tracker (Kipp & Zonen CM 11)	1	± 3 %
Direct-normal irradiance	W/m <sup>2</sup>	Pyrheliometer, mounted in an automatic sun-following tracker (Kipp & Zonen CH 1)	1	± 2 %
Infrared irradiance, façade plane	$W/m^2$	Pyrgeometers (Kipp & Zonen CG 4)	1	± 2 %
Outside air temperature, in front of façade	°C	Radiation shielded, mechanically ventilated thermocouples	2	± 0.5 K
Wind speed, in front of façade	m/s	Ultrasonic anemometer (WindMaster )	1	± 1.5 %
Horizontal illuminance	Lx	Luxmeter (Kipp & Zonen LuxLite, Minolta T-10W)	2	± 3 %
Pressure	hPa	Barometric Pressure Measuring Device (Vaisala PTA 427)	1	± 0.5 hPa
Relative humidity	%	Humidity Transmitter (Vaisala HMP 130Y Series)	1	± 1% (0-90%) ± 2% (90-100%)

Table 3.10. Parameters measured in the test cell, the external chamber and the guarded zone and

approximate accuracies according to manufacturer specifications.

Parameter	Unit	Type of sensor / measurement	Number	Accuracy
			of sensors	
Air temperatures, inside test cell	°C	Thermocouple, radiation shielded by two cylinders	18	± 0.3 K
Air temperatures, in external chamber	°C	Thermocouple, radiation shielded by two cylinders	5	± 0.3 K
Air temperatures, in guarded zone, 0.1 m in front of cell surface	°C	Thermocouple, radiation shielded by two cylinders	25	± 0.3 K
Surface temperatures, inner surface of cell envelope	°C	Thermocouple	30	± 0.3 K
Surface temperatures, outer surface of cell envelope	°C	Thermocouple	30	± 0.3 K
Heating power, inside test cell	W	Electric power (Infratek 106A)	1	± 0.1 %
Cooling power, inside test cell	W	Electromagnetic flowmeter (Endress+Hauser Promag 53H) and temperature difference measurement (PT100)	3	± 2 %
Illuminance, horizontal inside cell	Lx	Luxmeter (Minolta T-1H)	3	± 2 %

#### 3.6. Ground Reflectance Measurement

Artificial green turf was installed in front of the test cell to represent a typical outdoor surface. Hemispherical-hemispherical reflectance at each wavelength was determined by using angular dependent model for absorptance,  $\alpha(\theta)$ , [9] for incident angles between 0° and 80°, and a linear

model between 80° and 90°. This piecewise function is shown in Equation 3.3. Equation 3.4 was used to calculate the hemispherical-hemispherical reflectance,  $\rho_{hem}$  [10]. This integral was evaluated numerically using Engineering Equation Solver [11]. Directional-hemispherical reflectance at a normal incident angle was measured. Solar reflectance was determined according to European Standard EN 410 [7] by means of GLAD software [8] and the directional-hemispherical reflectance at a normal angle of incidence is provided in Table 3.11. A photograph of the artificial turf is shown in Figure 3.4. The specular components of the reflectance were measured at Basel University by Professor Peter Oelhafen and his research group for incident angles of 20°, 40°, and 60° and found to be less than 1%; therefore the surface was considered a Lambert surface [9].

$$\frac{\alpha(\theta)}{\alpha_n} = \begin{cases} 1 + 2.0345 \times 10^{-3} \,\theta - 1.99 \times 10^{-4} \,\theta^2 + 5.324 \times 10^{-6} \,\theta^3 - 4.799 \times 10^{-8} \,\theta^4 & 0^\circ \le \theta \le 80^\circ \\ -0.064\theta + 5.76 & 80^\circ \le \theta \le 90^\circ \end{cases}$$
(3.3)

where

 $\theta$  is the angle of incidence, °  $\alpha_n$  is the normal absorptance

$$\rho_{hem} = 2 \int_{0}^{90} (1 - \alpha(\theta)) \sin(\theta) \cos(\theta) d\theta$$
 (3.4)

Table 3.11. Ground reflectance.

	Hemispherical reflectance, %	Normal incident reflectance, %
Solar	14.8	8.8

## 3.7. Explanation of Experimental Data

The purpose of this series of experiments was to provide a well-documented description of the experiments and experimental data inputs and outputs that could be used to empirically validate building energy simulation programs. A description of the experiments and results from many building energy simulation programs are described in subsequent chapters of this report. However, the required inputs for simulating the exercises and the outputs used for comparisons are contained in Excel files that are described in Appendix A; the combined results and data from this report can be extremely useful for developers and modelers wishing to validate their own building energy simulation programs.

## **Chapter 4: Transient Characterization Experiment (Exercise 1)**

An experiment designed to evaluate the transient characteristics of the test cell was performed. Details concerning the test cell, thermophysical properties, experimental setup, and results are provided.

#### 4.1. Test Cell

An external chamber (Figure 4.1a) was mounted over the exterior wall with no window (Figure 4.1b) for climate control. The air temperatures in the guarded zone and the external chamber were maintained near 23°C, and the air inside the guarded cell was re-circulated and stirred to reduce thermal stratification. During the test, the re-circulating fans operated constantly and added an internal heat load of ~77 W. After an initial preconditioning phase of 50 hours, a pseudo-random heat source of ~196 W was turned on and off to provide an additional internal load. The heat source was located inside the test cell's re-circulation/conditioning apparatus and can therefore be considered purely convective.



Figure 4.1a. Photograph of test toom with external chamber.



Figure 4.1b. Outdoor test facility with removable façade element.

### 4.2. Thermophysical Properties

Temperature-dependent thermophysical properties were evaluated at the mean temperature of the construction elements averaged over time for the entire experiment; the mean temperature was computed as 28.38°C. Tables 4.1a to 4.1c contain fixed thermophysical properties for each construction element.

Table 4.1a. Ceiling, north, east and west wall construction evaluated at  $\theta = 28.38$ °C.

Layer number	Material	Thickness mm	Thermal conductivity W/m-K	Density kg/m <sup>3</sup>	Specific heat J/kg-K
1	Sheet steel	0.7	53.62	7837	460.8
2	PU foam	139	0.023098	30	1800
3	Sheet steel	0.7	53.62	7837	460.8

Table 4.1b. Floor construction evaluated at  $\theta = 28.38$ °C.

Layer number	Material	Thickness mm	Thermal conductivity W/m-K	Density kg/m <sup>3</sup>	Specific heat J/kg-K
1	Sheet steel	0.7	53.62	7837	460.8
2	PU foam	140	0.023098	30	1800
3	PU foam (higher density)	20	0.070	45	1800
4	Sheet steel with surface structure	2.5	53.62	7837	460.8

Table 4.1c. South wall construction evaluated at  $\theta = 28.38$ °C.

Layer number	Material	Thickness mm	Thermal conductivity W/m-K	Density kg/m <sup>3</sup>	Specific heat J/kg-K
1	Plywood	10	0.14133	850	1605
2	EPS foam	130	0.03716	28	1460
3	Plywood	10	0.14133	850	1605

## 4.3. Experimental Setup

Hourly averaged values (where 1 corresponds to a time from 0:00 to 1:00) for the measured mean surface temperatures (boundary conditions), test cell air temperatures and internal loads were used as inputs to the building energy simulation programs and are given in "Experiment 2.xls". Figure 4.2 shows the locations of the temperature sensors in cell and described in this file. Additional double-shielded thermocouples were added for subsequent experiments.

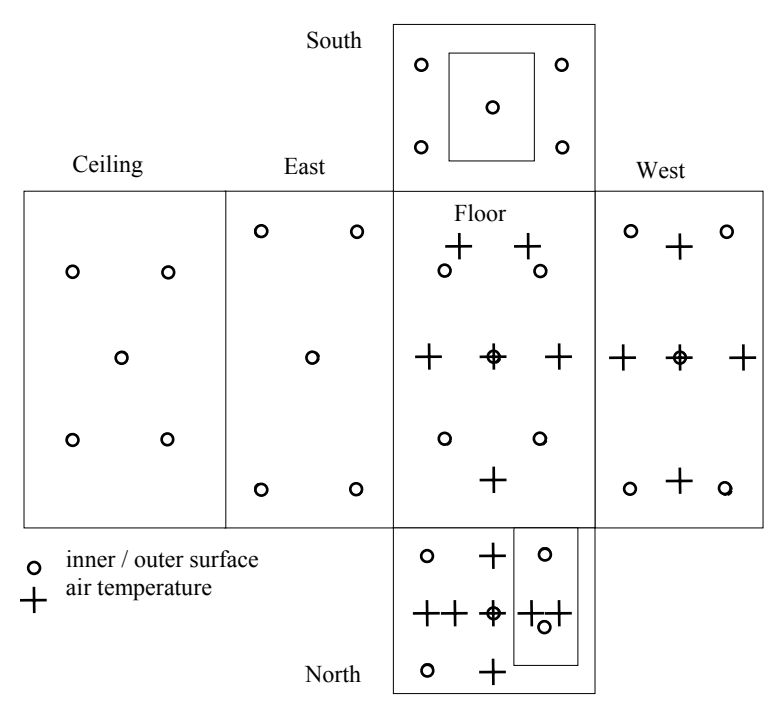


Figure 4.2. Location of temperature sensors.

Figure 4.3 contains a plot of the results for the experiment. Included in the plot are the mean cell temperature, mean surface temperatures, and the additional internal load introduced into the space.

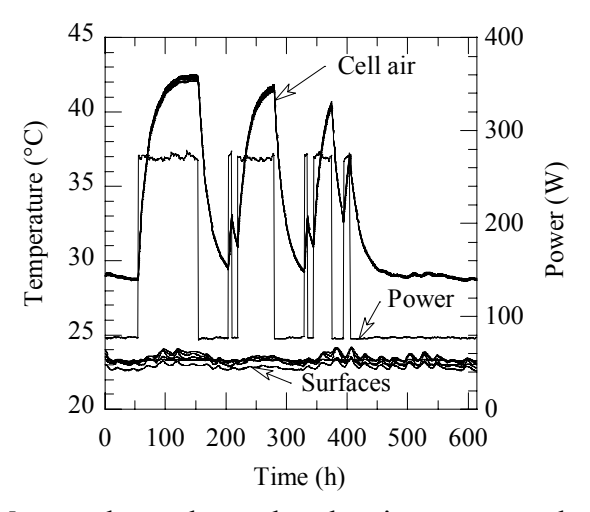
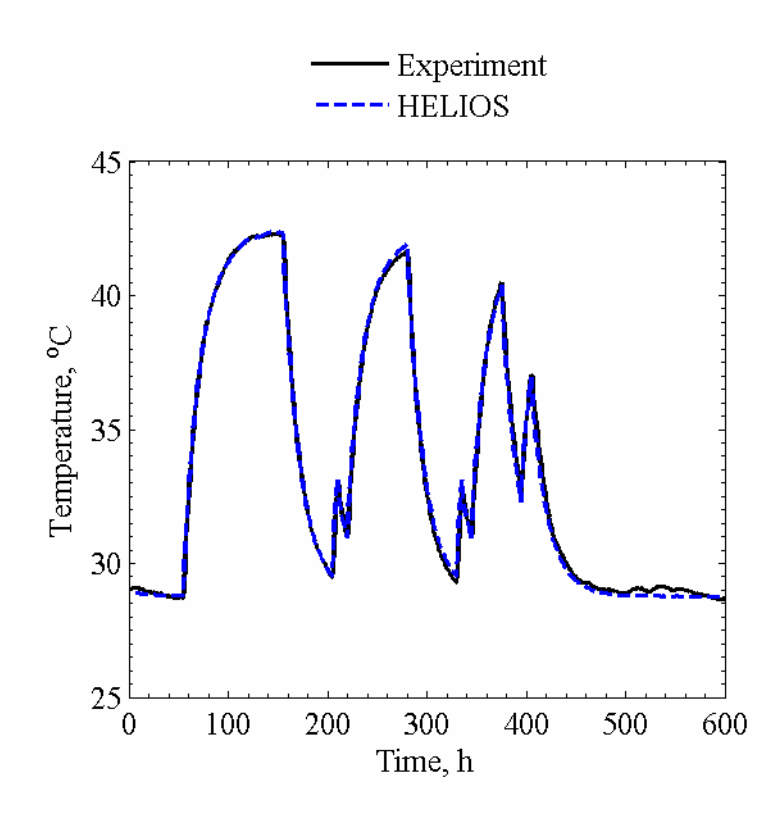


Figure 4.3. Measured pseudo-random heating power and temperatures.

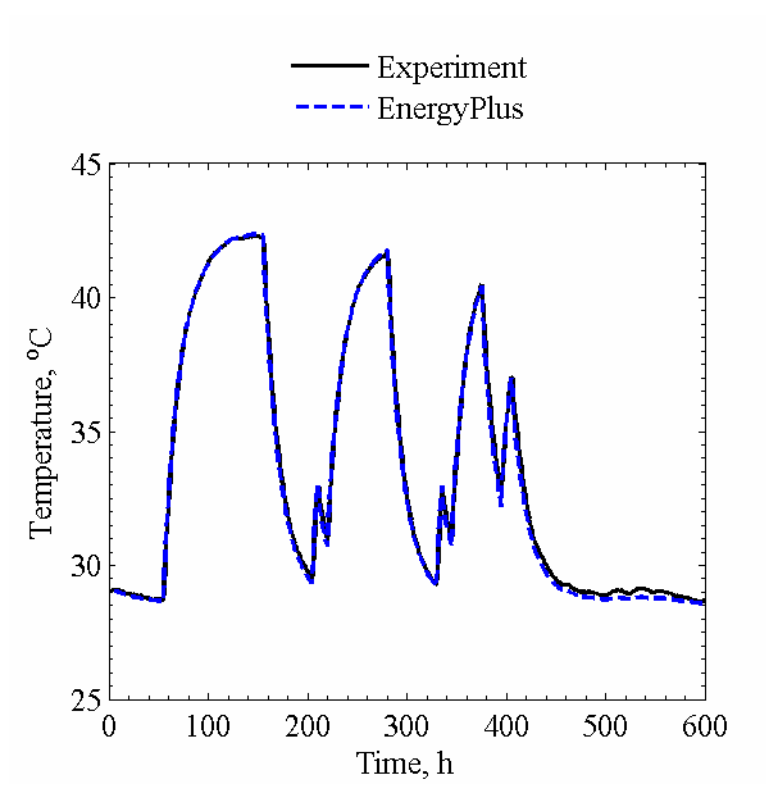
#### 4.4. Results

Test cell air temperature comparisons from the experiment and each building energy simulation program are contained in this section as well as a comprehensive set of statistical analysis for comparisons.

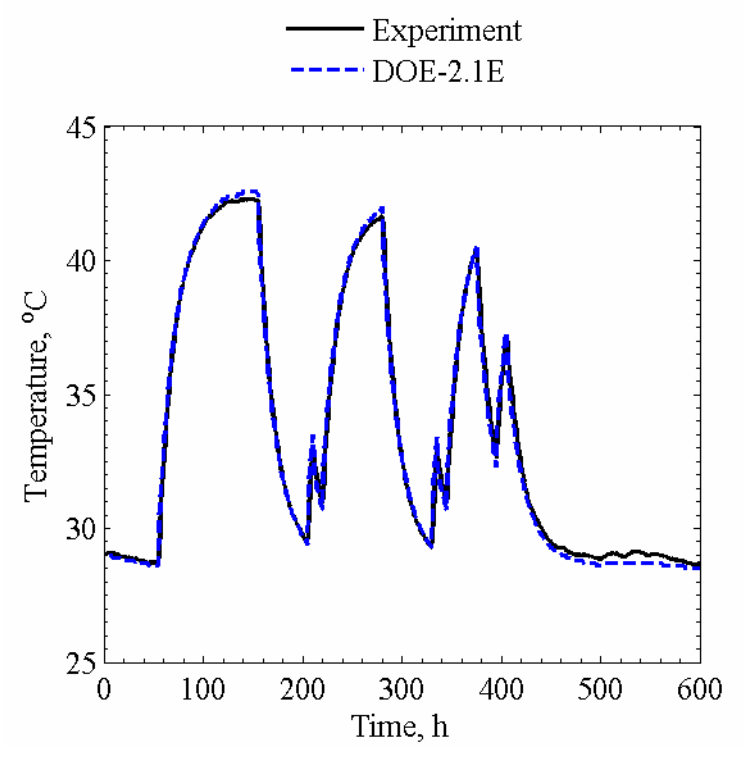
The measured and predicted test cell air temperatures from HELIOS, EnergyPlus, DOE-2.1E, and IDA-ICE are shown in Figures 4.4a to 4.4d, respectively. Other parameters used for diagnostic purposes that were not included were: convective heat transfer coefficients and inner surface temperatures for all construction elements.



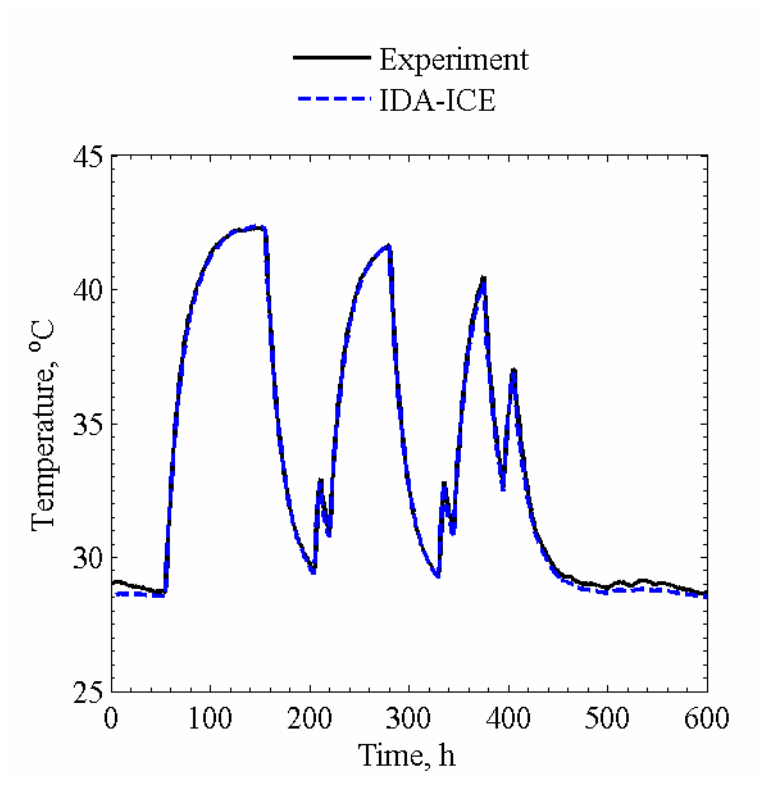
Figures 4.4a. Test cell air temperature comparisons for HELIOS.



Figures 4.4b. Test cell air temperature comparisons for EnergyPlus.



Figures 4.4c. Test cell air temperature comparisons for DOE-2.1E.



Figures 4.4d. Test cell air temperature comparisons for IDA-ICE.

The MCA was performed in EnergyPlus for all hours along with an assessment of experimental uncertainties for the test cell air temperatures. The hourly 95% credible limits for MCA, experiment, and sum are shown in Figure 4.5. An n-way factorial analysis was used to assess the sensitivity of the output test cell air temperature to uncertainties of input parameters. The 10 most influential parameters that impacted the predicted air temperature are shown in Table 4.2; these results include n-way factorial analysis for both forward and backward differencing. Statistical comparisons were performed employing the methodology described in Chapter 2 for all programs, and the results are displayed in Table 4.3.

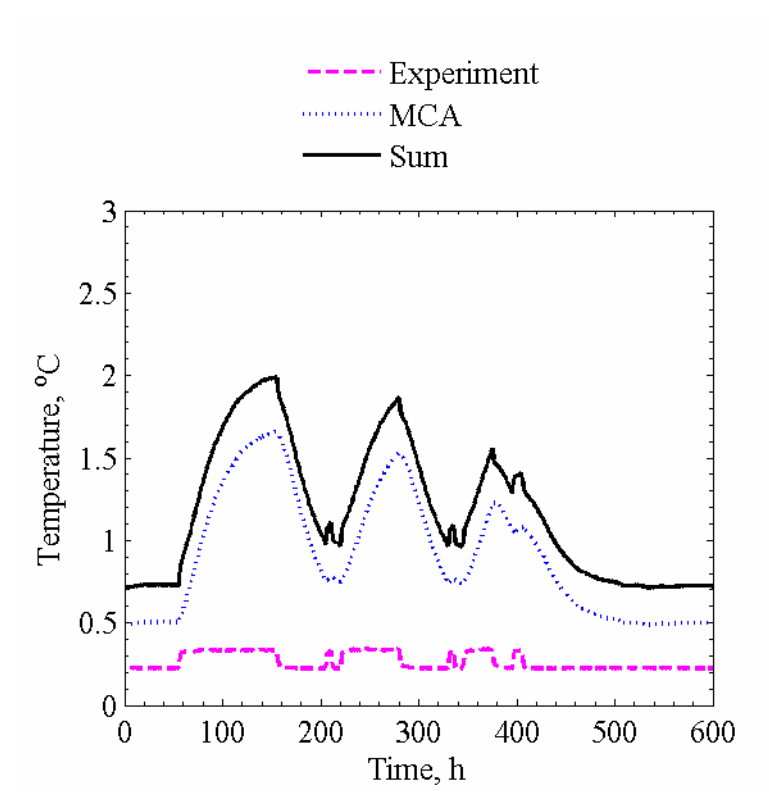


Figure 4.5. Experimental uncertainty, uncertainty of simulation results due to uncertainty in input parameters and total uncertainty.

Table 4.2. Overall uncertainty and 10 most influential parameter uncertainties that impacted the cell air temperature predictions in K.

Parameter	Forward	Backward
Overall uncertainty	0.454	0.481
Thermal bridge	-0.321	0.344
PU foam conductivity	-0.269	0.287
PU foam floor conductivity	-0.075	0.077
South wall surface temperature	0.057	-0.057
Ceiling surface temperature	0.055	-0.055
Floor surface temperature	0.053	-0.053
West wall surface temperature	0.046	-0.046
East wall surface temperature	0.046	-0.046
North wall surface temperature	0.044	-0.044
EPS foam conductivity	-0.042	0.043

Table 4.3. Statistical analysis for the test cell air temperature.

Parameter	Experiment	HELIOS	EnergyPlus	DOE-2.1E	DA-ICE
$\overline{x}$	33.5 °C	33.5 °C	33.4 °C	33.5 °C	33.4 °C
S	4.9 K	4.9 K	4.9 K	5.0 K	4.9 K
$x_{max}$	42.3 °C	42.4 °C	42.4 °C	42.6 °C	42.4 °C
$x_{min}$	28.7 °C	28.7 °C	28.6 °C	28.5 °C	28.5 °C
$\overline{D}$	•	0.0 K	0.1 K	0.1 K	0.1 K
$ \overline{D} $	-	0.2 K	0.2 K	0.3 K	0.2 K
$/D_{max}/$	Ī	1.0 K	0.7 K	1.2 K	0.6 K
$/D_{min}/$	Ī	0.0 K	0.0 K	0.0 K	0.0 K
$D_{rms}$	Ī	0.2 K	0.2 K	0.3 K	0.2 K
$/D/_{95\%}$	Ī	0.5 K	0.5 K	0.7 K	0.4 K
$\overline{OU}$	0.3 K	-	0.9 K	-	-
$\overline{\it UR}$	-	0.2	0.2	0.2	0.2
$UR_{max}$	-	1.1	0.8	1.4	0.7
$UR_{min}$	-	0.0	0.0	0.0	0.0
$ \overline{D} /\overline{x} \times 100\%$	-	0.5%	0.5%	0.8%	0.5%
$\overline{D}$ / $\overline{x} \times 100\%$	-	0.1%	0.4%	0.2%	0.4%

Based on these results, the conclusion was reached that the thermal bridges and thermophysical and optical properties in the test cell were well-described; these results provided a foundation for proceeding to experiments in this test cell that focused on assessing the impact of solar gains with and without shading devices. Further analysis and discussion of the experiment and results is provided by Manz et al. [12].

# **Chapter 5: Evaluation of Irradiation Models on Tilted Facades** (Exercise 2)

In preparation for the solar gain experiments, a preliminary exercise was designed to ascertain the accuracies of tilted surface radiation models from each building energy simulation. The experiment was performed from October 2 to October 26, 2004 at the EMPA outdoor test cell; the purpose of this exercise was to take two of three radiation measurement (direct-normal irradiance, diffuse irradiance, or global horizontal irradiance) along with the measured ground reflectance (quantified in Chapter 3) and predict the incident radiation (or global vertical irradiance) on the southwest façade.

The validation for this exercise focused on comparing measured global vertical solar irradiance on the exterior façade with predictions from each building energy simulation program. An assessment of the three components of solar irradiance (direct-normal, global horizontal, and diffuse horizontal) and the formulation of the various titled radiation models are given by Loutzenhiser et al. [2]. Plots for measured and prediction global vertical irradiance on the vertical façade are listed with corresponding figures as:

- HELIOS Perez 1987 (Figure 5.1a)
- EnergyPlus Perez 1990 (Figure 5.1b)
- DOE-2.1E Perez 1990 (Figure 5.1c)
- IDA-ICE Perez 1990 (Figure 5.1d)

Each figure contains two plots; the plot on the left are measurements of the vertical solar irradiance on the outside facade compared with predicted results from the building energy simulation program and 95% credible limits from both the experiment and the MCA all averaged over each hour of the day for the duration of the experiment. The plot on the right contains maximum, minimum, and mean absolute differences between measured and predicted global vertical irradiances for a given hour over the entire experiment. The same type of plot was used for comparing cooling powers for solar gain experiments discussed in subsequent chapters.

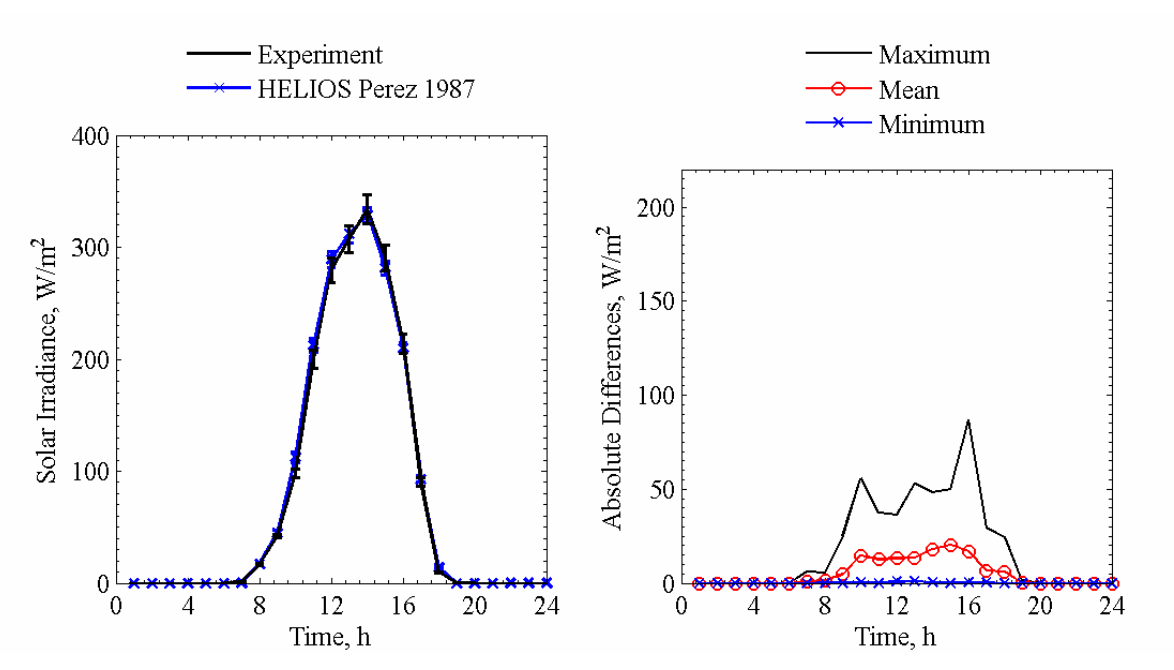


Figure 5.1a. Global vertical solar irradiance comparisons for HELIOS Perez 1987 averaged over each given hour of the day (left) and absolute maximum, mean, and minimum differences for a given hour of the day (right).

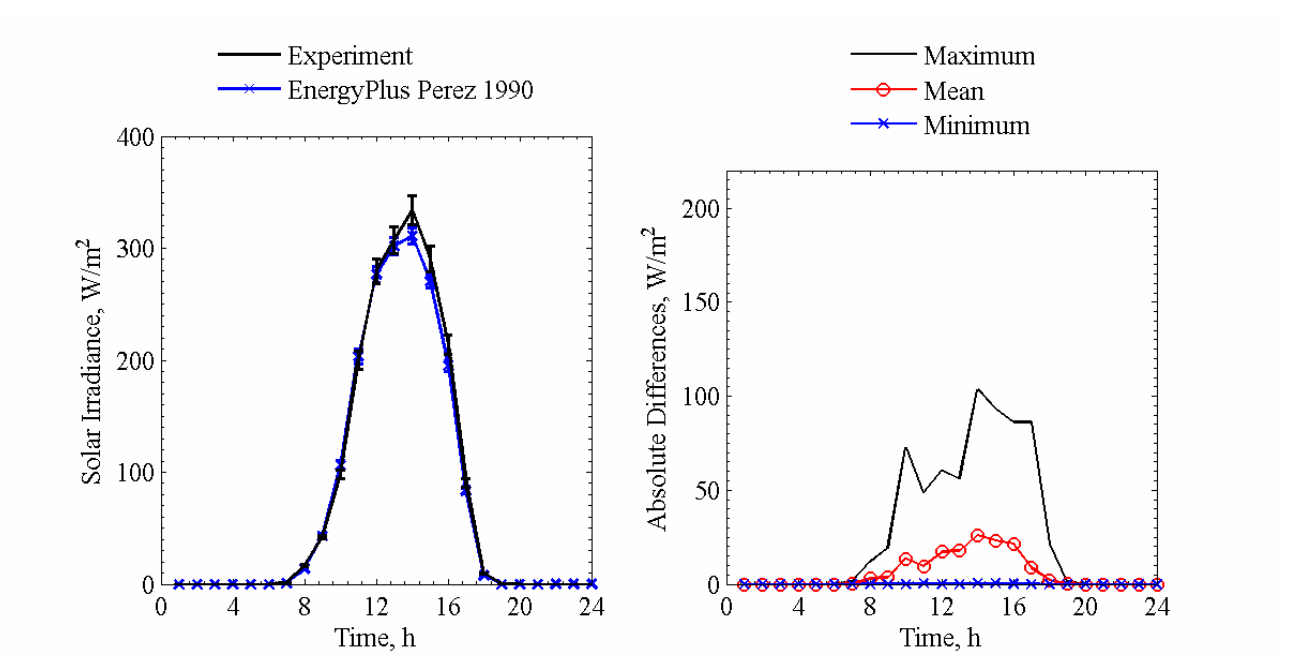


Figure 5.1b. Global vertical solar irradiance comparisons for EnergyPlus Perez 1990 averaged over each given hour of the day (left) and absolute maximum, mean, and minimum differences for a given hour of the day (right).

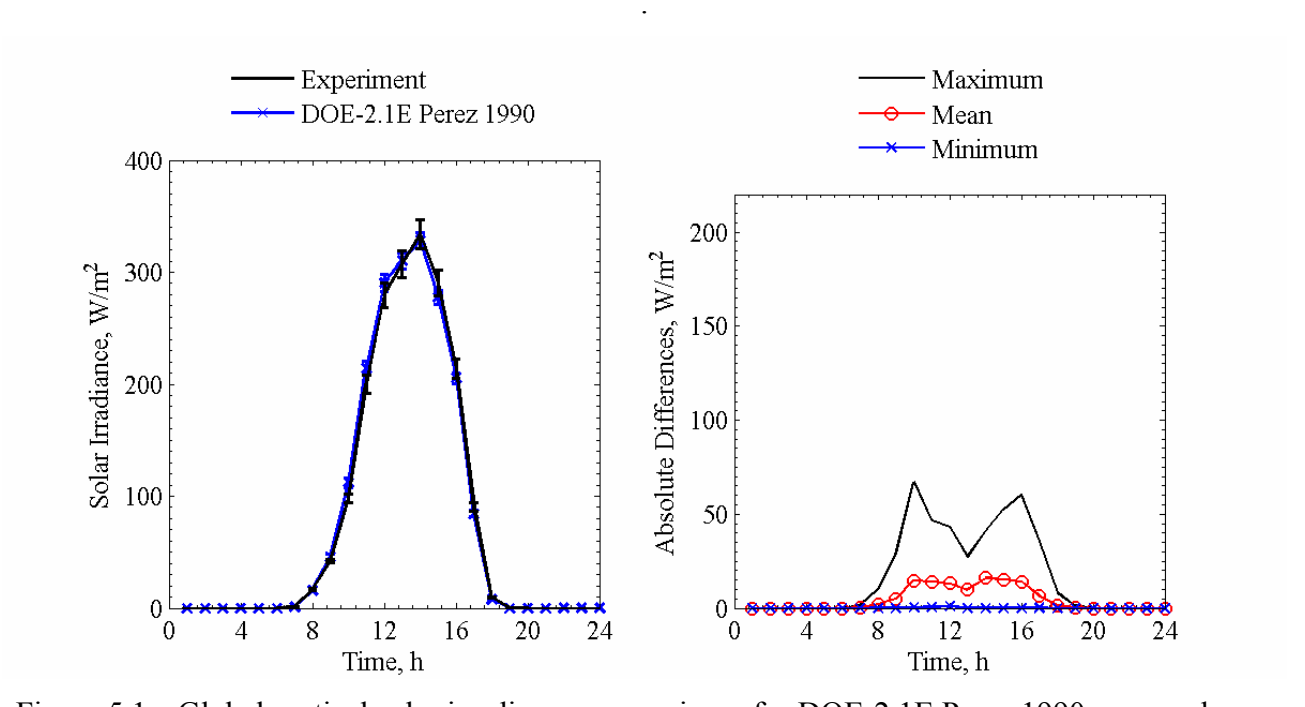


Figure 5.1c. Global vertical solar irradiance comparisons for DOE-2.1E Perez 1990 averaged over each given hour of the day (left) and absolute maximum, mean, and minimum differences for a given hour of the day (right).

21

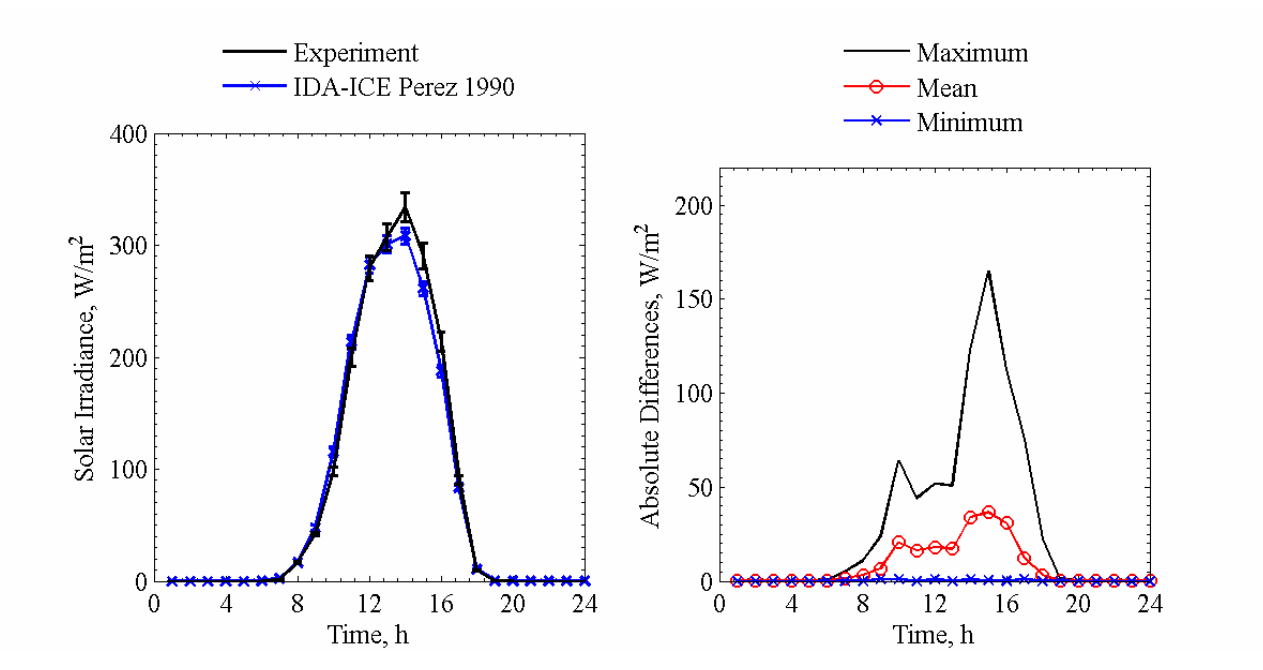


Figure 5.1d. Global vertical solar irradiance comparisons for IDA-ICE Perez 1990 averaged over each given hour of the day (left) and absolute maximum, mean, and minimum differences for a given hour of the day (right).

Table 5.1 contains overall, individual, and associated interactions from input uncertainties that impacted the global vertical solar irradiance predictions taken from the n-way factorial analysis. Statistical comparisons are contained in Table 5.2; the results were only analyzed when the solar altitude was greater than zero (when the sun was up).

Table 5.1. N-way factorial analyses to evaluate the sensitivities of outputs on input uncertainties.

Factorial analyses	Forward differencing W/m <sup>2</sup>	Backward differencing W/m²
Direct-normal solar irradiance	1.13	-1.10
Diffuse horizontal solar irradiance	1.37	-1.28
Ground reflectance	0.357	-0.357
Building azimuth	-0.499	0.500
Interactions between direct-normal and diffuse horizontal solar	-0.0560	-0.0831
irradiance		
Interaction between direct-normal solar irradiance and ground	0.00155	0.00158
reflectance		
Interaction between direct-normal solar irradiance and building	-0.00464	-0.00464
azimuth		
Interactions between diffuse horizontal solar irradiance and ground	0.00352	0.00380
reflectance		
Interactions between diffuse horizontal solar irradiance and building	-0.00267	-0.00264
azimuth		
Interactions between ground reflectance and building azimuth	No Interactions	No Interactions
Average overall uncertainty	2.40	2.40

Table 5.2. Statistical comparisons for Exercise 2.

	I	I			
Parameter	Experiment	HELIOS Perez 1990	EnergyPlus Perez 1990	DOE-2.1E Perez 1990	DA-ICE Perez 1990
$\overline{x}$	176.1 W/m <sup>2</sup>	179.2 W/m <sup>2</sup>	169.7 W/m <sup>2</sup>	177.2 W/m <sup>2</sup>	156.1 W/m <sup>2</sup>
S	$223.8 \text{ W/m}^2$	216.7 W/m <sup>2</sup>	$211.8 \text{ W/m}^2$	218.6 W/m <sup>2</sup>	190.2 W/m <sup>2</sup>
$x_{max}$	856.8 W/m <sup>2</sup>	812.0 W/m <sup>2</sup>	817.8 W/m <sup>2</sup>	820.4 W/m <sup>2</sup>	$743.5 \text{ W/m}^2$
	$0.2 \text{ W/m}^2$	$0.0 \text{ W/m}^2$	$0.3 \text{ W/m}^2$	$0.0 \text{ W/m}^2$	$0.4 \text{ W/m}^2$
$\frac{x_{min}}{\overline{D}}$	-	$-3.0 \text{ W/m}^2$	$6.4 \text{ W/m}^2$	$-1.1 \text{ W/m}^2$	$20.0 \text{ W/m}^2$
$ \overline{D} $	-	12.0 W/m <sup>2</sup>	$13.7 \text{ W/m}^2$	$10.5 \text{ W/m}^2$	26.0 W/m <sup>2</sup>
$/D_{max}/$	-	$87.0 \text{ W/m}^2$	$103.5 \text{ W/m}^2$	$67.1 \text{ W/m}^2$	$139.1 \text{ W/m}^2$
$ D_{min} $	-	$0.0 \text{ W/m}^2$	$0.0 \text{ W/m}^2$	$0.0 \text{ W/m}^2$	$0.0 \text{ W/m}^2$
$D_{rms}$	-	$18.7 \text{ W/m}^2$	$24.2 \text{ W/m}^2$	$17.0 \text{ W/m}^2$	$44.8 \text{ W/m}^2$
$/D/_{95\%}$	-	$44.8 \text{ W/m}^2$	$56.4 \text{ W/m}^2$	$40.3 \text{ W/m}^2$	$115.8 \text{ W/m}^2$
$\overline{OU}$	$6.9 \text{ W/m}^2$	-	$4.6 \text{ W/m}^2$	-	-
$\overline{UR}$	-	2.4	1.3	1.3	2.4
$UR_{max}$	-	71.3	12.4	20.4	17.0
$UR_{min}$	-	0.0	0.0	0.0	0.0
$ \overline{D} /\overline{x} \times 100\%$	-	6.8%	7.8%	5.9%	14.8%
$\overline{D}$ / $\overline{x} \times 100\%$	-	-1.7%	3.7%	-0.6%	11.3%

These results were used to identify the existing tilted surface radiation model that performed best in each building energy simulation program or to implement a different tilted radiation model into the code(s). This was also a vital step for identifying discrepancies in the solar gain experiments. In-depth analyses and discussion of these results is provided by Loutzenhiser et al. [2].

# **Chapter 6: Glazing Unit Only (Exercise 3)**

An experiment was performed in the test cell from October 2 to October 26, 2004 to evaluate the impact of solar gains through a glazing unit. Information about the glazing unit, thermophysical properties evaluated at mean envelope temperatures, the linear thermal transmittance of the glazing unit, and results are provided in subsequent sections.

#### **6.1. Description of the Experiment**

This section contains specific information about the experiment, including the following information:

- The mounting and properties of the glazing
- A two-dimensional steady-state heat transfer simulation and calorimetric measurements used to calculate the linear thermal transmittance of the mounting and spacer
- Thermophysical properties of the cell envelope

A photograph of the test cell taken during the experiment is shown in Figure 6.1.



Figure 6.1. A photograph of the test cell.

#### **6.1.1.** Glazing Unit Properties

The glazing unit for this experiment was mounted in the southwest exterior construction element of the test cell. The glazing properties from measured data are listed in Table 6.1. Measured optical properties for each glass pane as a function of wavelength from 250 nm to 2500 nm are contained in "Experiment 3.xls". Properties of the individual panes are described in Table 6.2. The integral inside and outside solar reflectances and solar transmittance were calculated according to European Standard EN 410 [7] in GLAD software [8]. The thermal transmittance due to the spacer and mounting was calculated from simulation and a calorimetric experiment described in a later section. For the individual panes of glass, the emittance was measured using an emissometer based on a calorimetric method. A dimensioned drawing of the exterior construction element as seen from this inside of the test cell showing the position of the glazing is presented in Figure 6.2. The dimensions in meters of the glazing in the figure correspond to the aperture height and width.

Table 6.1. Glazing unit properties.

Parameter	Quantity
Normal solar transmittance	42.9%
Normal solar exterior reflectance	25.2%
Normal solar interior reflectance	21.4%
Center-pane thermal transmittance	1.144 W/m <sup>2</sup> -K
Aperture glazing width	1.17 m
Aperture glazing height	1.42 m
Aperture glazing area	$1.66 \text{ m}^2$
Aperture perimeter length	5.18 m

Table 6.2a. Optical properties for the outer pane of glass (solar control Low-E).

Parameter	Quantity
Normal solar transmittance, %	50.9
Normal solar exterior reflectance, %	28.5
Normal solar interior reflectance, %	29.6
Outer emittance, %	89.4
Inner emittance, %	9.7

Table 6.2b. Optical properties for the inner pane of glass (clear float glass).

Parameter	Quantity
Normal solar transmittance, %	80.8
Normal solar exterior reflectance, %	7.6
Normal solar interior reflectance, %	7.6
Outer emittance, %	87.8
Inner emittance, %	88.7

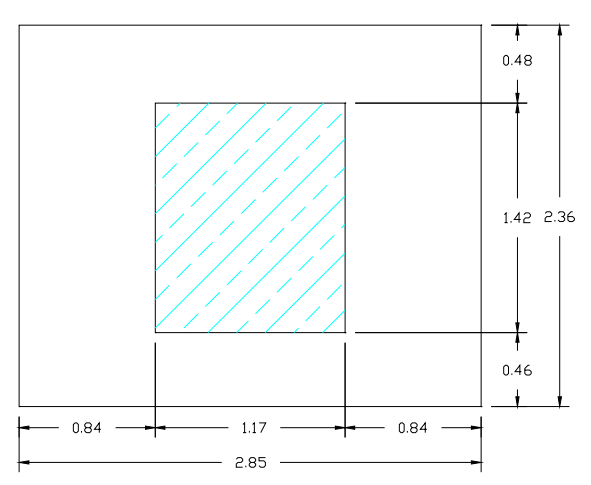


Figure 6.2. Position of the glazing in the exterior wall in meters seen from the inside of the test cell.

In addition to normal optical properties, angular dependent front reflectance, back reflectance, and transmittance were measured at various angles of incidents for the glazing unit from 300 nm to 1650 nm (properties from 1650 nm to 2500 nm were estimated using the value at 1650 nm) were measured at the University of Basel. The properties were integrated over the solar spectrum using European Standard EN 410 [7] in GLAD software [8] and are shown in Tables 6.3.

Table 6.3. Transmittance and as a function of incident angle.

Incident angle, °	0	15	30	45	50	55	60	65	67.5	70	72.5	75
Solar transmittance, %	42.1	41.7	40.9	38.9	37.6	35.8	33.2	29.5	27.2	24.6	21.6	18.4
Solar reflectance (front), %	-	26.7	26.6	27.6	28.4	30.0	32.3	35.9	38.5	41.6	45.0	49.4
Solar reflectance (back), %	-	24.6	24.7	26.2	27.3	29.3	32.2	36.7	39.7	43.4	47.4	52.6

#### 6.1.2. Linear Thermal Transmittance

The impact of the window spacer and construction used to mount the glazing in the test cell was simulated using a two-dimensional steady-state heat transfer software package called BISCO [13]. To simulate the aluminum spacer, a dimensioned cross-section provided by the manufacturer was used. Figure 6.3 shows a dimensioned drawing in millimeters of the spacer, the mounting construction and a portion of the exterior window and wall. BISCO simulation results coupled with calorimetric measurements [14] were used to quantify the impact of the spacer and the frame. From these calculations, the linear thermal transmittance was then computed.

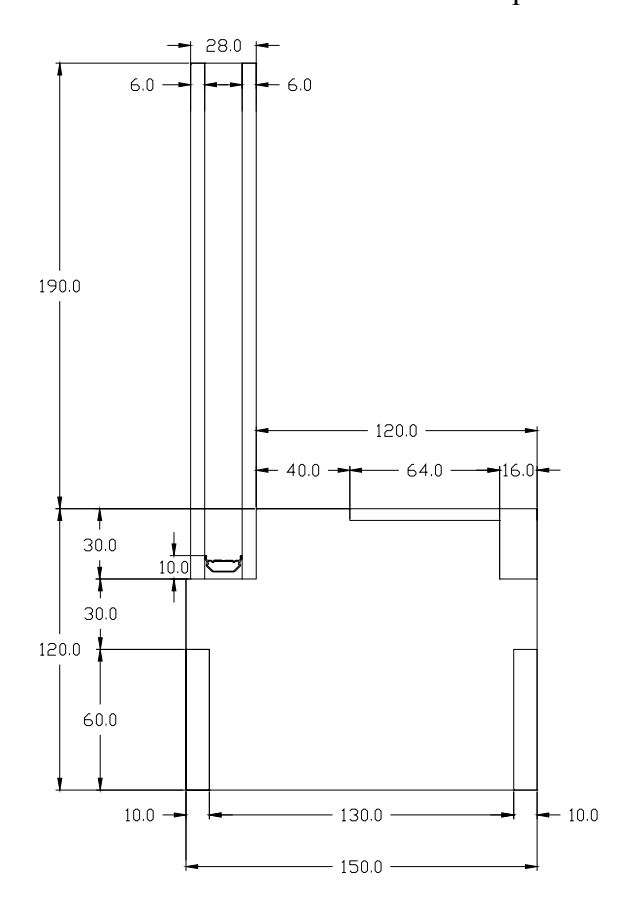


Figure 6.3. Dimensioned drawing of the spacer and frame in millimeters.

The thermal conductivities of the construction materials were required to perform the simulation. These properties were taken from literature, calculation, and in-house measurements. For temperature-dependent properties, the thermal conductivity was evaluated at a mean envelope temperature of 10°C. Table 6.4 provides a list of the quantities and color-coding of the materials and their respective thermal conductivities. An iterative procedure using the simulation results and the calorimetric measurements was employed to calculate the equivalent thermal conductivity for the argon cavity space—which factored in the impact of conduction, radiation, and convection. The

procedure simulated the spacer, calculated the linear thermal transmittance, and then recalculated a center-pane thermal transmittance.

Table 6.4. List of materials and their respective thermal conductivities.

Material	Thermal conductivity, W/m-K	Color-coding
Desiccant	0.130	
Aluminum	220.0	
Polyisobutylene	0.220	
Polysulfid	0.400	
Argon 90%/air 10%	0.02313	
Glass	1.0	
Plywood	0.1381	
Wood	0.110	
EPS Foam	0.03483	

The specified properties for the boundary conditions included the temperature and the heat transfer coefficients for the outside and inside of the frame; these values were taken from prEN ISO 10077-2 [6]. These results, as well as the color-codings, are presented in Table 6.5.

Table 6.5. Boundary condition properties.

Boundary condition	Temperature, °C	Heat transfer coefficient, W/m²-K	Color-coding
Inside air	20	7.7	
Outside air	0	25.0	

The bitmap of the cross-section of the glazing unit, spacer, and mounting used for the BISCO simulation of the frame and glazing construction and the spacer are shown in Figures 6.4a and 6.4b.

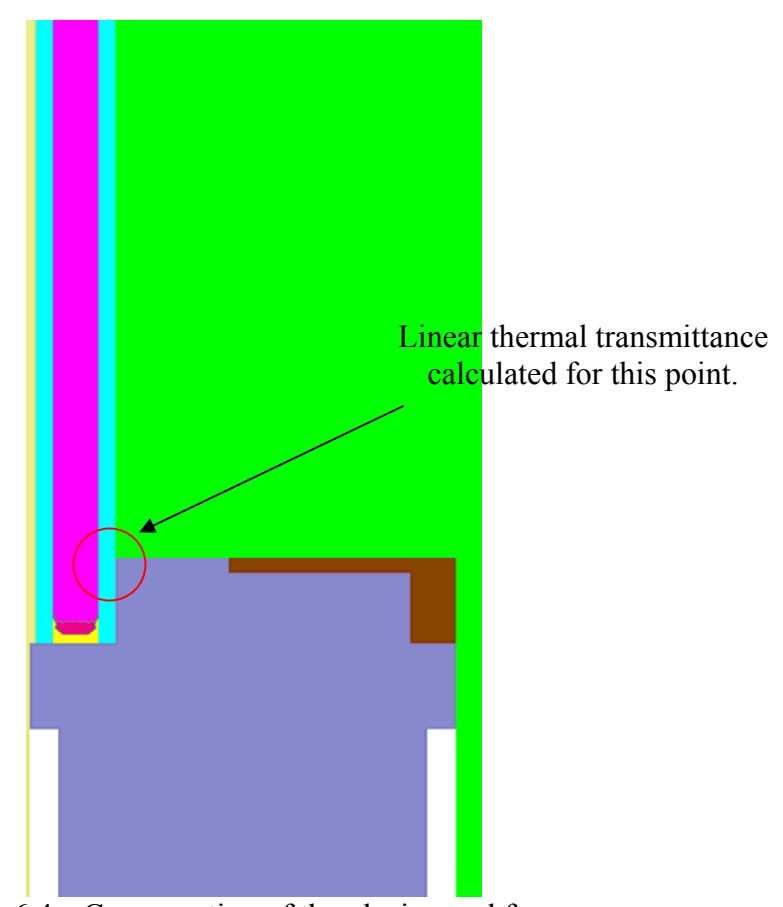


Figure 6.4a. Cross-section of the glazing and frame.

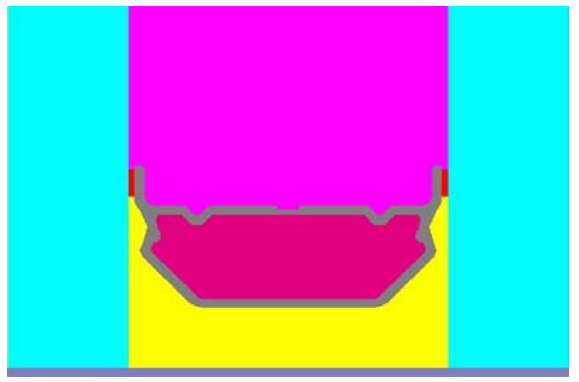


Figure 6.4b. Cross-section of the aluminum spacer.

For the BISCO simulation, the bitmap was divided up into 243,205 nodes and the heat transfer through the element was calculated as 6.72 W/m. Isotherm and heat flow line illustrations are shown in Figures 6.5a and 6.5b, respectively, to help visualize the two-dimensional heat flow path.

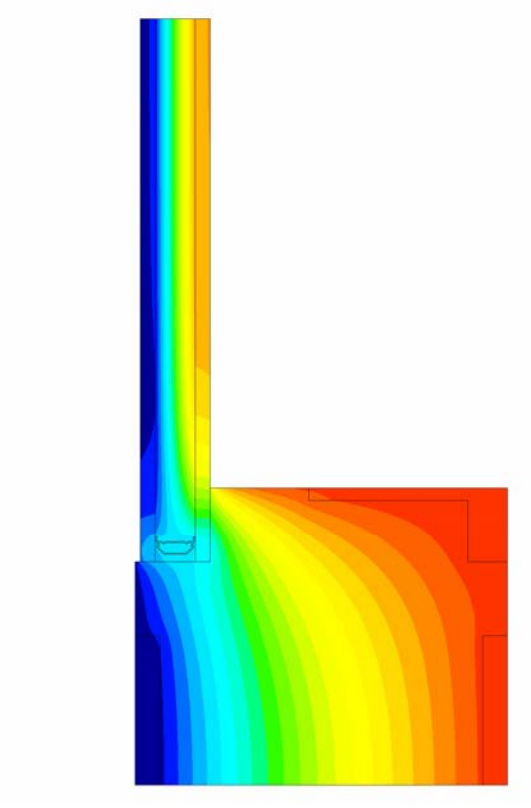


Figure 6.5a. Isotherm illustration from the BISCO simulation.

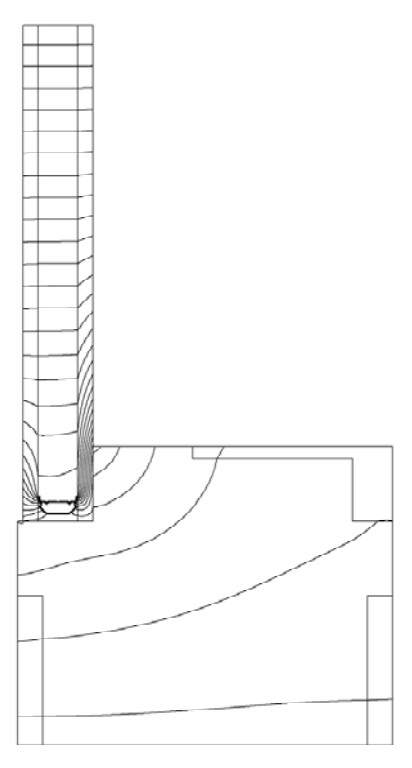


Figure 6.5b. Heat flow line illustration from the BISCO simulation.

One-dimensional heat transfer was calculated using Equation 6.1. A list of the additional parameters used for this calculation is shown in Table 6.6.

$$Q'_{I-D} = \left\{ L_{g}U_{g} + \frac{L_{w}}{\left(\frac{1}{h_{i}} + \frac{2d_{ply}}{\lambda_{ply}} + \frac{d_{eps}}{\lambda_{eps}} + \frac{1}{h_{o}}\right)} \right\} (\theta_{i} - \theta_{o})$$
(6.1)

where

 $L_g$  is the length of the glazing used from the simulation,

 $U_g$  is the center pane thermal transmittance of the glazing,

 $L_w$  is the length of the wall from the simulation,

 $h_i$  is the inside heat transfer coefficient,

 $d_{ply}$  is the width of the plywood,

 $\lambda_{ply}$  is the thermal conductivity of the plywood,

 $d_{eps}$  is the width of the eps foam,

 $\lambda_{eps}$  is the thermal conductivity of the eps foam,

 $h_o$  is the outside heat transfer coefficient,

 $\theta_l$  is the inside temperature, and

 $\theta_o$  is the outside temperature.

Table 6.6. Values of the variables used for the 1-D heat transfer calculation.

Parameter	Quantity
$L_{g}$	0.190 m
$U_{g}$	$1.144 \text{ W/m}^2\text{-K}$
$L_w$	0.120 m
$d_{ply}$	0.01 m
$d_{eps}$	0.130 m

Using the simulation conditions, the one-dimensional heat transfer was calculated to be 4.94 W/m. The linear thermal transmittance,  $\psi$ , was calculated using Equation 6.2 to be 0.08899 W/m-K.

$$\psi = \frac{Q_{BISCO}^{'} - Q_{1-D}^{'}}{\theta_i - \theta_o} \tag{6.2}$$

where

 $Q_{BISCO}$  is the heat transfer from the BISCO simulation.

#### 6.1.3. Thermophysical Properties of the Test Cell Envelope

The mean envelope temperatures of the construction elements are shown in Table 6.7. The thermophysical properties fixed at these mean envelope temperatures are contained in Tables 6.8a to 6.8c.

Table 6.7. Mean envelope temperatures for experiment.

Construction element	Mean temperature, °C
Ceiling, east, west, and north walls	22.78
Floor	22.72
South wall	17.49

Table 6.8a. Ceiling, north, east and west wall construction evaluated at 22.78°C.

Layer	Material	Thickness Thermal conductivity		Density	Specific heat
number		mm	W/m-K	kg/m <sup>3</sup>	J/kg-K
1	Sheet steel	0.7	53.62	7837	460.8
2	PU foam	139	0.02233	30	1800
3	Sheet steel	0.7	53.62	7837	460.8

Table 6.8b. Floor construction evaluated at 22.72°C.

Layer	Material	Thickness	Thermal conductivity	Density	Specific heat
number		mm	W/m-K	kg/m <sup>3</sup>	J/kg-K
1	Sheet steel	0.7	53.62	7837	460.8
2	PU foam	140	0.02232	30	1800
3	PU foam (higher density)	20	0.070	45	1800
4	Sheet steel with surface	2.5	53.62	7837	460.8
	structure				

Table 6.8c. South wall construction evaluated at 17.49°C.

Layer number	Material	Thickness mm	Thermal conductivity W/m-K	Density kg/m <sup>3</sup>	Specific heat J/kg-K
1	Plywood	10	0.1394	850	1605
2	EPS foam	130	0.03578	28	1460
3	Plywood	10	0.1394	850	1605

## 6.2. Results

The empirical validation for this exercise focused on comparing cooling power. Plots for cooling power from HELIOS, EnergyPlus, DOE-2.1E, IDA-PAR, IDA-SIA, and IDA-Detwind are shown in Figures 6.6a to 6.6f, respectively. Table 6.9 contains overall and 10 most influential input uncertainties that impacted the cooling power predictions taken from the n-way factorial analysis. A summary of the statistical comparisons is contained in Table 6.10.

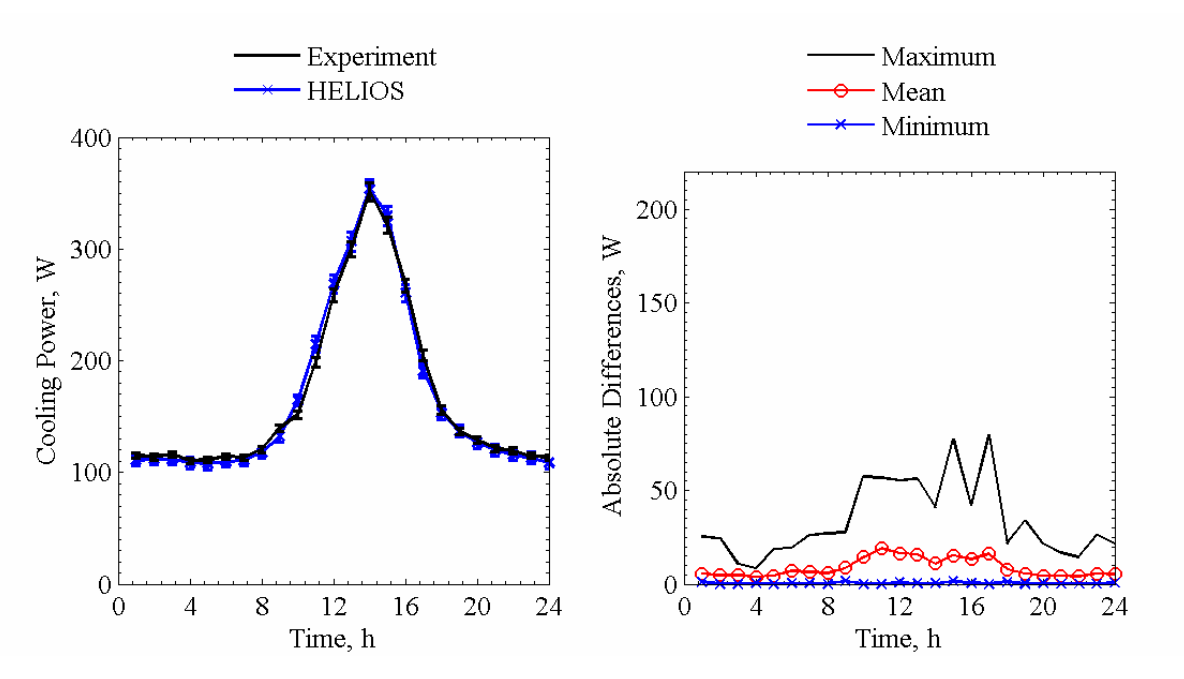


Figure 6.6a. Cooling power comparisons for HELIOS averaged over each given hour of the day (left) and absolute maximum, mean, and minimum differences for a given hour of the day (right).

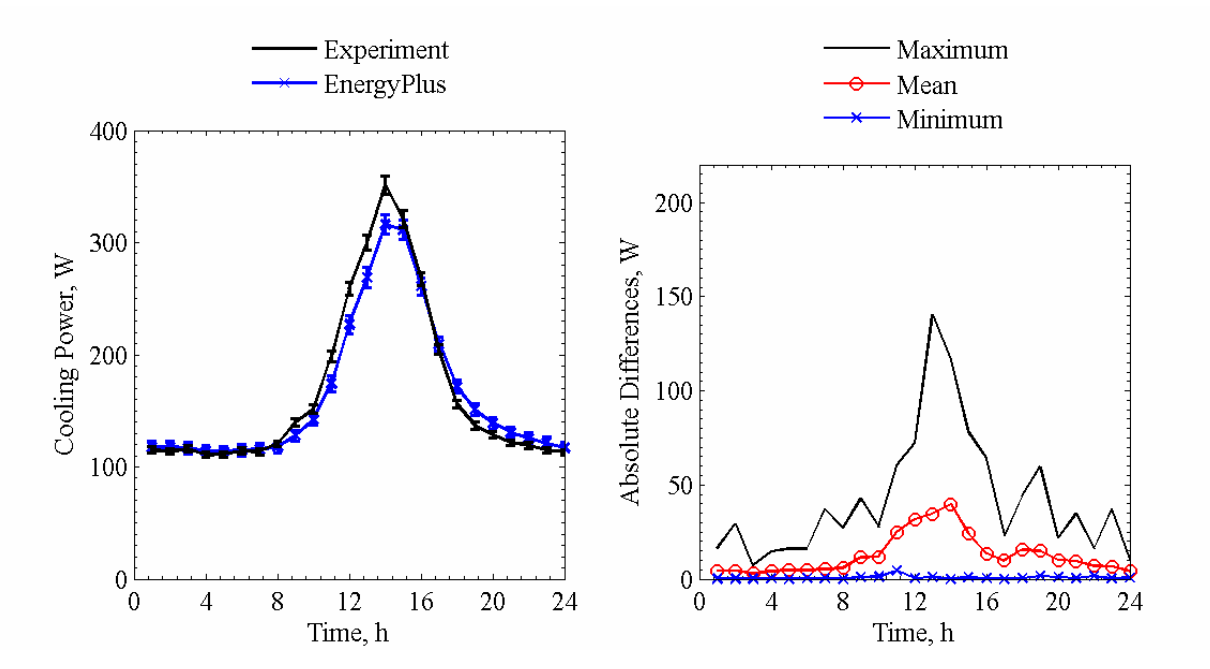


Figure 6.6b. Cooling power comparisons for EnergyPlus averaged over each given hour of the day (left) and absolute maximum, mean, and minimum differences for a given hour of the day (right).

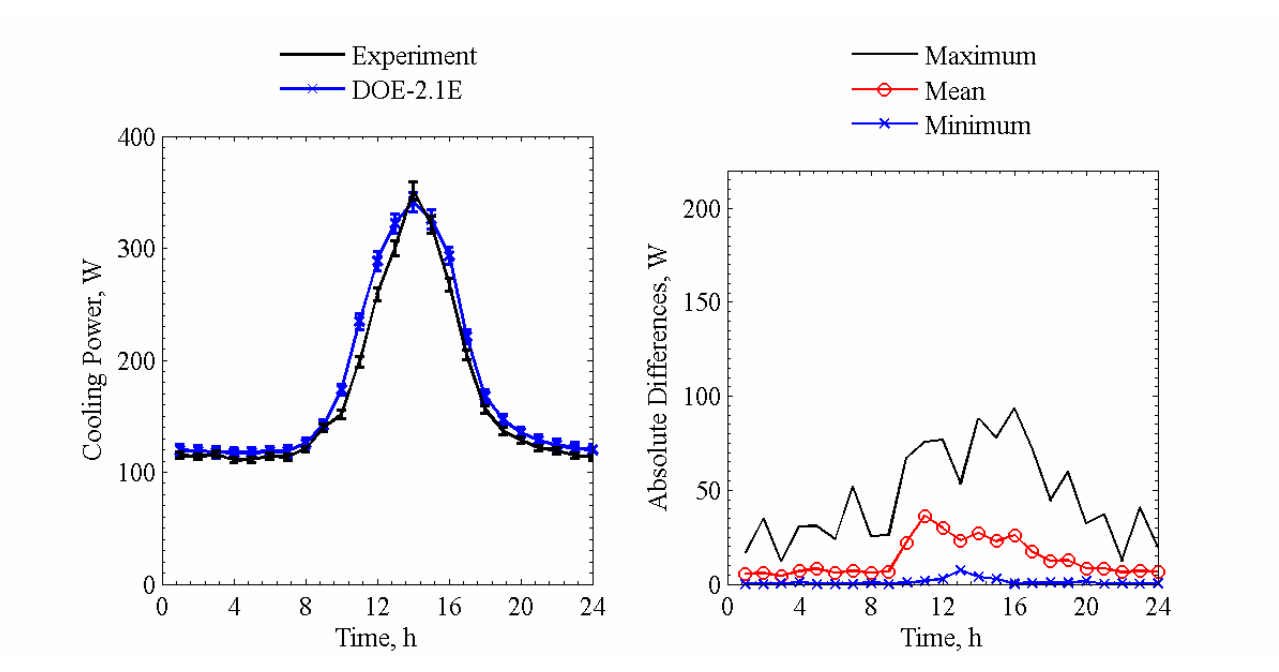


Figure 6.6c. Cooling power comparisons for DOE-2.1E averaged over each given hour of the day (left) and absolute maximum, mean, and minimum differences for a given hour of the day (right).

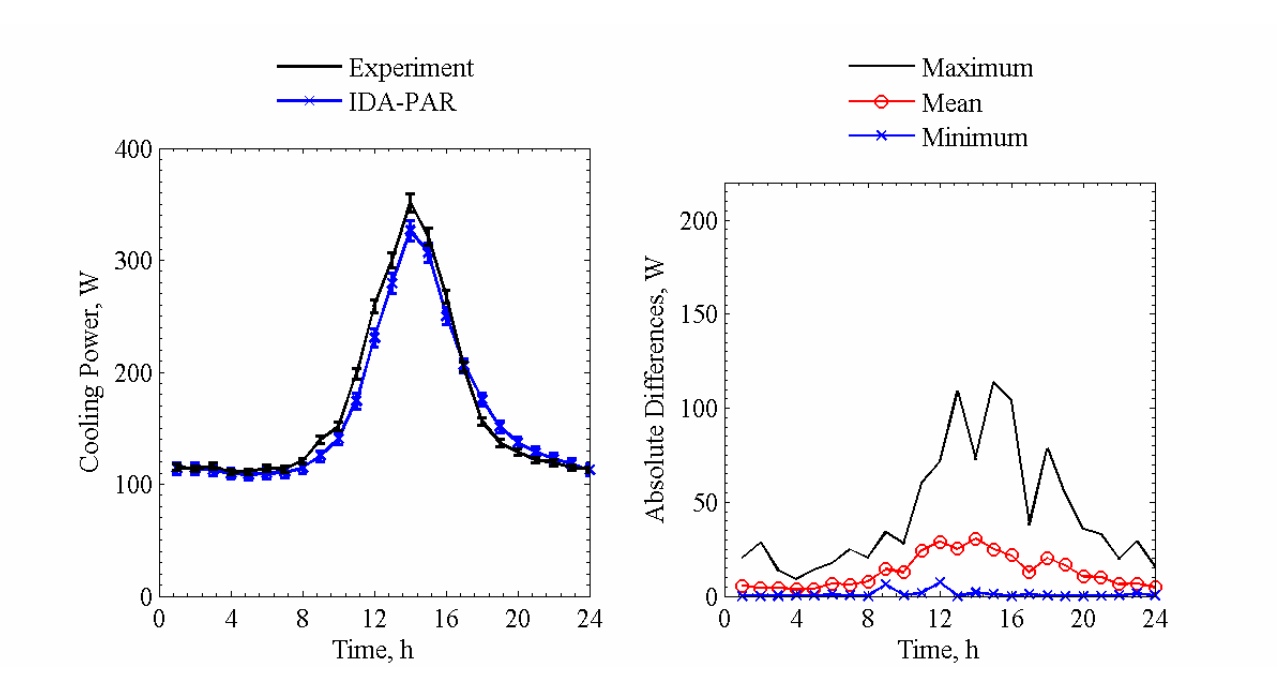


Figure 6.6d. Cooling power comparisons for IDA-PAR averaged over each given hour of the day (left) and absolute maximum, mean, and minimum differences for a given hour of the day (right).

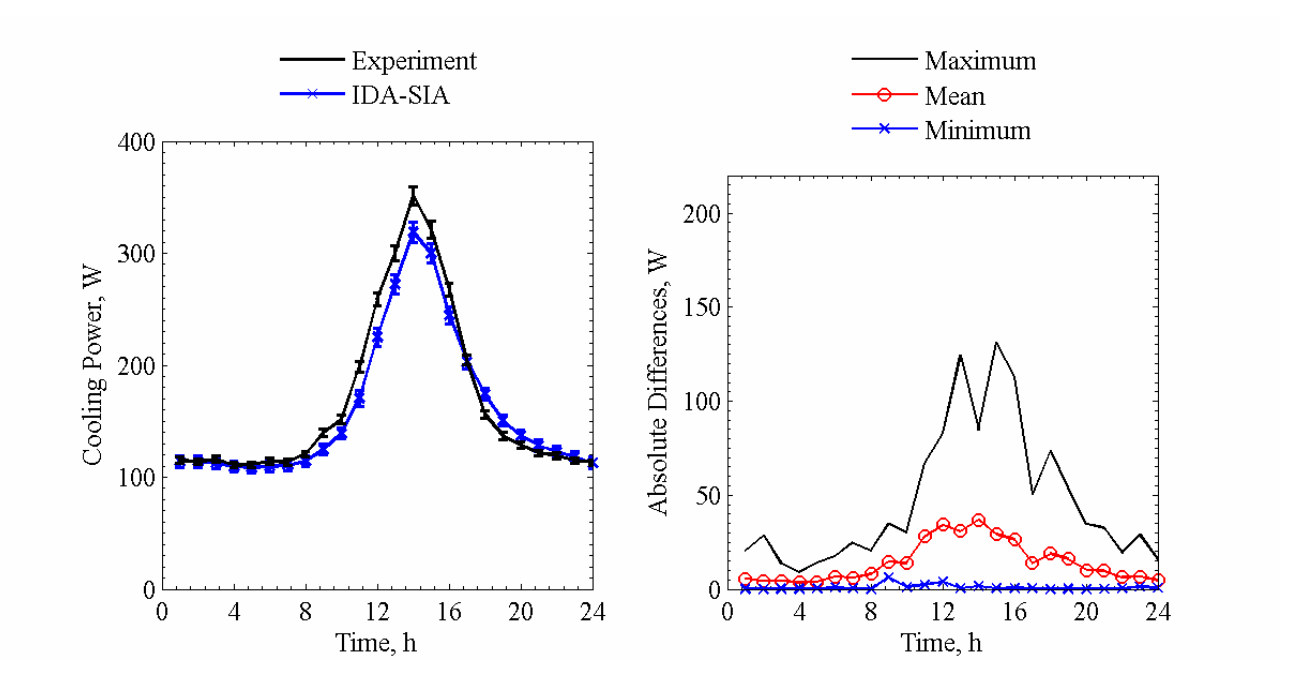


Figure 6.6e. Cooling power comparisons for IDA-SIA averaged over each given hour of the day (left) and absolute maximum, mean, and minimum differences for a given hour of the day (right).

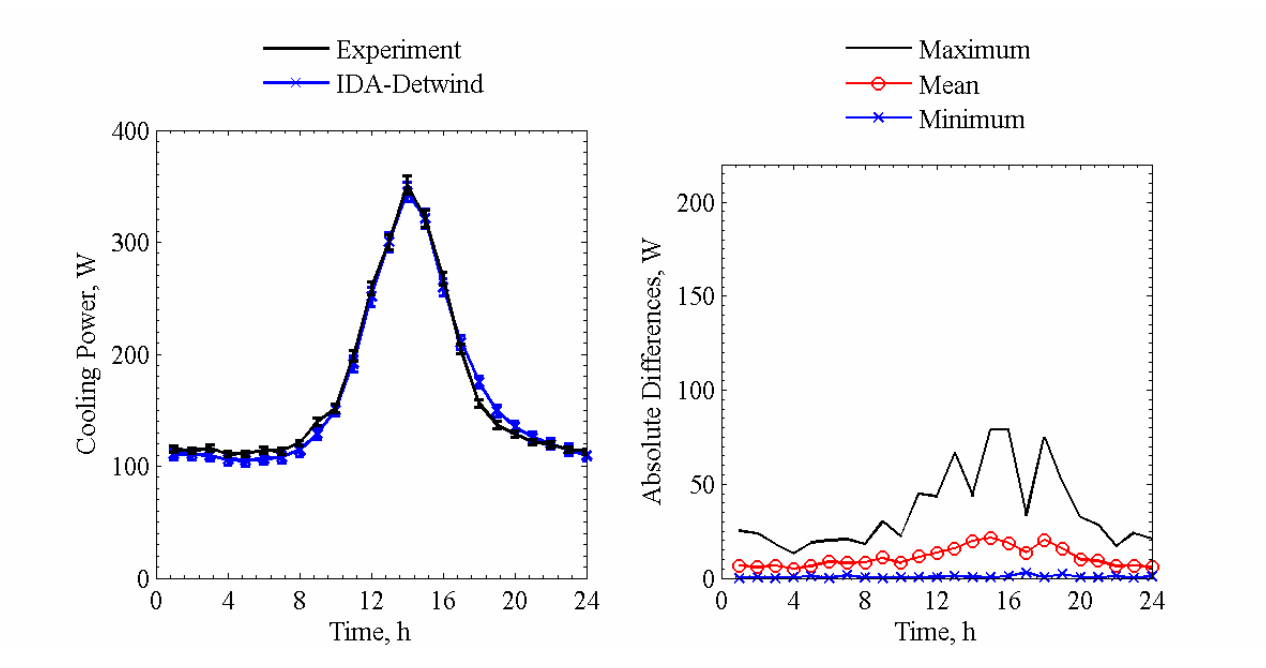


Figure 6.6f. Cooling power comparisons for IDA-Detwind averaged over each given hour of the day (left) and absolute maximum, mean, and minimum differences for a given hour of the day (right).

Table 6.9. Overall uncertainty and 10 most influential input parameters from the n-way factorial analyses in Watts.

Parameter	Forward	Backward
Overall uncertainty	3.08	3.06
Average inside air temperature	-1.82	1.82
Floor surface temperature	0.92	-0.92
Fan power	0.92	-0.92
Outside air temperature	0.82	-0.82
Ceiling surface temperature	0.73	-0.73
North wall surface temperature	0.52	-0.52
East wall surface temperature	0.46	-0.46
Outer pane transmittance	0.39	-0.39
Diffuse irradiance	0.39	-0.36
West wall surface temperature	0.38	-0.38

Table 6.10. Statistical comparisons for cooling power in Exercise 3.

	1	ilisticai co	1119 41110 0110	101 00011117	5 P 0 11 <b>0</b> 1 11	1	
Parameter	Experiment	HELIOS	EnergyPlus	DOE-2.1E	IDA-PAR	IDA-SIA	IDA-Detwind
$\overline{x}$	166.6 W	166.0 W	163.4 W	176.6 W	161.6 W	159.8 W	164.9 W
S	116.1 W	119.3 W	101.5 W	117.7 W	105.4 W	101.4 W	112.3 W
$x_{max}$	847.9 W	845.5 W	767.5 W	780.0 W	816.8 W	792.8 W	829.1 W
$x_{min}$	54.1 W	67.8 W	83.5 W	106.0 W	73.9 W	73.8 W	68.8 W
$\overline{D}$	-	0.7 W	3.2 W	-10.0 W	5.0 W	6.8 W	1.7 W
$ \overline{D} $	-	8.7 W	12.8 W	13.5 W	13.1 W	14.3 W	11.0 W
$ D_{max} $	-	79.6 W	140.5 W	93.6 W	114.0 W	131.4 W	79.0 W
$/D_{min}/$	-	0.0 W	0.1 W	0.0 W	0.0 W	0.0 W	0.1 W
$D_{rms}$	-	14.3 W	22.2 W	21.6 W	21.0 W	23.9 W	16.0 W
$/D/_{95\%}$	-	33.0 W	52.3 W	54.6 W	47.2 W	56.5 W	37.1 W
$\overline{OU}$	3.8 W	-	5.9 W	-	-	-	-
$\overline{UR}$	-	0.8	1.1	1.3	1.2	1.3	1.1
$UR_{max}$	-	6.1	9.3	9.3	8.5	8.4	8.0
$UR_{min}$	-	0.0	0.0	0.0	0.0	0.0	0.0
$ \overline{D} /\overline{x} \times 100\%$	-	5.2%	7.7%	8.1%	7.8%	8.6%	6.6%
$\overline{D}/\overline{x} \times 100\%$	-	0.4%	1.9%	-6.0%	3.0%	4.1%	1.0%

Program-to-program comparisons were also used to try to diagnose differences between the programs. One of these parameters useful in assessing solar gain models is the transmitted solar power through the glazing unit. Figure 6.7 contains a plot of the transmitted solar power averaged over each given hour of the day through the glazing unit for all programs.

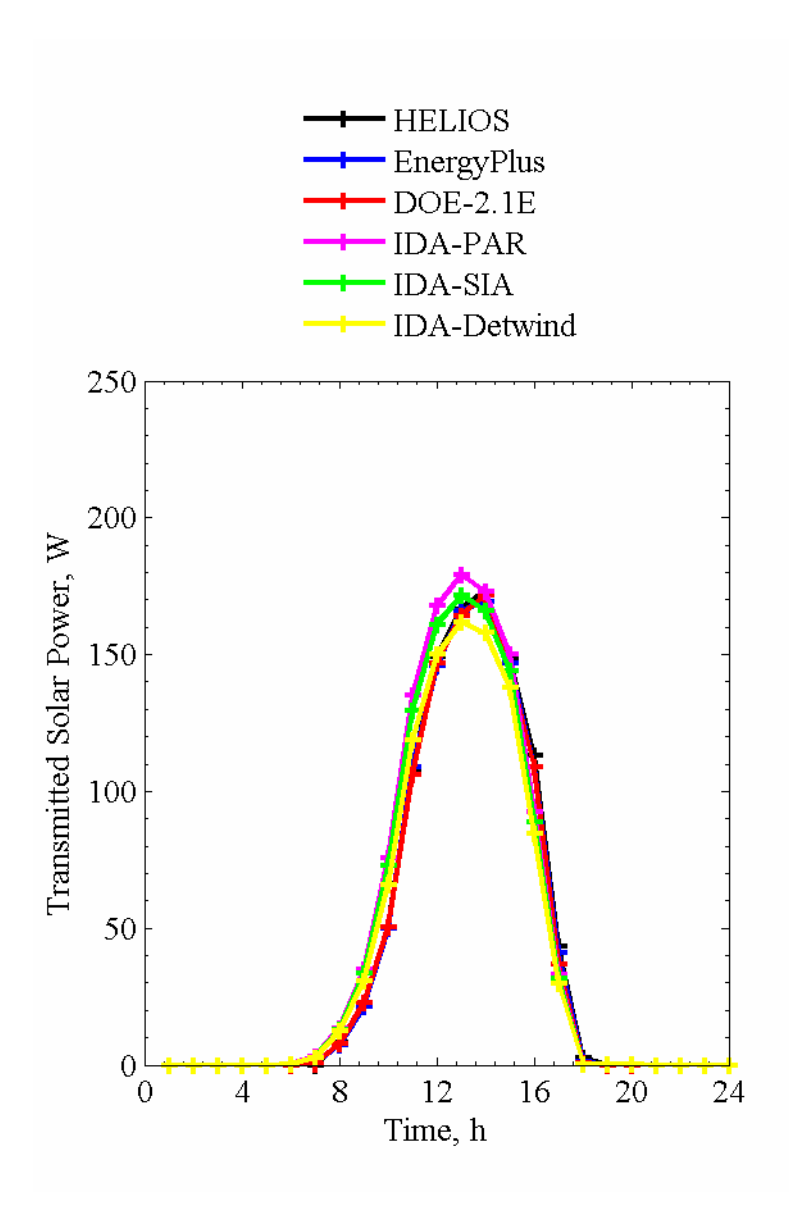


Figure 6.7. Transmitted solar power averaged over each given hour of the day.

Small differences were seen in the transmitted solar power which indicated that the window models were very similar. Therefore, many of the discrepancies in the predicted cooling powers from each simulation are a result of variations in internal and external heat transfer from convection and long-wave radiation and the modeling of internal short-wave radiation. In-depth analyses and discussion of these results is provided by Loutzenhiser et al. [15].

# **Chapter 7: Glazing Unit with Exterior Shading Screen (Exercise 4)**

An experiment designed to evaluate the impact of solar gains through a glazing unit with a diffuse exterior shading screen was run in the test cell from March 23 to April 16, 2005. Information concerning the properties and mounting of the exterior shading screen is provided.

### 7.1. Description of the Experiment

This section contains specific information about the experiment including the following information:

- Geometry and optical properties of the exterior shading screen
- Thermophysical properties of test cell envelope

### 7.1.1. Geometry and Optical Properties of the Exterior Shade Screen

For this experiment, an exterior shading screen was installed 10 cm from the glazing and is pictured in Figure 7.1. The shade was mounted to allow air to flow between gap of the external shade and the glazing; a dimensioned drawing of the shade position relative to the glazing is shown in Figure 7.2.



Figure 7.1. Photograph of the exterior shade mounted on the test cell.

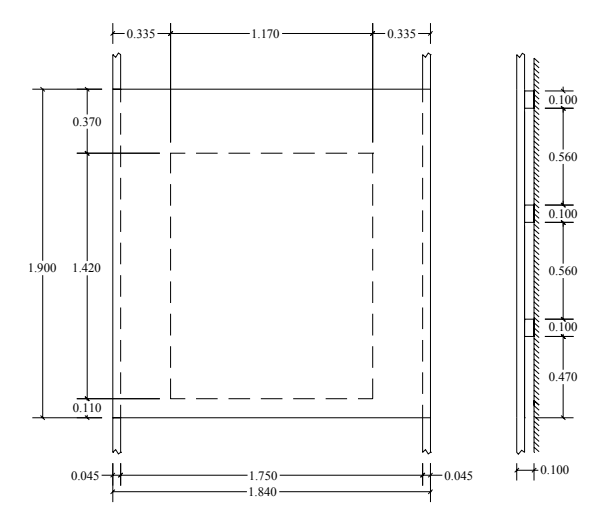


Figure 7.2. Dimensioned drawing of the external shade in meters relative to the glazing unit.

The optical properties of the shading screen were measured at normal incident angles using a spectrometer. The transmittance and reflectance as a function of wavelength from 250 nm to 2500 nm are contained in "Experiment 4.xls". The optical properties integrated over the solar spectrum for the shading screen were computed according to European Standard EN 410 [7] using GLAD software [8] and are shown in Table 7.1.

Table 7.1. Optical properties of the exterior shade.

Property	Quantity
Normal solar transmittance, %	21.5
Normal solar reflectance, %	59.6

### 7.1.2. Thermophysical Properties of the Test Cell Envelope

The mean envelope temperatures of the construction elements are shown in Table 7.2. The thermophysical properties fixed at these mean envelope temperatures are contained in Tables 7.3a to 7.3c.

Table 7.2. Mean envelope temperatures for experiment.

Construction element	Mean temperature, °C
Ceiling, east, west, and north walls	22.58
Floor	22.34
South wall	16.34

Table 7.3a. Ceiling, north, east and west wall construction evaluated at 22.58°C.

Layer number	Material	Thickness mm	Thermal conductivity W/m-K	Density kg/m <sup>3</sup>	Specific heat J/kg-K
1	Sheet steel	0.7	53.62	7837	460.8
2	PU foam	139	0.02230	30	1800
3	Sheet steel	0.7	53.62	7837	460.8

Table 7.3b. Floor construction evaluated at 22.34°C.

Layer	Material	Thickness	Thermal conductivity	Density	Specific heat
number		mm	W/m-K	kg/m <sup>3</sup>	J/kg-K
1	Sheet steel	0.7	53.62	7837	460.8
2	PU foam	140	0.02227	30	1800
3	PU foam (higher density)	20	0.070	45	1800
4	Sheet steel with surface structure	2.5	53.62	7837	460.8

Table 7.3c. South wall construction evaluated at 16.34°C.

Layer number	Material	Thickness mm	Thermal conductivity W/m-K	Density kg/m³	Specific heat J/kg-K
1	Plywood	10	0.1384	850	1605
2	EPS foam	130	0.03564	28	1460
3	Plywood	10	0.1384	850	1605

#### 7.2. Results

The empirical validation for this exercise focused on comparing cooling power. Plots for cooling power from HELIOS, EnergyPlus, DOE-2.1E, and IDA-SIA are shown in Figures 7.3a to 7.3d, respectively. Two plots are contained in each figure. Table 7.4 contains the overall and 10 most influential input uncertainties that impacted the cooling power predictions taken from the n-way factorial analysis. A summary of the statistical comparisons is contained in Table 7.5.

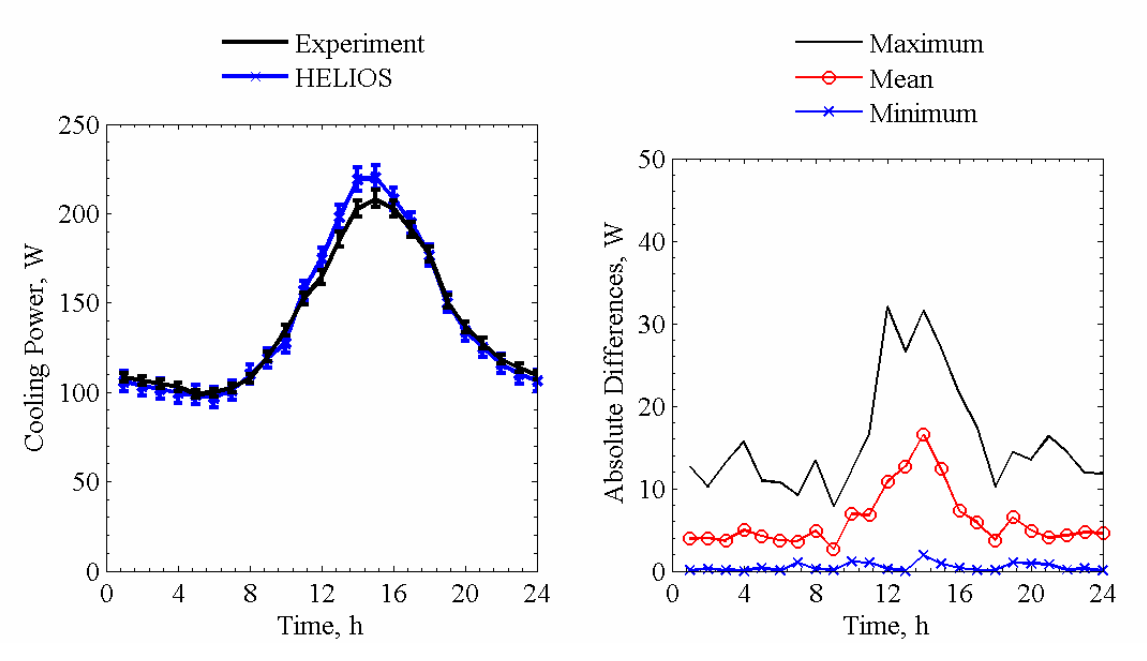


Figure 7.3a. Cooling power comparisons for HELIOS averaged over each given hour of the day (left) and absolute maximum, mean, and minimum differences for a given hour of the day (right).

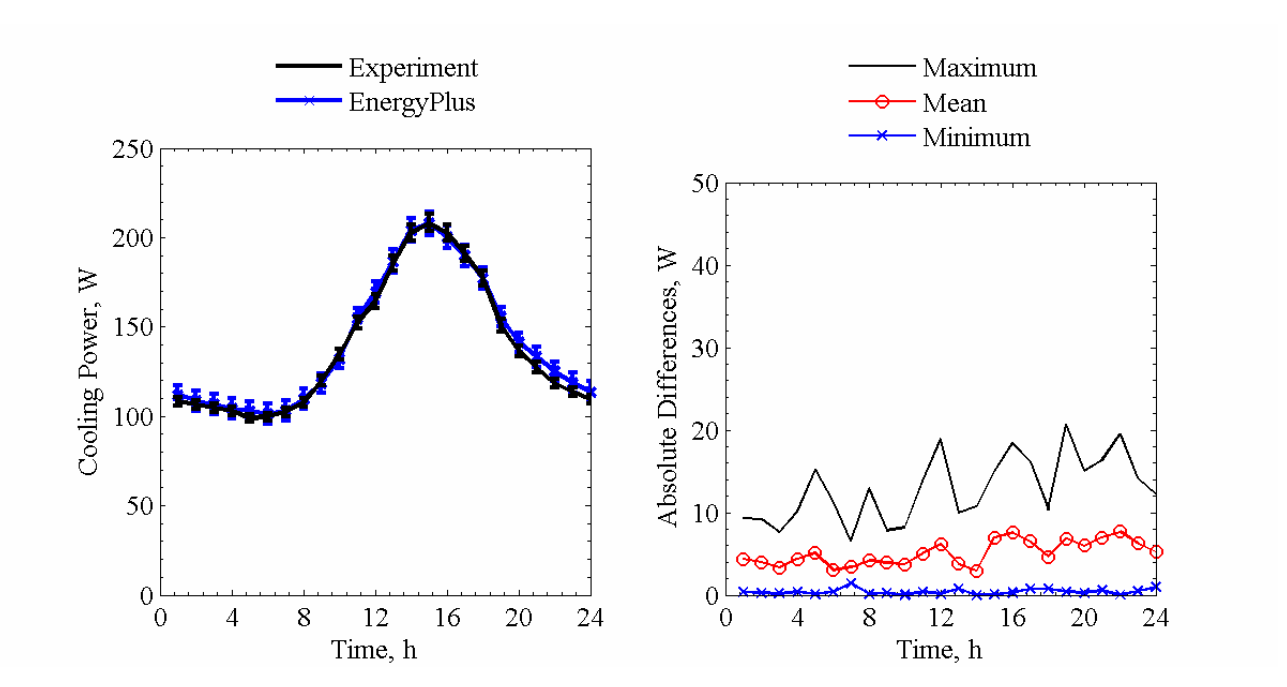


Figure 7.3b. Cooling power comparisons for EnergyPlus averaged over each given hour of the day (left) and absolute maximum, mean, and minimum differences for a given hour of the day (right).

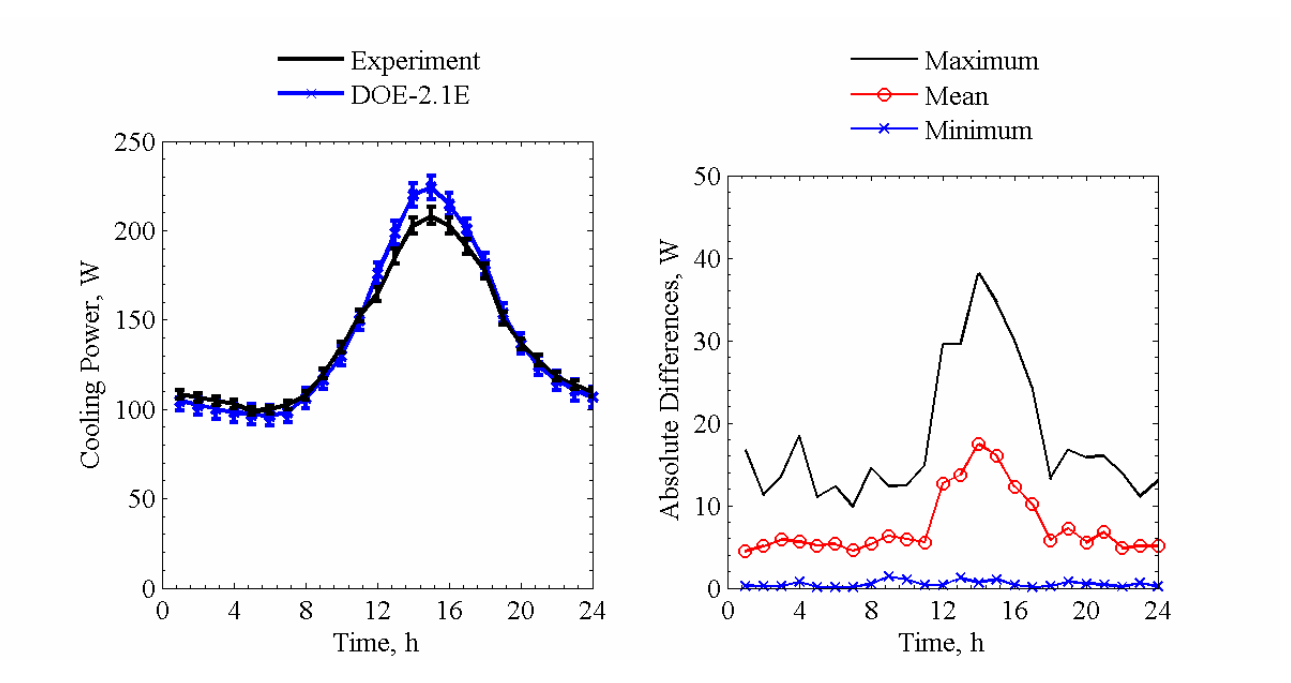


Figure 7.3c. Cooling power comparisons for DOE-2.1E averaged over each given hour of the day (left) and absolute maximum, mean, and minimum differences for a given hour of the day (right).

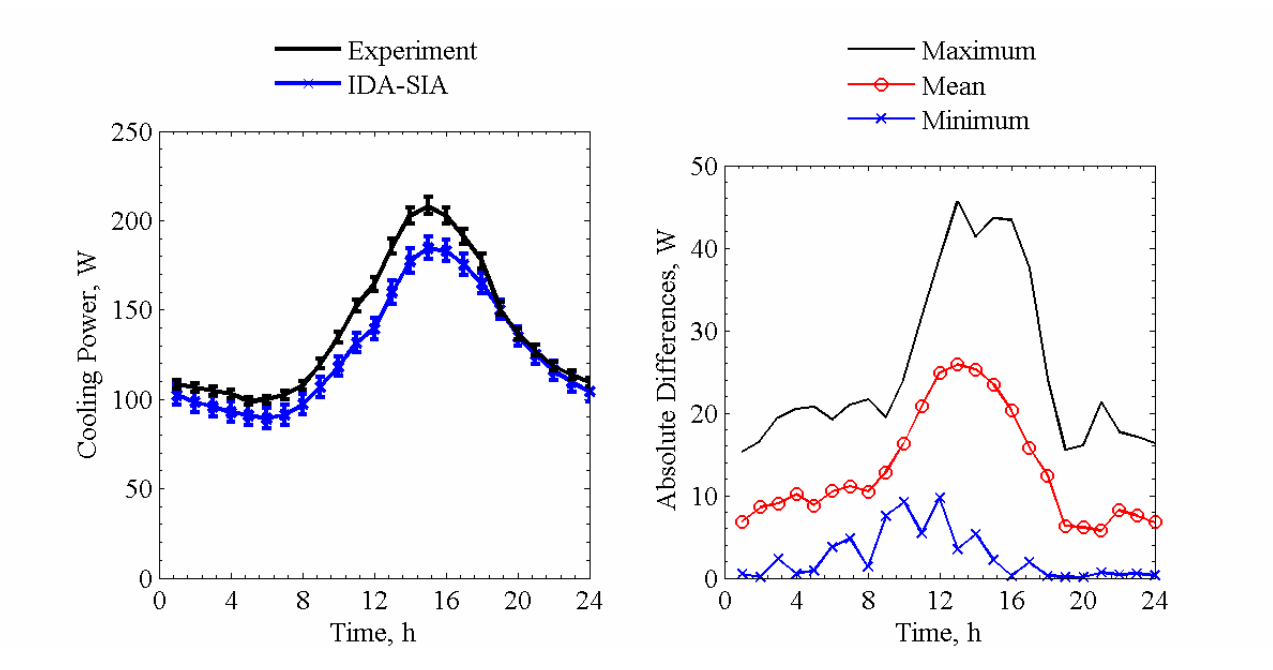


Figure 7.3d. Cooling power comparisons for IDA-SIA averaged over each given hour of the day (left) and absolute maximum, mean, and minimum differences for a given hour of the day (right).

Table 7.4. Overall uncertainty and 10 most influential input parameters from the n-way factorial analyses in Watts.

Parameter	Forward	Backward
Overall uncertainty	3.04	3.04
Average room air temperature	-1.83	1.83
Floor surface temperature	1.29	-1.30
Ceiling surface temperature	1.02	-1.02
Fan power	0.91	-0.91
Outside air temperature	0.89	-0.89
East wall surface temperature	0.68	-0.68
North wall surface temperature	0.50	-0.50
West wall surface temperature	0.37	-0.37
Transmittance of the outer glazing	0.18	-0.19
Diffuse horizontal solar irradiance	0.17	-0.18

Table 7.5. Statistical comparisons for cooling power in Exercise 4.

Parameter	Experiment	HELIOS	EnergyPlus	DOE-2.1E	IDA-SIA
$\overline{x}$	138.6 W	139.7 W	140.7 W	140.1 W	126.6 W
S	50.4 W	55.4 W	48.1 W	57.1 W	44.4 W
$x_{max}$	317.4 W	332.6 W	303.4 W	337.0 W	277.4 W
$x_{min}$	73.2 W	78.2 W	84.5 W	83.0 W	65.1 W
$\overline{D}$	-	-1.2 W	-2.1 W	-1.6 W	11.9 W
$ \overline{D} $	-	6.2 W	5.1 W	7.6 W	13.1 W
$/D_{max}/$	-	32.0 W	20.7 W	38.1 W	45.6 W
$/D_{min}/$	-	0.0 W	0.0 W	0.1 W	0.1 W
$D_{rms}$	-	8.6 W	6.5 W	10.3 W	16.5 W
$/D/_{95\%}$	-	19.2 W	13.3 W	23.9 W	36.6 W
$\overline{OU}$	3.14 W	-	5.8 W	-	-
$\overline{UR}$		0.6	0.6	0.8	1.4
$UR_{max}$	-	2.9	2.6	2.8	3.8
$UR_{min}$	-	0.0	0.0	0.0	0.0
$ \overline{D} /\overline{x} \times 100\%$	-	4.4%	3.7%	5.5%	9.5%
$\overline{D}/\overline{x} \times 100\%$	-	-0.9%	-1.5%	-1.1%	8.6%

Figure 7.4 contains a plot of the transmitted solar power for a given hour of the day through the glazing unit and exterior shading screen for all programs.

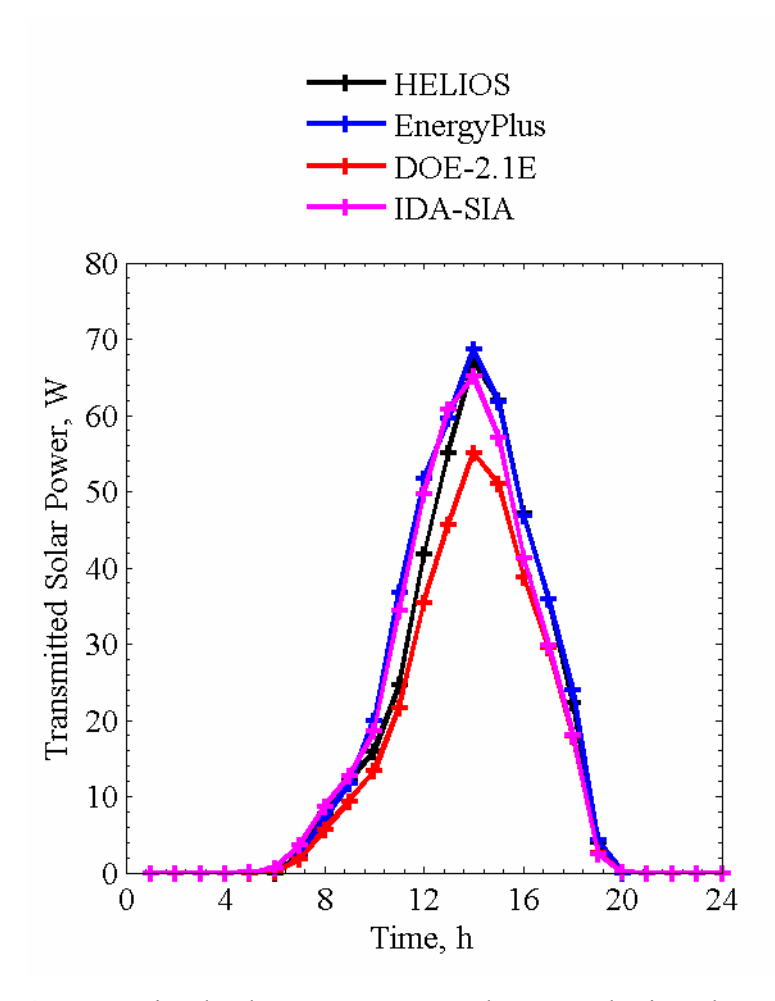


Figure 7.4. Transmitted solar power averaged over each given hour of the day.

The optical models used in each building energy simulation program used different assumptions to account for the shading screen; this in conjunction with modeling of air gap and associated long-wave radiation exchange caused additional differences in predicted cooling power. However, the magnitude of the transmitted solar power was significantly reduced compared with the glazing only experiment resulting in closer cooling power predictions. In-depth analyses and discussion of these results is provided by Loutzenhiser et al. [16].

# **Chapter 8: Glazing Unit with an Interior Shading Screen (Exercise 5)**

An experiment designed to evaluate the impact of solar gains through a glazing with a diffuse interior shading screen was run from June 8 to July 2, 2005. Information about the mounting of the interior shade and other parameters are provided in this chapter.

### 8.1. Description of the Experiment

This section contains specific information about the experiment, which includes the following information:

- Geometry and optical properties of the interior shading screen
- Thermophysical properties of the test cell envelope

## 8.1.1. Geometry and Optical Properties of the Interior Shade Screen

For this experiment, an interior shading screen was installed 16 cm from the glazing and is pictured in Figure 8.1. The shade was mounted to allow air to flow between gap of the interior shade and the glazing unit; a dimensioned drawing of the shade position relative to the glazing is shown in Figure 8.2.

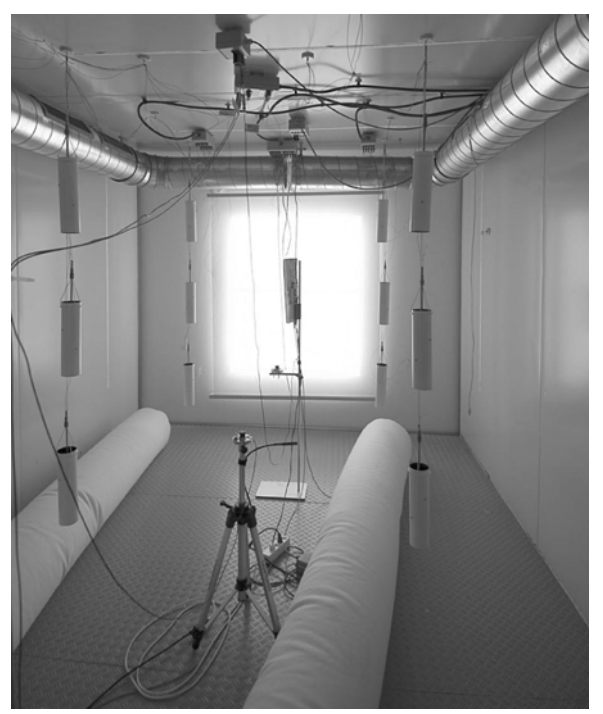


Figure 8.1. Photograph of the interior shade mounted on the test cell.

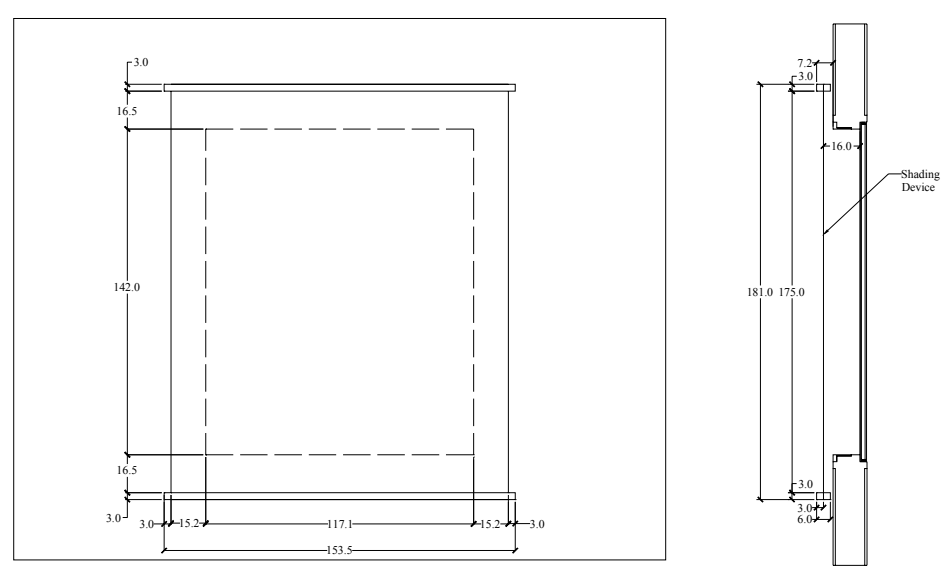


Figure 8.2. Dimensioned drawing of the interior shade in centimeters relative to the glazing.

The optical properties of the shade were measured at normal incident angles using a spectrometer. The transmittance and reflectance as a function of wavelength from 250 nm to 2500 nm and are contained in "Experiment 5.xls". The optical properties for the interior shade were integrated over the solar spectrum according to EN 410 [7] using GLAD software [8] and are shown in Table 8.1.

Table 8.1. Optical properties of the interior shading screen.

Property	Quantity
Normal solar transmittance, %	30.4
Normal solar reflectance, %	59.4

## 8.1.2. Thermophysical Properties of the Test Cell Envelope

The mean envelope temperatures of the construction elements are shown in Table 8.2. The thermophysical properties fixed at these mean envelope temperatures are contained in Tables 8.3a to 8.3c.

Table 8.2. Mean envelope temperatures for experiment.

Construction element	Mean temperature, °C
Ceiling, east, west, and north walls	22.83
Floor	22.75
South wall	20.91

Table 8.3a. Ceiling, north, east and west wall construction evaluated at 22.83°C.

Layer	Material	Thickness	Thermal conductivity	Density	Specific heat
number		mm	W/m-K	Kg/m <sup>3</sup>	J/kg-K
1	Sheet steel	0.7	53.62	7837	460.8
2	PU foam	139	0.02234	30	1800
3	Sheet steel	0.7	53.62	7837	460.8

Table 8.3b. Floor construction evaluated at 22.75°C.

Layer number	Material	Thickness mm	Thermal conductivity W/m-K	Density kg/m <sup>3</sup>	Specific heat J/kg-K
1	Sheet steel	0.7	53.62	7837	460.8
2	PU foam	140	0.02233	30	1800
3	PU foam (higher density)	20	0.070	45	1800
4	Sheet steel with surface Structure	2.5	53.62	7837	460.8

Table 8.3c. South wall construction evaluated at 20.91°C.

Layer	Material	Thickness	Thermal conductivity	Density	Specific heat
number		mm	W/m-K	Kg/m <sup>3</sup>	J/kg-K
1	Plywood	10	0.1404	850	1605
2	EPS foam	130	0.03622	28	1460
3	Plywood	10	0.1404	850	1605

#### 8.2. Results

The empirical validation for this exercise focused on comparing cooling power. Plots for cooling power from HELIOS, EnergyPlus, DOE-2.1E, and IDA-SIA are shown in Figures 8.3a to 8.3d, respectively. Table 8.4 contains the overall and 10 most influential input uncertainties that impacted the cooling power predictions taken from the n-way factorial analysis. A summary of the statistical comparisons is contained in Table 8.5.

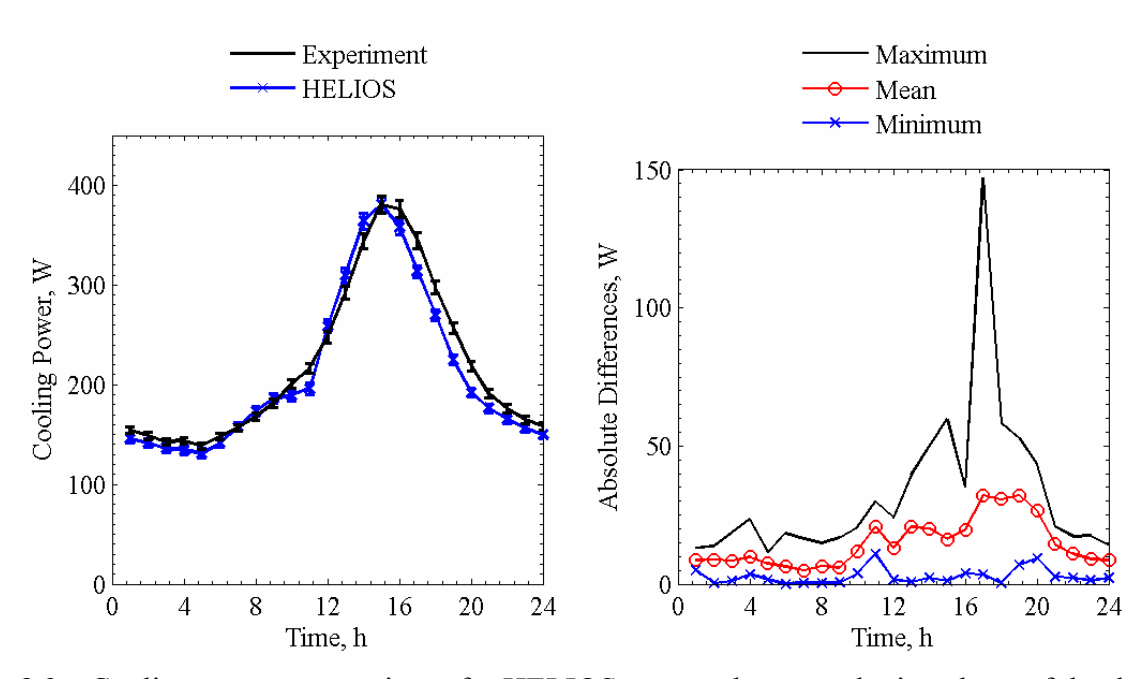


Figure 8.3a. Cooling power comparisons for HELIOS averaged over each given hour of the day (left) and absolute maximum, mean, and minimum differences for a given hour of the day (right).

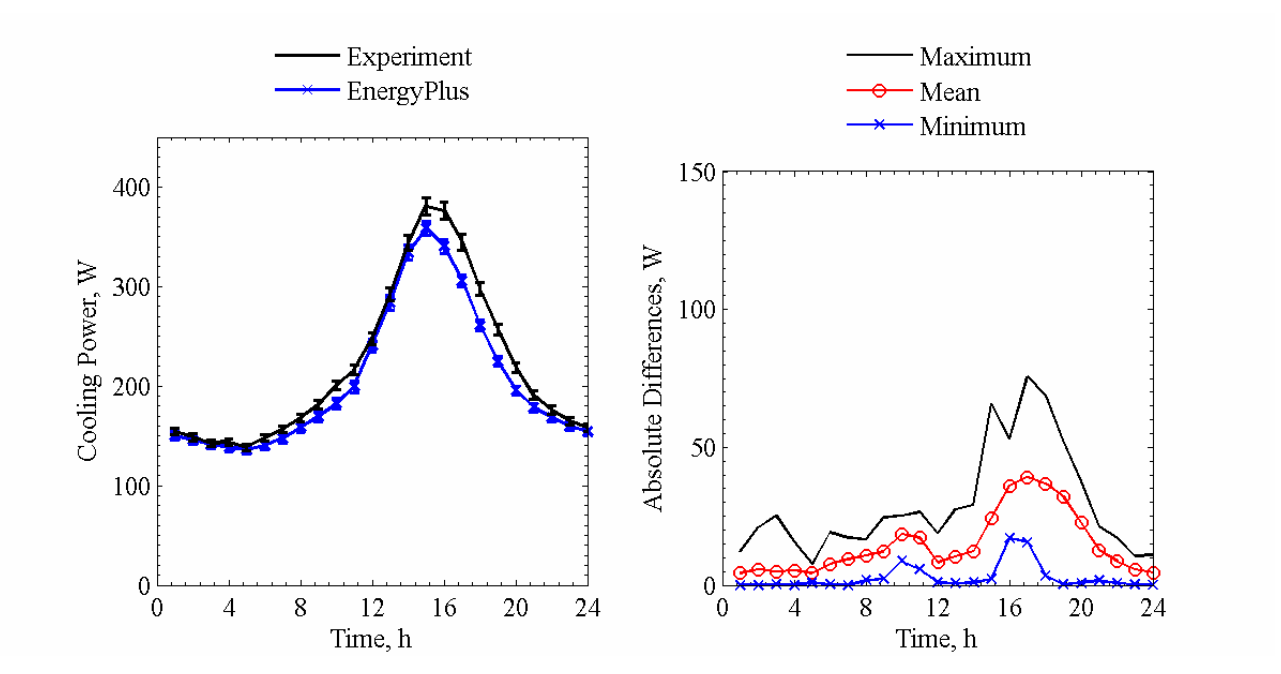


Figure 8.3b. Cooling power comparisons for EnergyPlus averaged over each given hour of the day (left) and absolute maximum, mean, and minimum differences for a given hour of the day (right).

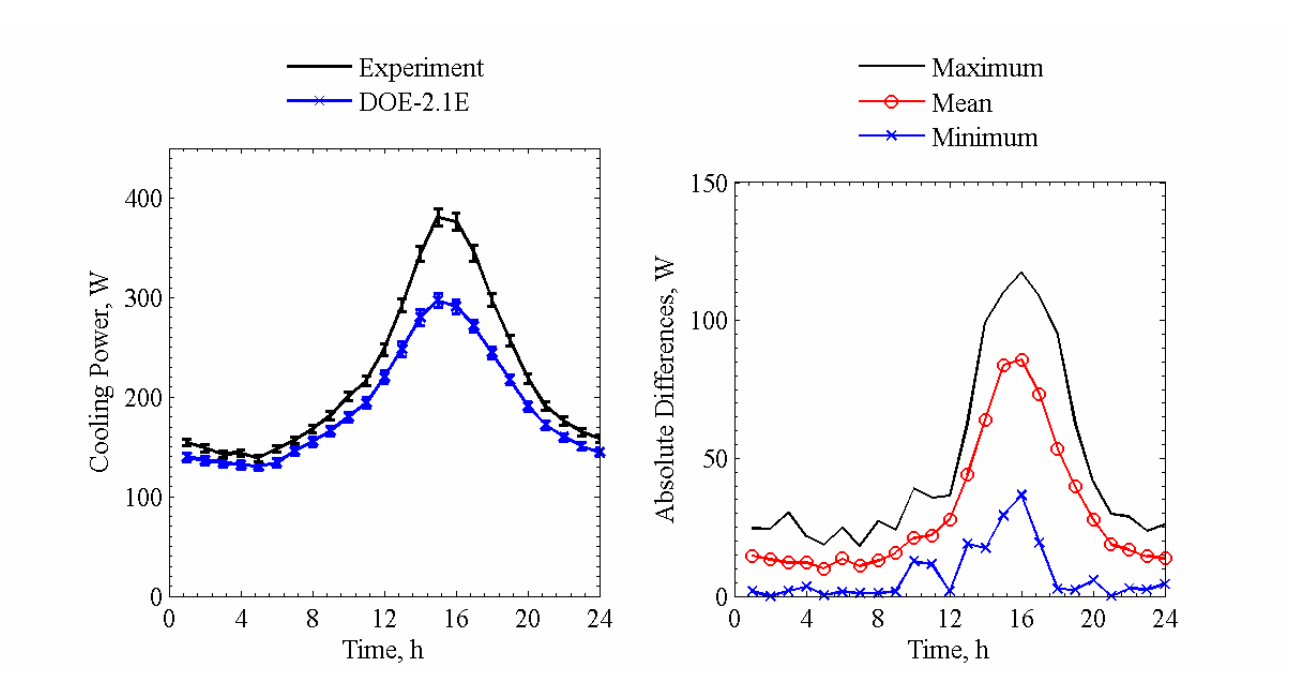


Figure 8.3c. Cooling power comparisons for DOE-2.1E averaged over each given hour of the day (left) and absolute maximum, mean, and minimum differences for a given hour of the day (right).

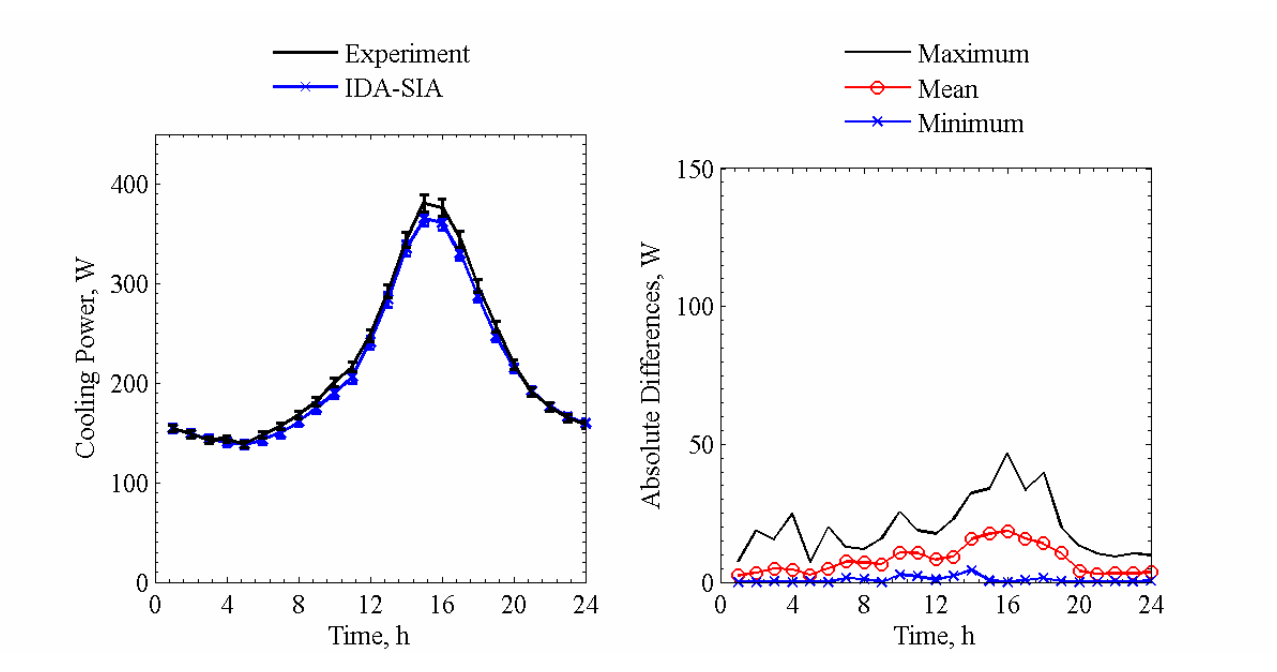


Figure 8.3d. Cooling power comparisons for IDA-SIA averaged over each given hour of the day (left) and absolute maximum, mean, and minimum differences for a given hour of the day (right).

Table 8.4. Overall uncertainty and 10 most influential input parameters from the n-way factorial analyses in Watts.

Parameter	Forward	Backward
Overall uncertainty	2.66	2.63
Average room air temperature	-1.39	1.40
Fan power	0.89	-0.89
Outside air temperature	0.88	-0.87
North wall surface temperature	0.71	-0.71
Ceiling surface temperature	0.60	-0.60
West wall surface temperature	0.48	-0.48
Floor surface temperature	0.40	-0.39
Inner glazing front reflectance	-0.37	0.29
Transmittance of the outer glazing	0.36	-0.32
Diffuse horizontal solar irradiance	0.34	-0.34

Table 8.5. Statistical comparisons for cooling power in Exercise 5.

Parameter	Experiment	SOГТЭН	EnergyPlus	DOE-2.1E	IDA-SIA
$\overline{x}$	218.7 W	210.4 W	204.8 W	188.9 W	212.9 W
S	85.2 W	85.3 W	76.5 W	58.8 W	79.6 W
$x_{max}$	459.4 W	441.5 W	419.5 W	342.0 W	431.7 W
$\chi_{min}$	100.6 W	107.3 W	119.9 W	119.0 W	111.5 W
$\overline{D}$	-	8.2 W	13.9 W	29.7 W	5.8 W
D	-	14.8 W	14.7 W	30.1 W	8.0 W
$ D_{max} $	-	146.9 W	75.7 W	117.4 W	46.7 W
$ D_{min} $	•	0.1 W	0.1 W	0.0 W	0.0 W
$D_{rms}$	•	19.9 W	20.2 W	40.6 W	11.1 W
/D/ <sub>95%</sub>	•	40.6 W	44.0 W	94.8 W	24.7 W
$\overline{OU}$	4.9 W	ı	5.2 W	-	-
$\overline{\it UR}$	-	1.4	1.3	2.6	0.7
$UR_{max}$	-	11.3	5.8	7.7	3.2
$UR_{min}$	=	0.0	0.0	0.0	0.0
$ \overline{D} /\overline{x} \times 100\%$	-	6.7%	6.7%	13.8%	3.7%
$\overline{D}$ / $\overline{x} \times 100\%$	-	3.8%	6.4%	13.6%	2.6%

Figure 8.4 contains a plot of the transmitted solar power for a given hour of the day through the glazing unit and interior shading screen for all programs.

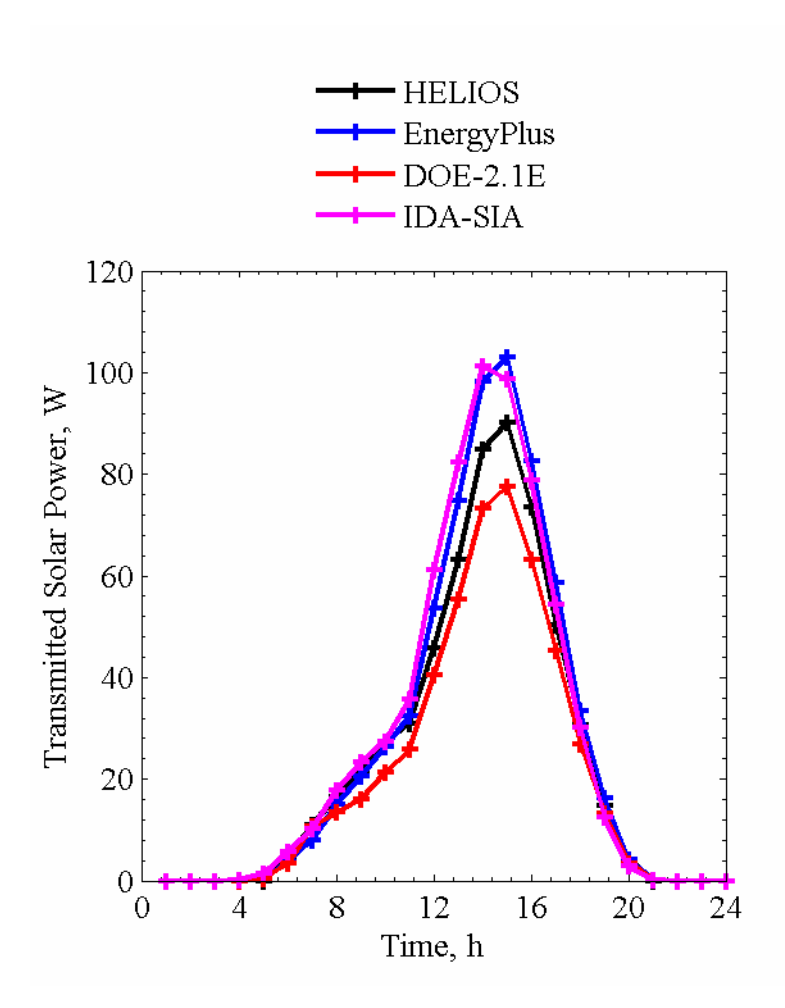


Figure 8.4. Transmitted solar power averaged over each given hour of the day.

Many of the same modeling challenges and differences in the optical model from the exterior shading screen exercise were also apparent in this simulation exercise. In-depth analyses and discussion of these results is provided by Loutzenhiser et al. [16].

# **Chapter 9: Glazing Unit with Exterior Venetian Blind (Exercise 6)**

An experiment designed to evaluate the impact of solar gains through a glazing unit with an exterior Venetian blind assembly was run in the EMPA test cell from July 16 to September 5, 2005. The first part of the experiment was performed with the slats in the horizontal position, and the second part was with the outer slat blade (farthest from the glazing unit) tilted downward toward the ground at a 45° angle; the slat position was changed on August 16, 2005 at 7:00 AM. Information about exterior Venetian blind mounting and the results from this exercise are provided.

### 9.1. Description of the Experiment

This section contains specific information about the experiment, which includes the following information:

- Geometry and optical properties of the exterior Venetian blind assembly
- Thermophysical properties of the test cell envelope

### 9.1.1. Geometry and Optical Properties of the Exterior Venetian Blind Assembly

For this experiment, an exterior Venetian blind assembly was installed 1.0 cm from the exterior glazing surface and is pictured in Figure 9.1. A dimensioned drawing of the blind position relative to the glazing unit and the geometry of the blind slat are shown in Figures 9.2 and 9.3, respectively.



Figure 9.1. Photograph of the exterior blind mounted in front of the test cell.

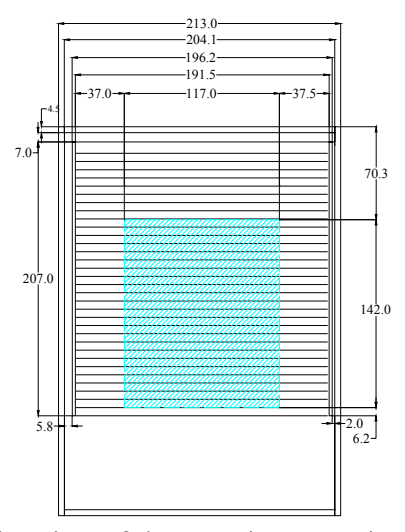


Figure 9.2. Dimensioned drawing of the exterior Venetian blind in centimeters relative to the glazing.

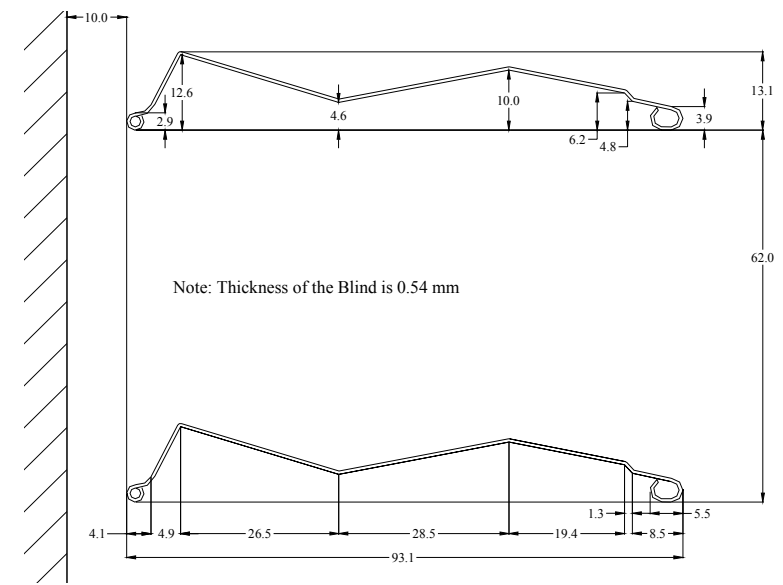


Figure 9.3. Dimensioned blind relative to the glazing in millimeters.

The optical properties of the exterior blind were measured at normal incident angles using a spectrometer. The transmittance and reflectance as a function of wavelength from 250 nm to 2500 nm can be found in "Experiment 6.xls". The solar reflectance, computed according to European Standard EN 410 [7] using GLAD software [8], and hemispherical emittance, measured with an emissometer based on a calorimetric method, are shown in Table 9.1.

Table 9.1. Optical properties of the slat surfaces.

Property	Quantity
Normal solar reflectance, %	44.1
Hemispherical emittance, %	86.2

## 9.1.2. Thermophysical Properties of the Test Cell Envelope

Table 9.2 contains the mean envelope temperatures for both blind slat positions. The thermophysical properties evaluated at these mean envelope temperatures are contained in Tables 9.3a to 9.3c for the Venetian blinds horizontally positioned and Tables 9.4a to 9.4c when tilted downward 45°.

Table 9.2. Mean envelope temperatures for the experiments.

Construction element	Mean temperature, °C		
	Horizontal	45° Downward	
Ceiling, east, west, and north walls	22.72	20.83	
Floor	22.72	20.83	
South wall	20.82	20.90	

Table 9.3a, Ceiling, north, east and west wall construction evaluated at 22.72°C

Layer number	Material	Thickness mm	Thermal conductivity W/m-K	Density kg/m <sup>3</sup>	Specific heat J/kg-K
1	Sheet steel	0.7	53.62	7837	460.8
2	PU foam	139	0.02232	30	1800
3	Sheet steel	0.7	53.62	7837	460.8

Table 9.3b. Floor construction evaluated at 22.72°C.

Layer	Material	Thickness	Thermal conductivity	Density	Specific heat	
number		mm	W/m-K	kg/m <sup>3</sup>	J/kg-K	
1	Sheet steel	0.7	53.62	7837	460.8	
2	PU foam	140	0.02232	30	1800	
3	PU foam (higher density)	20	0.070	45	1800	
4	Sheet steel with surface structure	2.5	53.62	7837	460.8	

Table 9.3c. South wall construction evaluated at 20.82°C.

Layer number	Material	Thickness mm	Thermal conductivity W/m-K	Density kg/m <sup>3</sup>	Specific heat J/kg-K
1	Plywood	10	0.1400	850	1605
2	EPS foam	130	0.03620	28	1460
3	Plywood	10	0.1400	850	1605

Table 9.4a. Ceiling, north, east and west wall construction evaluated at 22.83°C.

Layer number	Material	Thickness mm	Thermal conductivity W/m-K	Density kg/m <sup>3</sup>	Specific heat J/kg-K
1	Sheet steel	0.7	53.62	7837	460.8
2	PU foam	139	0.02234	30	1800
3	Sheet steel	0.7	53.62	7837	460.8

Table 9.4b. Floor construction evaluated at 22.83°C.

Layer number	Material	Thickness mm	Thermal conductivity W/m-K	Density kg/m <sup>3</sup>	Specific heat J/kg-K
1	Sheet steel	0.7	53.62	7837	460.8
2	PU foam	140	0.02232	30	1800
3	PU foam (higher density)	20	0.070	45	1800
4	Sheet steel with surface structure	2.5	53.62	7837	460.8

Table 9.4c. South wall construction evaluated at 20.90°C.

Layer number	Material	Thickness mm	Thermal conductivity W/m-K	Density kg/m <sup>3</sup>	Specific heat J/kg-K
1	Plywood	10	0.1400	850	1605
2	EPS foam	130	0.03621	28	1460
3	Plywood	10	0.1400	850	1605

#### 9.2. Results

The empirical validation for this exercise focused on comparing the measured cooling power in the test cell during the experiment with the predicted cooling powers from each building energy simulation program. Results are provided in two sections to reflect and assess the performances of the building energy simulation programs for both Venetian blind slat positions.

#### 9.2.1. Horizontally Positioned Venetian Blind Slat Position

Plots for cooling power from HELIOS and EnergyPlus are shown in Figures 9.4a and 9.4b, respectively. Comparisons were made for a 20 day period from July 24 to August 12, 2005. Two plots are contained in each figure. Table 9.5 contains the overall and the 10 most influential input uncertainties that impacted the cooling power predictions taken from the n-way factorial analysis. A summary of the statistical comparisons is contained in Table 9.6.

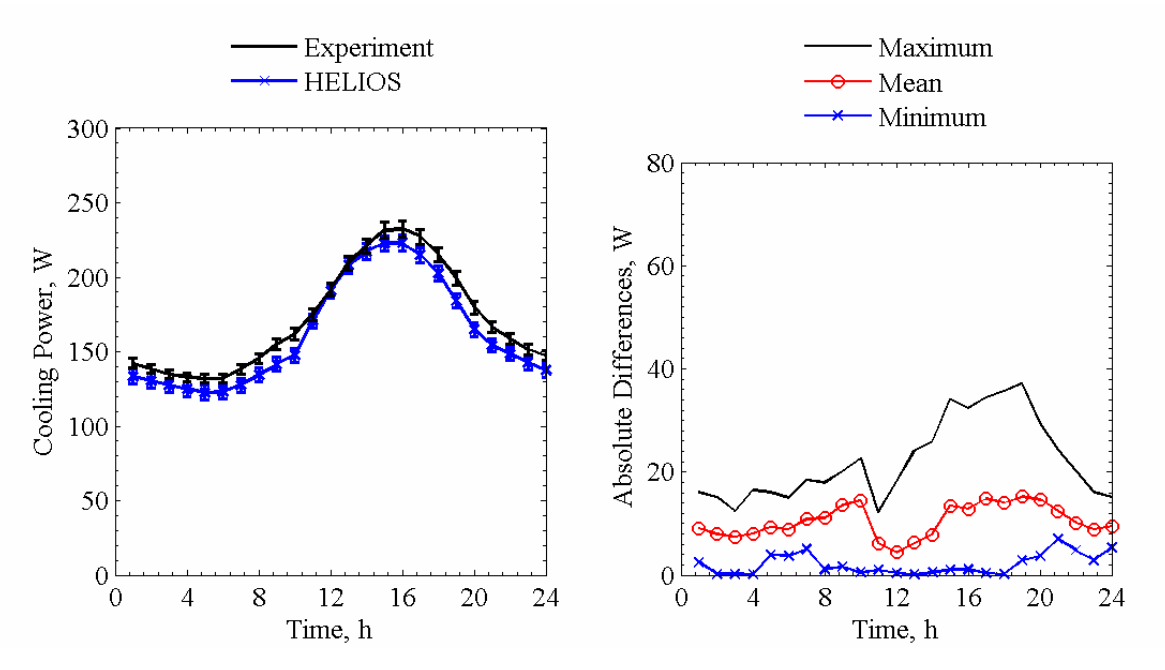


Figure 9.4a. Cooling power comparisons for HELIOS averaged over each given hour of the day (left) and absolute maximum, mean, and minimum differences for a given hour of the day (right).

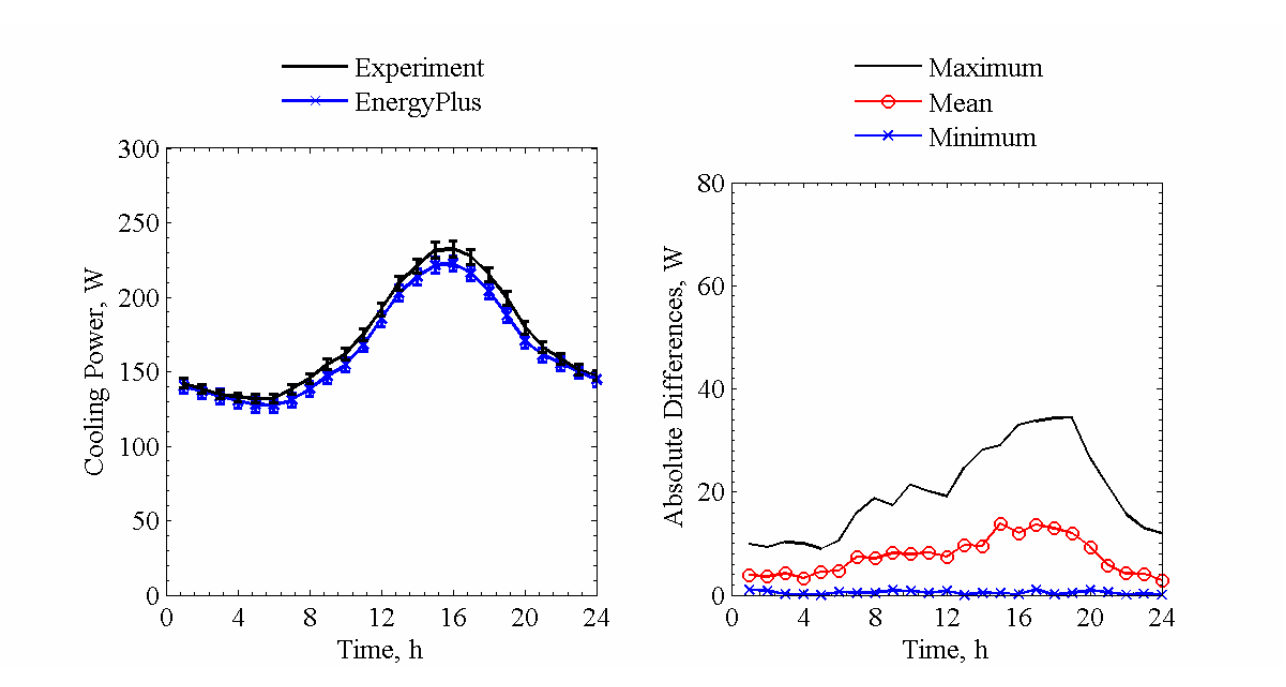


Figure 9.4b. Cooling power comparisons for EnergyPlus averaged over each given hour of the day (left) and absolute maximum, mean, and minimum differences for a given hour of the day (right).

Table 9.5. Overall uncertainty and 10 most influential input parameters from the n-way factorial analyses in Watts.

Parameter	Forward	Backward
Overall uncertainty	2.28	2.28
Average inside air temperature	-1.36	1.37
Fan power	0.89	-0.89
Outside air temperature	0.82	-0.82
North wall temperature	0.71	-0.71
Ceiling temperature	0.60	-0.60
West wall surface temperature	0.47	-0.47
Floor surface temperature	0.39	-0.39
East wall surface temperature	0.32	-0.32
Diffuse horizontal solar irradiance	0.23	-0.22
Global horizontal infrared irradiance	0.18	-0.18

Table 9.6. Statistical comparisons for cooling power in Exercise 6 with slats horizontally positioned.

Parameter	Experiment	HELIOS	EnergyPlus	
$\overline{x}$	171.6 W	162.3 W	165.4 W	
S	43.2 W	41.8 W	38.5 W	
$x_{max}$	330.4 W	298.1 W	297.4 W	
$x_{min}$	102.4 W	95.5 W	102.8 W	
$\overline{D}$	-	9.4 W	6.2 W	
$ \overline{D} $	-	10.5 W	7.5 W	
$/D_{max}/$	-	37.2 W	34.4 W	
$ D_{min} $	-	0.1 W	0.0 W	
$D_{rms}$	-	12.4 W	10.4 W	
$D_{rms} = D_{l95\%}$	-	22.7 W	22.8 W	
$\overline{OU}$	3.9 W	-	4.8 W	
$\overline{\it UR}$	-	1.2 3.2	0.8	
$UR_{max}$	-	3.2	3.0	
$UR_{min}$	-	0.0	0.0	
$ \overline{D} /\overline{x} \times 100\%$	-	6.1%	4.4%	
$\overline{D}$ / $\overline{x} \times 100\%$	-	5.5%	3.6%	

Figure 9.5 contains a plot of the transmitted solar power for a given hour of the day through the glazing unit and horizontally positioned exterior Venetian blind slats for all programs.

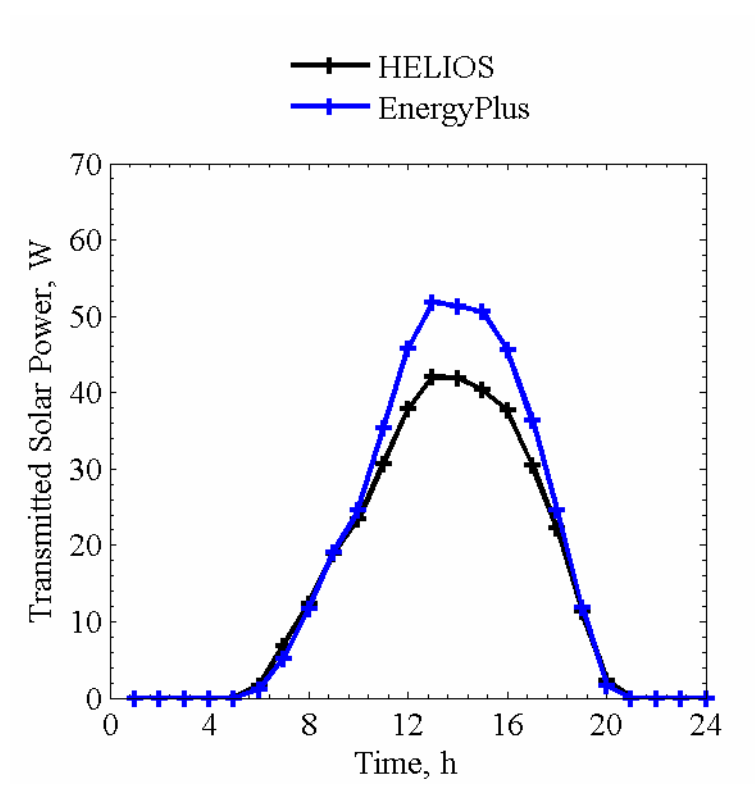


Figure 9.5. Transmitted solar power averaged over each given hour of the day.

#### 9.2.2. Tilted 45° Downward Venetian Blind Slat Position

Plots for cooling power from HELIOS and EnergyPlus are shown in Figures 9.6a and 9.6b, respectively. To account for the change in slat blade angle, comparisons were made for a 20 day period from August 17 to September 5, 2005. Table 9.7 contains overall and 10 most influential input uncertainties that impacted the cooling power predictions taken from the n-way factorial analysis. A summary of the statistical comparisons is contained in Table 9.8.

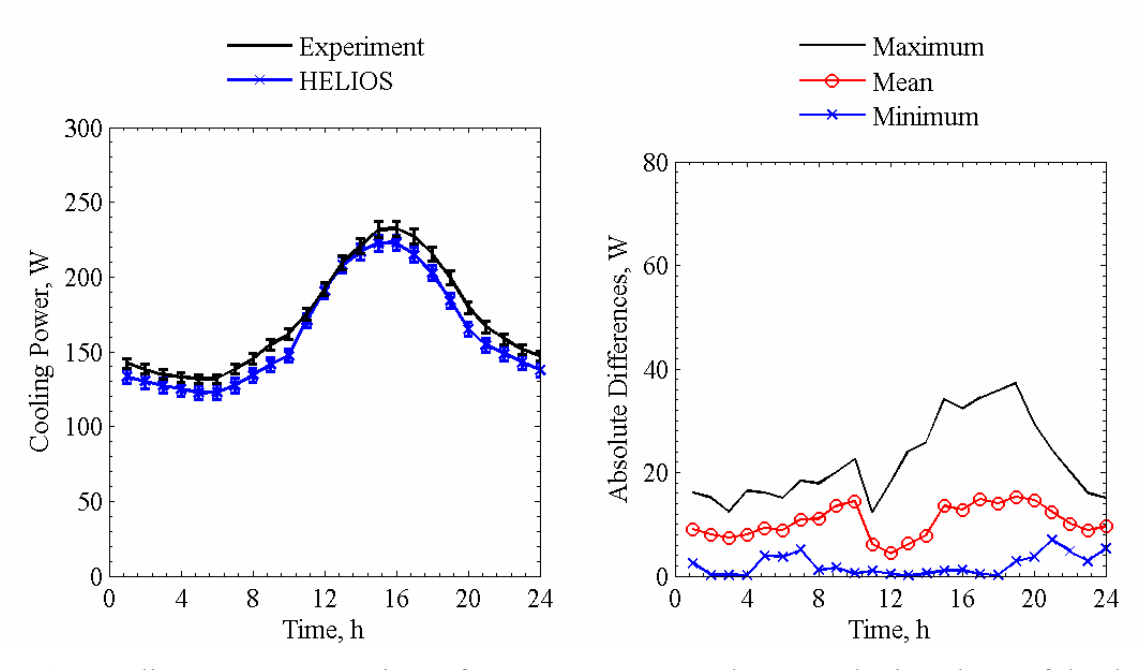


Figure 9.6a. Cooling power comparisons for HELIOS averaged over each given hour of the day (left) and absolute maximum, mean, and minimum differences for a given hour of the day (right).

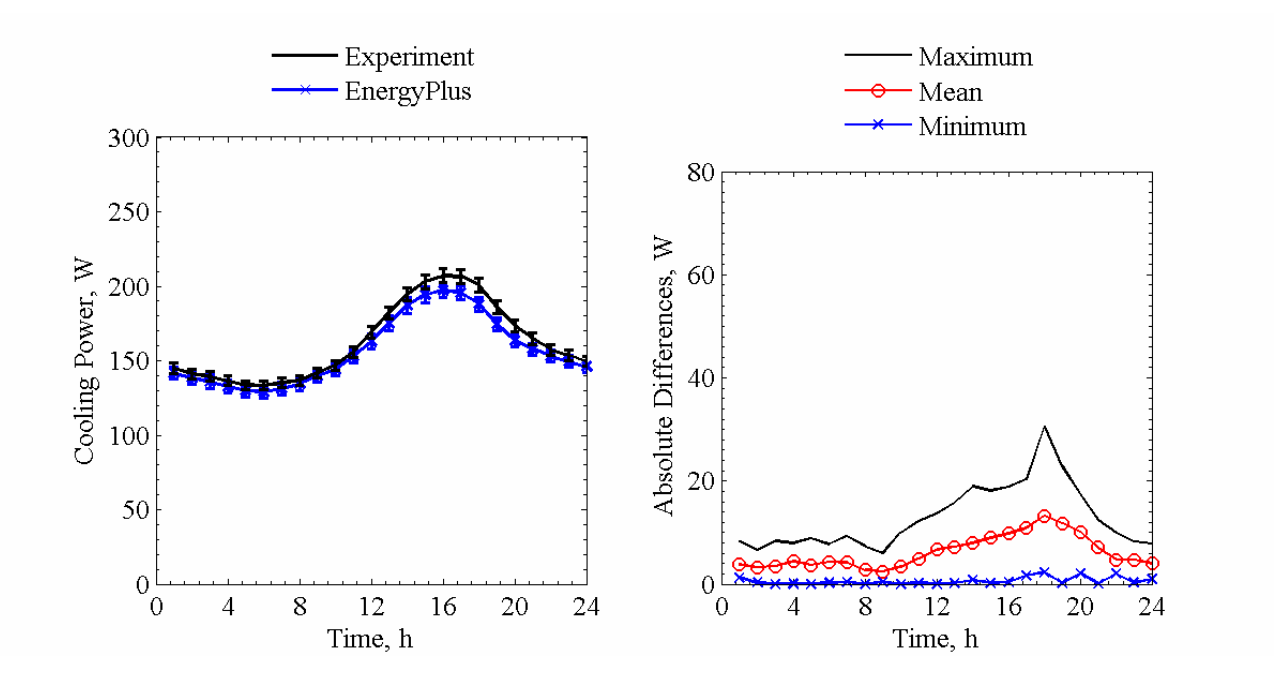


Figure 9.6b. Cooling power comparisons for EnergyPlus averaged over each given hour of the day (left) and absolute maximum, mean, and minimum differences for a given hour of the day (right).

Table 9.7. Overall uncertainty and 10 most influential input parameters from the n-way factorial analyses in Watts.

Parameter	Forward	Backward
Overall uncertainty	2.22	2.22
Average inside air temperature	-1.36	1.36
Fan power	0.893	-0.893
Outside air temperature	0.824	-0.821
North wall surface temperature	0.708	-0.708
Ceiling surface temperature	0.598	-0.596
West wall temperature	0.471	-0.470
Floor surface temperature	0.388	-0.388
East wall surface temperature	0.315	-0.315
Global horizontal infrared irradiance	0.144	-0.143
Ground reflectance	0.125	-0.123

Table 9.8. Statistical comparisons for cooling power in Exercise 6 with slats tilted 45° downward.

Parameter	Experiment	HELIOS	EnergyPlus
$\overline{x}$	162.2 W	157.4 W	156.4 W
S	32.2 W	36.1 W	28.1 W
$x_{max}$	260.6 W	253.9 W	242.7 W
$x_{min}$	112.7 W	100.2 W	107.8 W
$\overline{D}$	-	4.8 W	5.8 W
D	-	9.5 W	6.2 W
$ D_{max} $	-	35.5 W	30.5 W
$ D_{min} $	-	0.0 W	0.0 W
$D_{rms}$	-	11.0 W	7.9 W
$/D/_{95\%}$	-	19.8 W	16.5 W
$\overline{OU}$	3.7 W	-	4.4 W
$\overline{UR}$	-	1.2	0.7
$UR_{max}$	-	3.7	3.1
$UR_{min}$	-	0.0	0.0
$ \overline{D} /\overline{x} \times 100\%$	-	5.8%	3.8%
$\overline{D}/\overline{x} \times 100\%$	-	3.0%	3.6%

Figure 9.7 contains a plot of the transmitted solar power for a given hour of the day through the glazing unit and 45° downward positioned exterior Venetian blind slats for all programs.

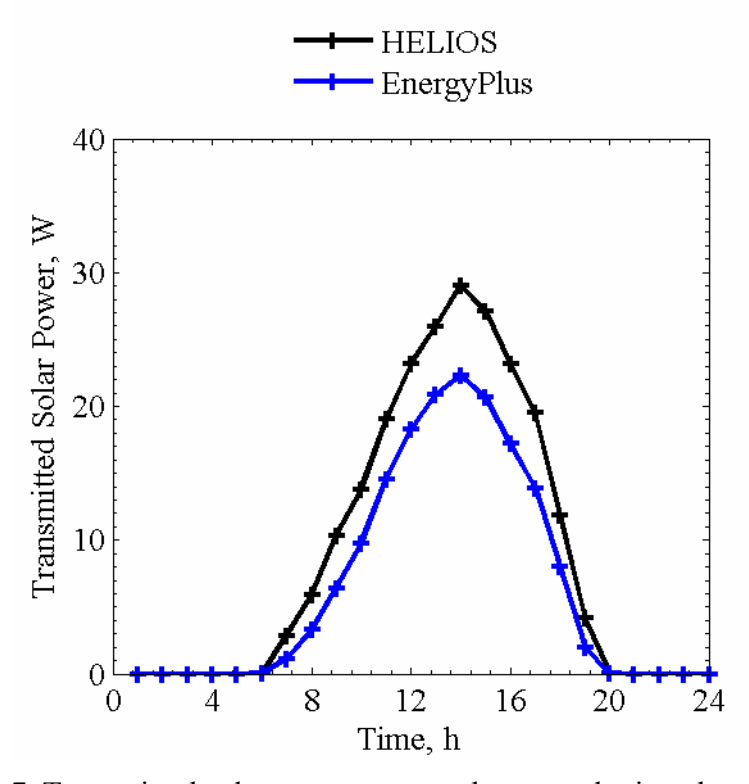


Figure 9.7. Transmitted solar power averaged over each given hour of the day.

Because of the complexities associated with modeling blind assemblies, not all participants simulated this exercise. Overall, the magnitude of the transmitted solar power into the test cell was

quite low but not uniform from program to program. Different assumptions for modeling the blind assembly discussed in the modelers' reports provide additional insight into this discrepancy.

# **Chapter 10: Glazing Unit with Interior Mini-blind (Exercise 7)**

Two components of an experiment were run in the EMPA test cell designed to evaluate the impact of solar gains through a glazing unit with mini-blinds at two different slat positions. The first component was performed with the slats in the horizontal position and was run from October 10, 2005 to November 11, 2005 and the second component, with the outer blind slats (closest to the window) tilted downward at a 45° angle, was run from March 27, 2006 to May 20, 2006.

#### 10.1. Description of the Experiment

This section contains specific information about the experiment, which includes the following information:

- Geometry of interior mini-blind assembly and blind slat optical properties
- Thermophysical properties of the test cell envelope

# 10.1.1. Geometry of Interior Mini-blind Assembly and Blind Slat Optical Properties

For this experiment, an interior mini-blind assembly was installed and the dimensions relative to the glazing unit and the blind slats are shown in Figures 10.1 and 10.2, respectively.

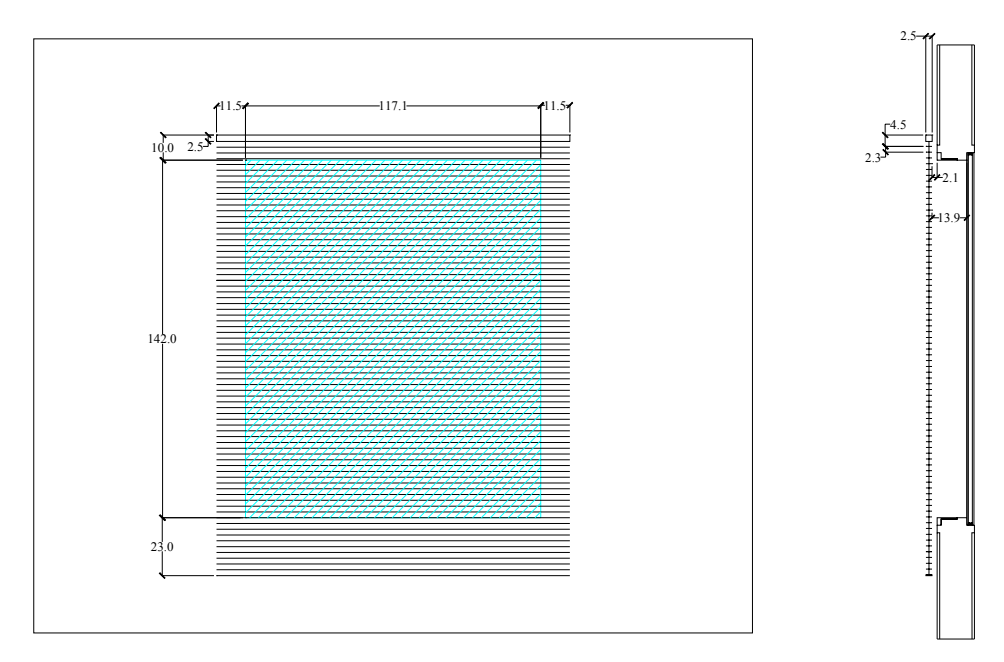


Figure 10.1. Dimensioned drawing of the internal mini-blinds in centimeters relative to the glazing.

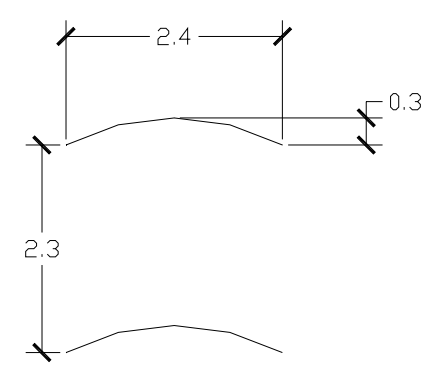


Figure 10.2. Dimension internal mini-blinds relative to the glazing in centimeters.

The optical properties of the interior mini-blind slats were measured at normal incident angles using a spectrometer. The reflectance as a function of wavelength from 250 nm to 2500 nm can be found in "Experiment 7a.xls" and "Experiment 7b.xls". The solar reflectance, computed according to EN 410 [7] using GLAD software [8], and the hemispherical emittance, measured with an emissometer based on a calorimetric method, are given in Table 10.1.

Table 10.1. Optical properties of the slat surfaces.

Property	Quantity
Normal solar reflectance, %	63.9
Hemispherical emittance, %	72.1

#### 10.1.2. Thermophysical Properties of the Test Cell Envelope

The mean envelope temperatures of the construction elements for both experiments are shown in Table 10.2. The thermophysical properties evaluated at these mean envelope temperatures are contained in Tables 10.3a to 10.3c for the mini-blind assembly horizontally positioned and Tables 10.4a to 10.4c when tilted downward 45°.

Table 10.2. Mean envelope temperatures for the experiments.

Construction element	Mean te	Mean temperature, °C		
	Horizontal	45° Downward		
Ceiling, east, west, and north walls	22.58	22.94		
Floor	22.58	22.94		
South wall	16.96	15.52		

Table 10.3a. Ceiling, north, east and west wall construction evaluated at 22.58°C.

Layer number	Material	Thickness mm	Thermal conductivity W/m-K	Density kg/m <sup>3</sup>	Specific heat J/kg-K
1	Sheet steel	0.7	53.62	7837	460.8
2	PU foam	139	0.02230	30	1800
3	Sheet steel	0.7	53.62	7837	460.8

Table 10.3b. Floor construction evaluated at 22.72°C.

Layer number	Material	Thickness mm	Thermal conductivity W/m-K	Density kg/m <sup>3</sup>	Specific heat J/kg-K
1	Sheet steel	0.7	53.62	7837	460.8
2	PU foam	140	0.02230	30	1800
3	PU foam (higher density)	20	0.070	45	1800
4	Sheet steel with surface	2.5	53.62	7837	460.8
	Structure				

Table 10.3c. South wall construction evaluated at 16.96°C.

Layer number	Material	Thickness mm	Thermal conductivity W/m-K	Density kg/m <sup>3</sup>	Specific heat J/kg-K
1	Plywood	10	0.1393	850	1605
2	EPS foam	130	0.03571	28	1460
3	Plywood	10	0.1393	850	1605

Table 10.4a. Ceiling, north, east and west wall construction evaluated at 22.94°C.

Layer number	Material	Thickness mm	Thermal conductivity W/m-K	Density kg/m <sup>3</sup>	Specific heat J/kg-K
1	Sheet steel	0.7	53.62	7837	460.8
2	PU foam	139	0.02235	30	1800
3	Sheet steel	0.7	53.62	7837	460.8

Table 10.4b. Floor construction evaluated at 22.94°C.

Layer number	Material	Thickness mm	Thermal conductivity W/m-K	Density kg/m <sup>3</sup>	Specific heat J/kg-K
1	Sheet steel	0.7	53.62	7837	460.8
2	PU foam	140	0.02235	30	1800
3	PU foam (higher density)	20	0.070	45	1800
4	Sheet steel with surface structure	2.5	53.62	7837	460.8

Table 10.4c. South wall construction evaluated at 15.52°C.

Layer number	Material	Thickness mm	Thermal conductivity W/m-K	Density kg/m <sup>3</sup>	Specific heat J/kg-K
1	Plywood	10	0.1391	850	1605
2	EPS foam	130	0.03553	28	1460
3	Plywood	10	0.1391	850	1605

#### 10.2. Results

Results for cooling power are provided in two sections to assess the performances of the building energy simulation programs for both mini-blind slat positions.

# 10.2.1. Horizontally Positioned Mini-Blind Slat Position

Plots for cooling power from HELIOS and EnergyPlus are shown in Figures 10.3a to 10.3b, respectively. Two plots are contained in each figure. The plot of the left contains results and 95% credible limits averaged at each hour of day for the duration of the experiment and the plot on the right contains maximum, mean, and minimum absolute differences for each hour of the day during the comparison period. Table 10.5 contains overall and 10 most influential input uncertainties that impacted the cooling power predictions taken from the n-way factorial analysis. A summary of the statistical comparisons is contained in Table 10.6.

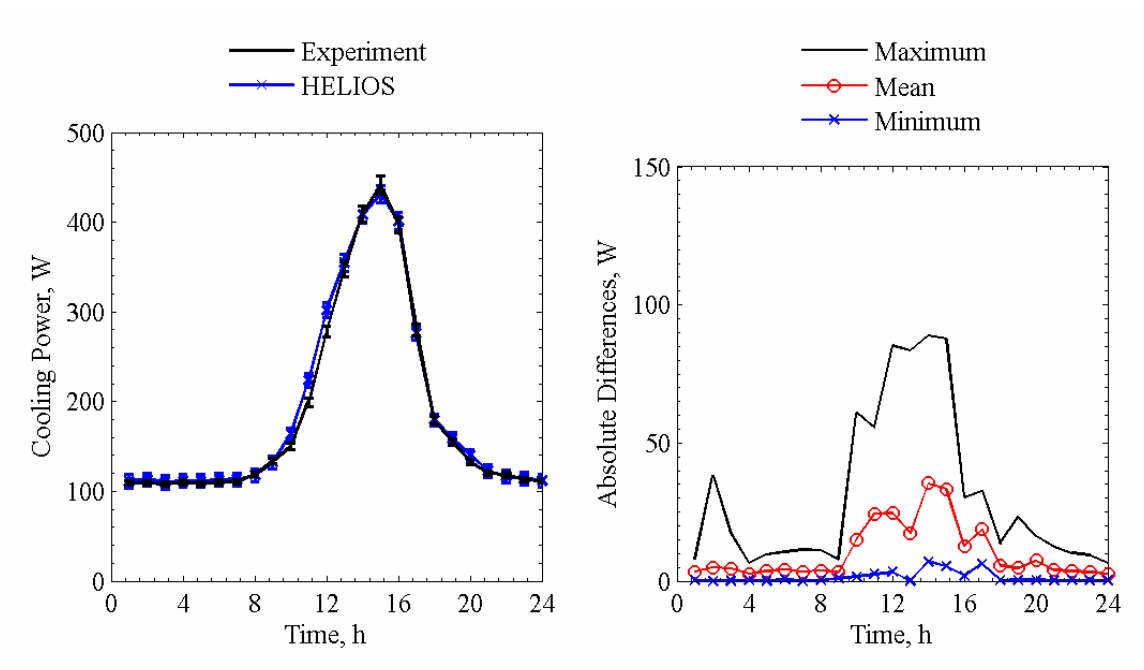


Figure 10.3a. Cooling power comparisons for HELIOS averaged over each given hour of the day (left) and absolute maximum, mean, and minimum differences for a given hour of the day (right).

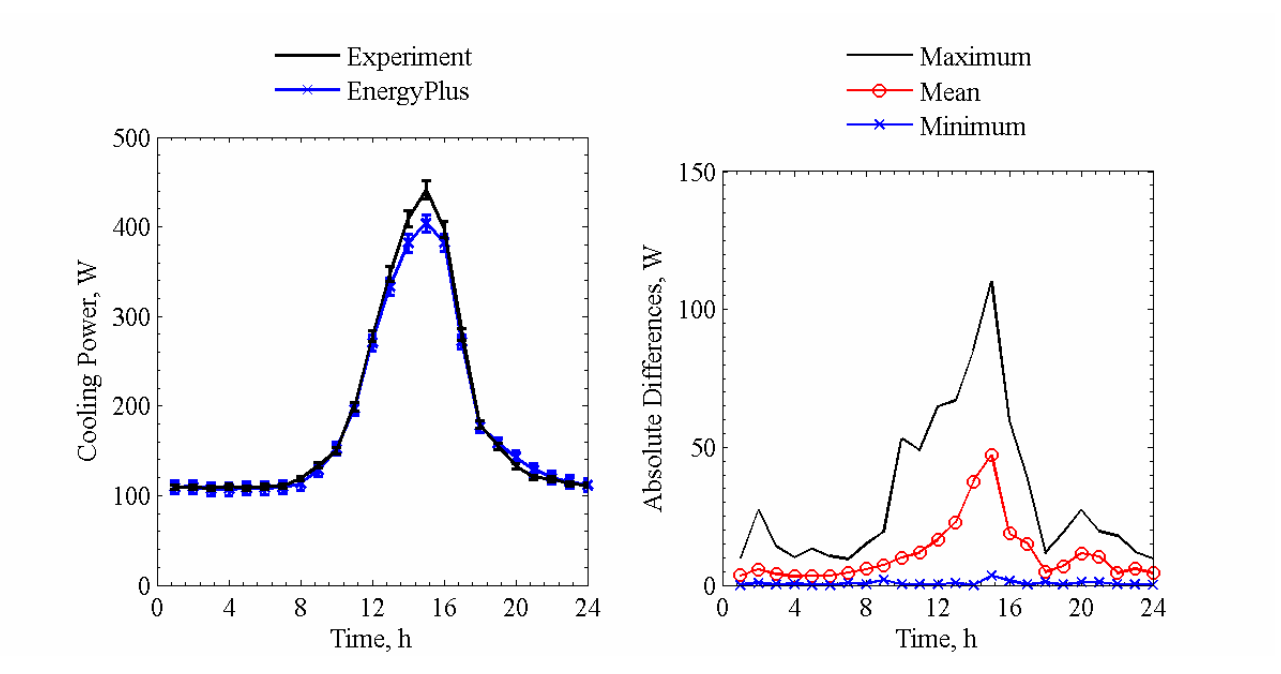


Figure 10.3b. Cooling power comparisons for EnergyPlus averaged over each given hour of the day (left) and absolute maximum, mean, and minimum differences for a given hour of the day (right).

Table 10.5. Overall uncertainty and 10 most influential input parameters from the n-way factorial analyses in Watts.

Parameter	Forward	Backward
Overall uncertainty	4.20	4.10
West wall surface temperature	2.13	-2.13
Floor surface temperature	1.78	-1.78
Average air temperature	-1.68	1.68
East wall surface temperature	1.04	-1.04
Fan power	0.90	-0.90
Ceiling surface temperature	0.82	-0.82
Outside air temperature	0.71	-0.71
North wall surface temperature	0.66	-0.66
Global horizontal infrared irradiance	0.47	-0.48
Front reflectance of inner glass pane	-0.44	0.15

Table 10.6. Statistical comparisons for cooling power in Exercise 7 with slats horizontally positioned.

Parameter	Experiment	HELIOS	EnergyPlus
	Exp	HE	Ene
$\overline{x}$	185.4 W	189.1 W	181.2 W
S	138.0 W	135.4 W	127.5 W
$x_{max}$	747.0 W	723.2 W	676.2 W
	79.8 W	82.5 W	80.7 W
$\frac{x_{min}}{\overline{D}}$	-	-3.7 W	4.2 W
D	-	10.3 W	11.2 W
$/D_{max}/$	-	89.0 W	110.1 W
$/D_{min}/$	-	0.1 W	0.0 W
$D_{rms}$	-	17.5 W	20.2 W
D <sub>rms</sub>  D  <sub>95%</sub>	-	38.1 W	51.4 W
$\overline{OU}$	4.2 W	-	7.6 W
$\overline{UR}$	-	0.8	0.8
$UR_{max}$	-	5.4	5.0
$UR_{min}$	-	0.0	0.0
$ \overline{D} /\overline{x} \times 100\%$	-	5.5%	6.1%
$\overline{D}/\overline{x} \times 100\%$	-	-2.0%	2.3%

Figure 10.4 contains a plot of the transmitted solar power for a given hour of the day through the glazing unit and horizontally positioned interior mini-blind slats for all programs.

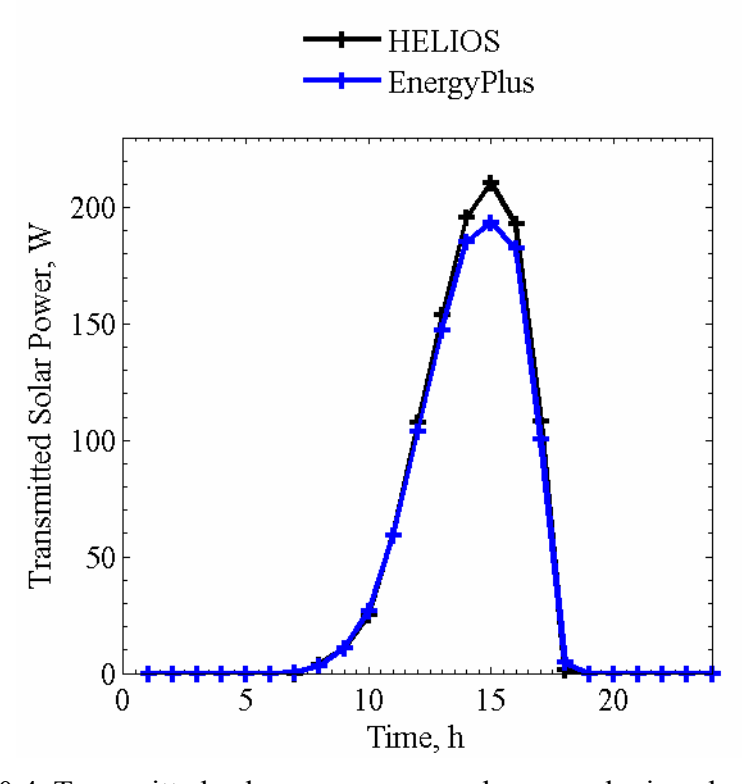


Figure 10.4. Transmitted solar power averaged over each given hour of the day.

### 10.2.2. Tilted 45° Downward Mini-Blind Slat Position

Plots for cooling power from HELIOS and EnergyPlus are shown in Figures 10.5a to 10.5b, respectively. Table 10.7 contains overall and the 10 most influential input uncertainties that impacted the cooling power predictions taken from the n-way factorial analysis. A summary of the statistical comparisons is contained in Table 10.8.

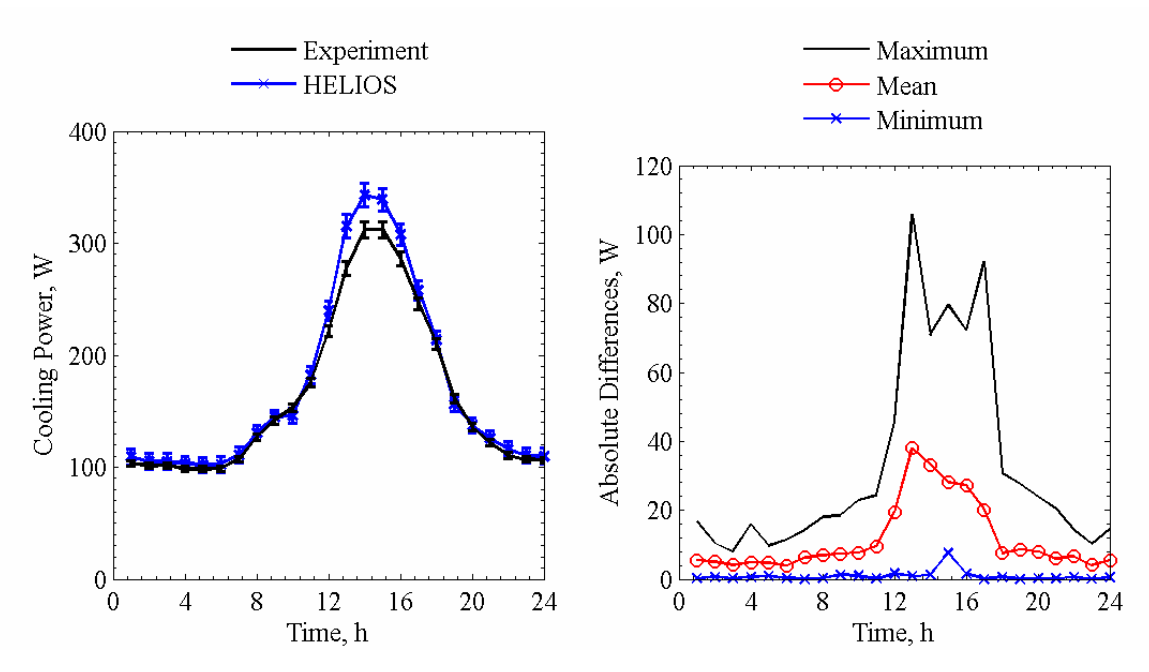


Figure 10.5a. Cooling power comparisons for HELIOS averaged over each given hour of the day (left) and absolute maximum, mean, and minimum differences for a given hour of the day (right).

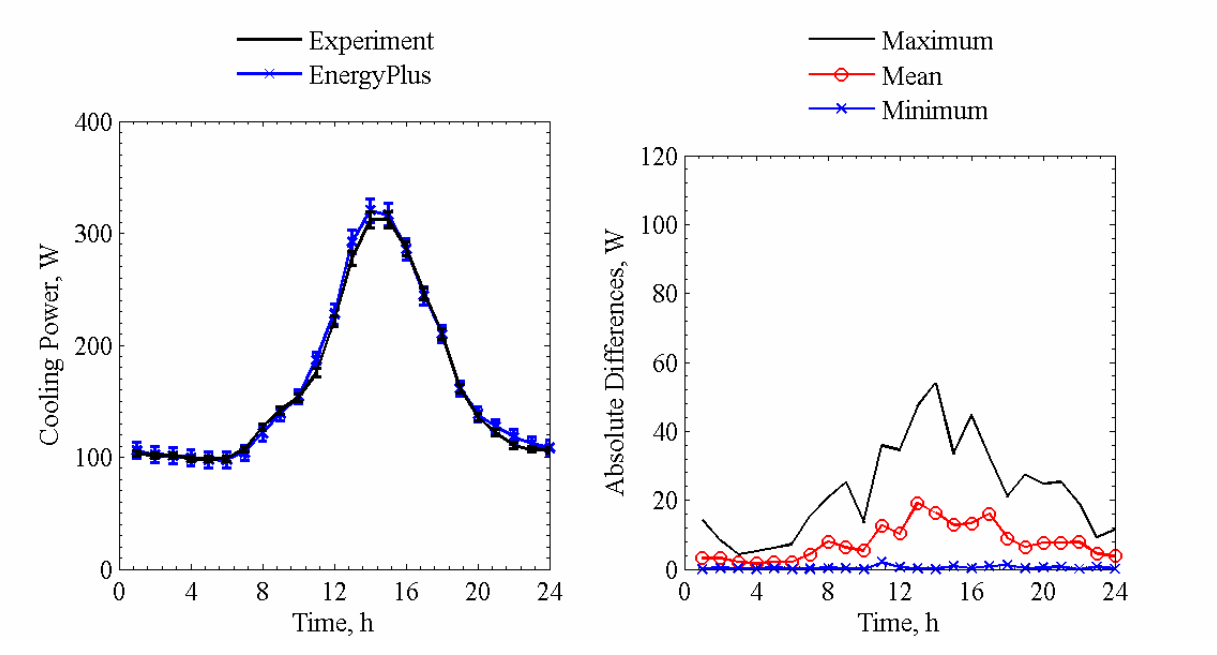


Figure 10.5b. Cooling power comparisons for EnergyPlus averaged over each given hour of the day (left) and absolute maximum, mean, and minimum differences for a given hour of the day (right).

Table 10.7. Overall uncertainty and 10 most influential input parameters from the n-way factorial analyses in Watts.

Parameter	Forward	Backward
Overall uncertainty	4.27	4.11
West wall surface temperature	2.13	-2.13
Floor surface temperature	1.77	-1.77
Average air temperature	-1.68	1.68
East wall surface temperature	1.04	-1.03
Fan power	0.87	-0.87
Ceiling surface temperature	0.82	-0.82
Outside air temperature	0.74	-0.74
North wall surface temperature	0.66	-0.66
Front reflectance of inner glass pane	-0.50	0.10
Global horizontal infrared irradiance	0.43	-0.43

Table 10.8. Statistical comparisons for cooling power in Exercise 7 with slats tilted 45° downward.

Parameter	Experiment	HELIOS	EnergyPlus
$\overline{x}$	163.1 W	171.4 W	165.4 W
S	97.8 W	108.5 W	100.6 W
$x_{max}$	519.9 W	577.9 W	546.0 W
$\mathcal{X}_{min}$	66.7 W	77.4 W	66.4 W
$\frac{x_{min}}{\overline{D}}$	-	-8.2 W	-2.3 W
$ \overline{D} $	-	11.6 W	7.8 W
$ D_{max} $	-	105.9 W	53.8 W
$ D_{min} $	-	0.0 W	0.0 W
$D_{rms}$	-	19.1 W	11.9 W
/D/ <sub>95%</sub>	-	45.8 W	28.7 W
$\overline{OU}$	3.7 W	-	7.6 W
$\overline{UR}$	-	0.9	0.6
$UR_{max}$	-	6.9	3.1
$UR_{min}$	-	0.0	0.0
$ \overline{D} /\overline{x} \times 100\%$	-	7.1%	4.8%
$\overline{D}/\overline{x} \times 100\%$	-	-5.1%	-1.4%

Figure 10.6 contains a plot of the transmitted solar power for a given hour of the day through the glazing unit and 45° downward positioned exterior Venetian blind slats for all programs.

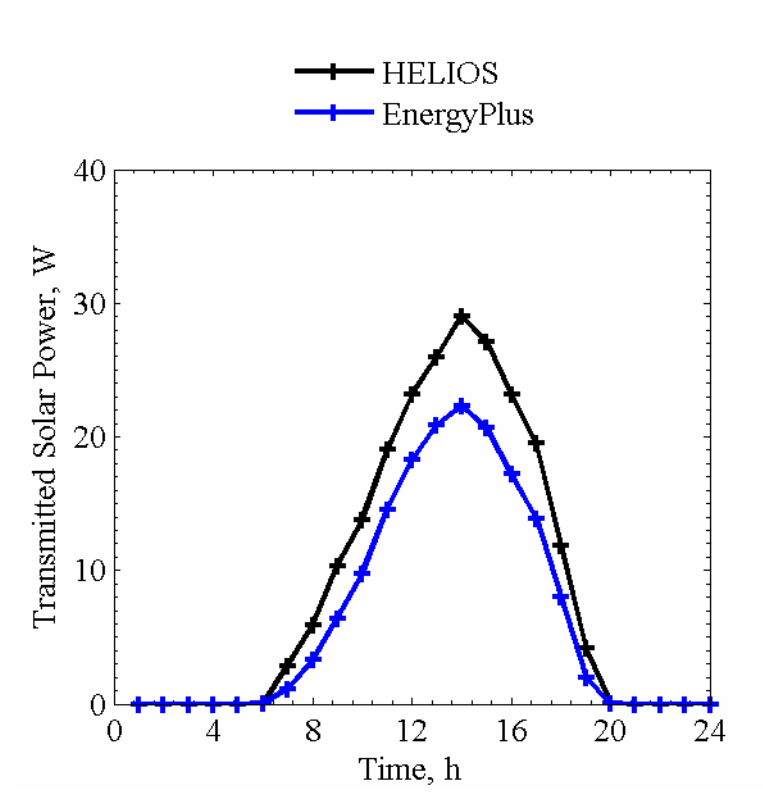


Figure 10.6. Transmitted solar power averaged over each given hour of the day.

Differences like those seen for the exterior blind assembly exercise were also apparent for this exercise.

# **Chapter 11: Window (Exercise 8)**

An experiment was run from June 25 to July 19, 2006 in the EMPA test cell that was designed to evaluate the impact of solar gains through a window (i.e. glazing unit and window frame). Information about the window, thermophysical properties evaluated at mean envelope temperatures, thermal bridges, and results from various programs are provided in this chapter.

# 11.1. Description of the Experiment

This section contains specific information about the experiment, which includes the following information:

- The placement and properties of the window
- A two-dimensional steady-state heat transfer simulation and hotbox measurements used to calculate the thermal bridges
- Thermophysical properties of the test cell envelope

A photograph of the test cell during the experiment is shown in Figure 11.1.



Figure 11.1. A photograph of the test cell.

### 11.1.1. Window Properties

For this experiment, a window was mounted in the southwest exterior wall of the test cell. The glazing unit properties from measured data are listed in Table 11.1. Additional measurements for the individual panes of glass as a function of wavelength are provided in "Experiment 8.xls". Properties of the individual panes are described in Table 11.2. The inside and outside reflectance and transmittance were calculated using European Standard EN 410 [7] with GLAD software [8]. For the individual panes of glass, the emittances were measured using an emissometer based on a calorimetric method. A dimensioned drawing of the exterior wall as seen from this inside of the test cell showing the position of the glazing is presented in Figure 11.2. The dimensions in meters of the glazing in the figure correspond to the aperture height and width. The window frame was painted white and the solar reflectance and emittance of the frame were approximated with the same optical properties of the exterior surface of 76.6% and 93%, respectively.

Table 11.1. Window optical properties.

Parameter	Quantity
Normal solar transmittance	53.7%
Normal solar exterior reflectance	23.3%
Normal solar interior reflectance	22.4%

Table 11.2a. Optical properties for the outer pane of glass (Clear Float Glass).

Parameter	Quantity
Normal solar transmittance	83.6%
Normal solar exterior reflectance	7.8%
Normal solar interior reflectance	7.7%
Outer emittance	85.3%
Inner emittance	87.3%

Table 11.2b. Optical properties for the inner pane of glass (Low-E Pro).

Parameter	Quantity
Normal solar transmittance	62.5%
Normal solar exterior reflectance	24.9%
Normal solar interior reflectance	20.0%
Outer emittance	8.5%
Inner emittance	87.3%

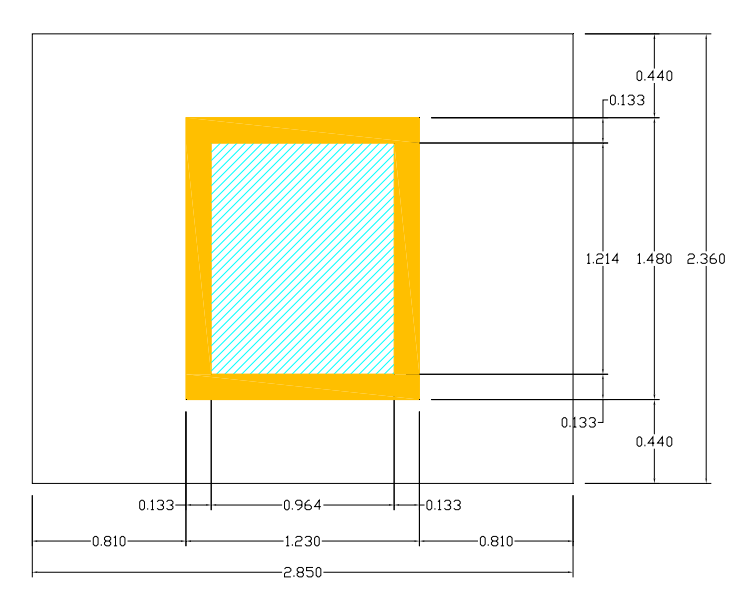


Figure 11.2. Position of the glazing in the exterior wall in meters (inside view).

# 11.1.2. Thermal Transmittances and Bridges

The impact of the thermal bridges due to the spacer, window frame, and mounting were all computed. The calculations for the linear thermal transmittances for the spacer and mounting and the overall thermal conductance of the window frame are described in this section using a two-dimensional software package called BISCO [13] and calorimetric measurements from the hotbox [17]. The results from the thermal bridge calculations and center-pane thermal transmittance and conductance of the window described in this section are summarized in Table 11.3. Preliminary quantities used for computing these properties are provided in another section.

Table 11.3. Summary of computed and measured thermal bridge properties and center-pane glazing properties.

Description	Symbol	Quantity
Center-pane thermal transmittance of the glazing unit	$U_C$	1.163 W/m <sup>2</sup> -K
Center-pane thermal conductance of the glazing unit	$\Lambda_C$	$1.449 \text{ W/m}^2\text{-K}$
Linear thermal transmittance for the spacer	$\psi_{sp}$	0.073 W/m-K
Thermal conductance of the window frame	$\Lambda_{WF}$	$1.643 \text{ W/m}^2\text{-K}$
Linear thermal transmittance for the mounting	$\psi_M$	-0.028 W/m-K

A dimensioned drawing of a cross section of the glazing unit, window frame, and mounting is shown in Figure 11.3. Table 11.4 contains a list of the materials used in the simulation, thermal conductivities, and coloring codings that correspond to Figure 11.3. The thermal conductivities were taken from literature and in-house measurements; temperature dependent thermophysical properties were fixed as the average between the outer and inner air temperatures for the south wall.

Table 11.4. Materials and thermal conductivities

Material	Thermal Conductivity, W/m-K	Color-coding		
Desiccant	0.130			
Aluminum	220.0			
Steel	50.0			
Stainless steel (spacer)	17.0			
Polyisobutylene	0.200			
Butyl	0.240			
Argon 90%/Air 10%	0.029			
Glass	1.0			
Frame	0.110			
Plywood	0.1381			
EPS foam	0.03483			
Soft rubber	0.100			
Weather stripping	0.050			
Insulation panel (Figure 11.4 right)	0.0409			

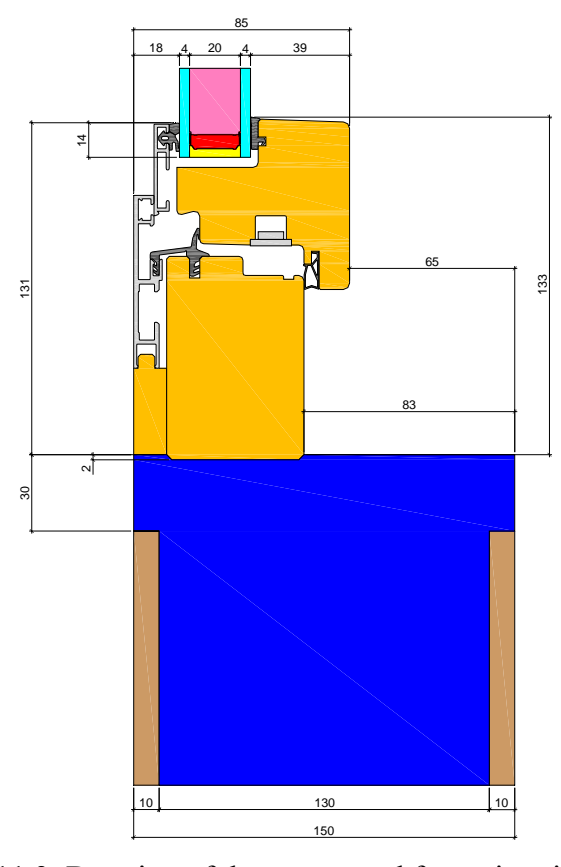


Figure 11.3. Drawing of the spacer and frame in millimeters.

# 11.1.2.1. Linear Thermal Transmittance of the Spacer

The impact of the spacer was calculated using a two-dimensional drawing of the spacer/frame assembly. The linear thermal transmittance of the spacer was evaluated according to preEN ISO 10077-2 [6]. During the hotbox measurements, the heat flux through the center of the window pane was measured and a center-pane thermal transmittance was computed. From this measurement, an equivalent conductivity was computed in the argon filled glazing cavity that factored in the impact of conduction, convection, and radiation. The thermal transmittance was also used to compute an equivalent thermal conductivity of the insulation panel for replacing the glazing unit in the frame as (which deviates slightly from standard which specifies a fixed equivalent thermal conductivity). Figures 11.4 show the bitmaps used for the simulations. Equivalent thermal conductivities of the air cavities were calculated according to preEN ISO 10077-2. The linear thermal transmittance due to the spacer,  $\psi_{sp}$ , was computed using Equation 11.1 using results from the BISCO simulations.

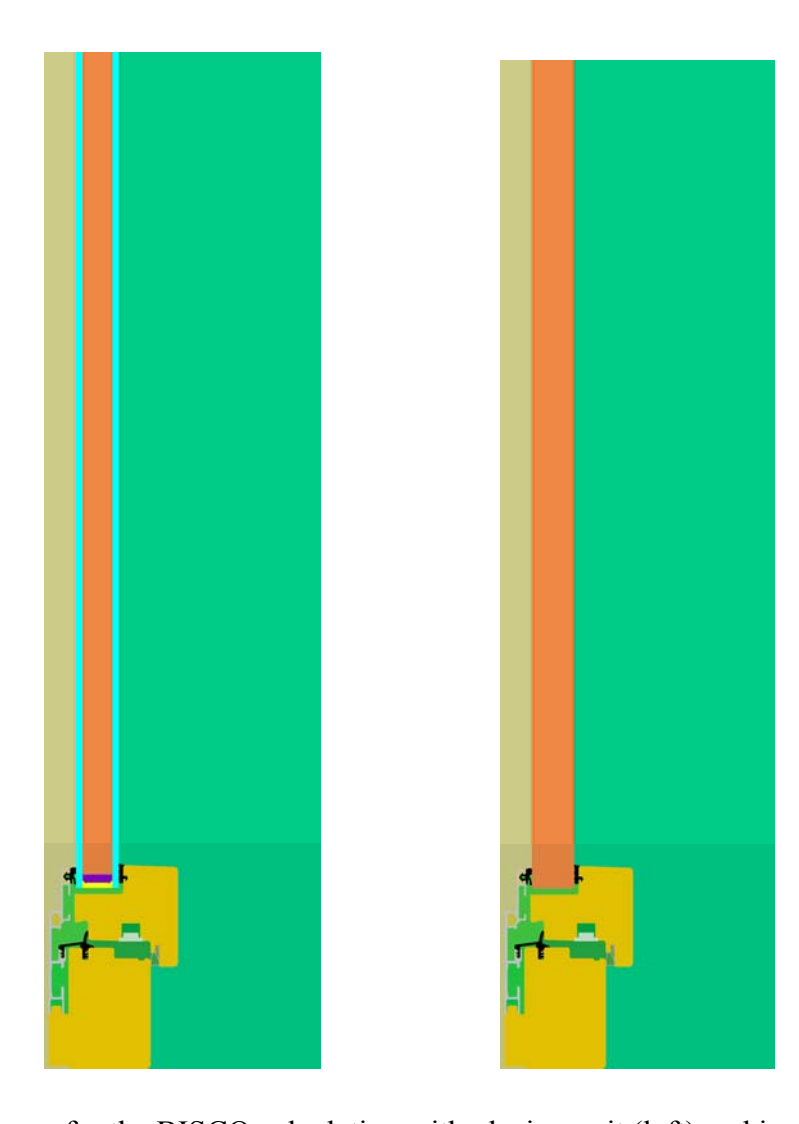


Figure 11.4. Bitmaps for the BISCO calculation with glazing unit (left) and insulation panel (right).

$$\psi_{sp} = \frac{Q'_{sp} - Q'_{ins}}{\theta_i - \theta_s} \tag{11.1}$$

where

 $Q'_{sp}$  is the heat flow per unit length from the BISCO simulation through the glazing unit and window frame,

Q'ins is the heat flow per unit length from the BISCO simulation through the insulation panel and window frame.

 $\theta_i$  is the inside air temperature, and

 $\theta_i$  is the outside air temperature.

#### 11.1.2.2. Thermal Conductance of the Window Frame

The thermal transmittance of the window frame was computed by using the BISCO simulation and the results from the linear thermal transmittance for the spacer and the one-dimensional heat transfer assumed by the building energy simulation programs. For this calculation, the window frame was assumed to have fixed height. Linear temperature profiles were assumed across the window frame for the steady one-dimensional heat transfer calculation. The thermal conductance (note this is not thermal transmittance because it does not include heat transfer coefficients) of the frame,  $\Lambda_{WF}$ , was calculated using Equation 11.2.

$$\Lambda_{WF} = \left[ \frac{L_{WF}}{\frac{Q'_{sp}}{\theta_i - \theta_o} - \psi_{sp} - L_{GL}U_c} - \frac{1}{h_i} - \frac{1}{h_o} \right]^{-1}$$
(11.2)

where

 $L_{WF}$  is the height of the window frame for the simulation,

 $L_{GL}$  is the height the glazing unit extends out past the frame in the two-dimensional simulation,

 $h_i$  is the inside combined heat transfer coefficient, and

 $h_o$  is the outside combined heat transfer coefficient.

# 11.1.2.3. Linear Thermal Transmittance Due to Mounting

A linear thermal transmittance due to the mounting of the window in the frame was computed by coupling BISCO simulation results with hotbox measurements. Therefore the results for the calculation also include thermal bridges from the spacer and frame {non-homogeneities (i.e. screws, and frames) and corner effects from the window frame and the spacer}. For this calculation, an assumption was made that the outer wall was composed entirely of homogeneous layered material specified for the building energy simulation programs; however, this is not the case because an additional 30 mm of insulation was added near the edge of the window opening for mounting the window. This additional thermal resistance is also included in the linear thermal transmittance computation to quantify mounting effects. The hotbox measurements were also considered quasisteady state and a linear temperature profiles across each material were assumed for the one-dimensional calculations. Measured film coefficients from the experiment were used for computing this quantity instead of the combined heat transfer coefficients used in the simulations. Equation 11.3 was used to calculate the one-dimensional thermal transmittance,  $UA_{1D}$ , through the window frame, outside wall, and the glazing unit. Temperature dependent thermophysical properties were fixed at the mean temperature of the hot and cold chambers.

$$UA_{1D} = A_{wall} \left( R_C + \frac{2d_p}{\lambda_p} + \frac{d_e}{\lambda_e} + R_H \right)^{-1} + A_{WF} \left( R_C + \frac{1}{\Lambda_{WF}} + R_H \right)^{-1} + A_{GL} \left( R_C + \frac{1}{\Lambda_C} + R_H \right)^{-1}$$
(11.3)

where

 $A_{wall}$  is the area of the outside wall in the hotbox,

 $R_C$  is the measured film resistance of the air in the cold chamber,

 $R_H$  is the measured film resistance of the air in the hot chamber,

 $d_p$  is the width of the plywood,

 $\lambda_p$  is the thermal conductivity of the plywood,

 $d_e$  is the width of the eps foam,

 $\lambda_e$  is the thermal conductivity of the eps foam,

 $A_{WF}$  is the area of the window frame, and

 $A_{GL}$  is the exposed area of the glazing unit.

The linear thermal transmittance of the mounting,  $\psi_M$ , was calculated using Equation 11.4. The quantity computed from Equation 11.4 was negative (Table 11.4), indicating that the thermal resistance in one-dimension plus the additional thermal bridging from the spacer and frame was less than the measurements.

$$\psi_{M} = \frac{Q_{HB}}{\theta_{H} - \theta_{C}} - UA_{1D} - \psi_{SP}P_{SP} - P_{M}$$
(11.4)

where

 $Q_{HB}$  is the total heat transfer through the construction element,

 $\theta_H$  is the temperature of the hot chamber of the hot box,  $\theta_C$  is the temperature of the cold chamber of the hot box,

 $P_{SP}$  is the perimeter of the exposed glazing unit, and

 $P_M$  is the outer perimeter of the window frame.

A BISCO simulation was also run to examine the heat flow and a picture of the frame, mounting, and spacer with heat flow lines are shown in Figure 11.5.

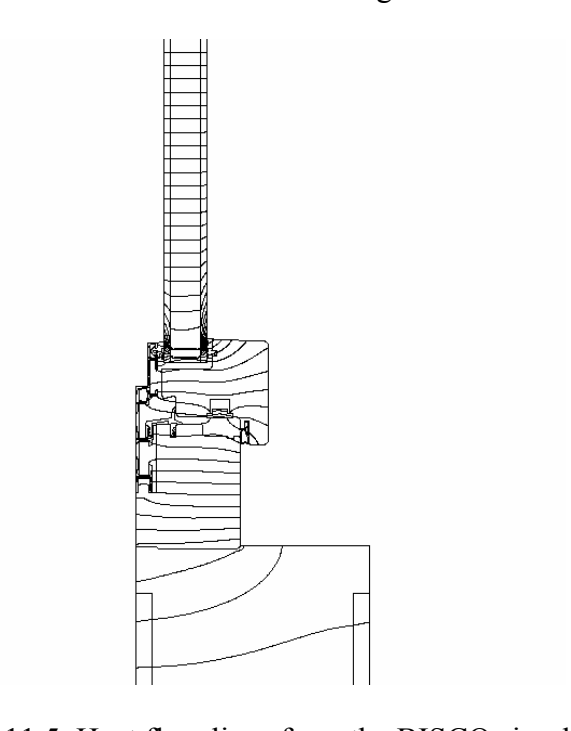


Figure 11.5. Heat flow lines from the BISCO simulation.

# 11.1.2.4. Quantities Used for the Calculations

The quantities used for computing the impact of the thermal bridges from the simulation and the hotbox measurements are contained in Tables 11.5a and 11.5b, respectively.

Table 11.5a. Values used for the BISCO simulations.

Description	Symbol	Quantity
Width of the eps foam	$d_e$	0.130 m
Width of the plywood	$d_p$	0.010 m
Inside combined heat transfer coefficient for the simulation	$h_i$	$7.7 \text{ W/m}^2\text{-K}$
Outside combined heat transfer coefficient for the simulation	$h_o$	$25.0 \text{ W/m}^2\text{-K}$
Height of the window frame for the simulation	$L_{WF}$	0.133 m
Height the glazing unit extends out past the frame in the two-	$L_{GL}$	0.55 m
dimensional simulation		
Inside air temperature	$\theta_{i}$	20.0 °C
Outside air temperature	$\theta_o$	0.0 °C
Heat flow per unit length from the BISCO simulation through	$Q'_{sp}$	17.67 W/m
the glazing unit and window frame	•	
Heat flow per unit length from the BISCO simulation through the	$Q$ ' $_{ins}$	16.21 W/m
insulation panel and window frame		

Table 11.5b. Measurements from the hotbox.

Description	Symbol	Quantity
Area of the wall	$A_{wall}$	$3.196 \text{ m}^2$
Area of the glazing	$A_{GL}$	$1.170 \text{ m}^2$
Area of the window frame	$A_{W\!F}$	$0.650 \text{ m}^2$
Width of the eps foam	$d_e$	0.130 m
Width of the plywood	$d_p$	0.010 m
Perimeter of the exposed glazing unit	$P_{SP}$	4.356 m
Outer perimeter of the window frame	$P_{M}$	5.420 m
Measured film resistance of the air in the cold chamber	$R_C$	$0.057 \text{ m}^2\text{-K/W}$
Measured film resistance of the air in the hot chamber	$R_H$	$0.134 \text{ m}^2\text{-K/W}$
Thermal conductivity of the plywood for the experiment	$\lambda_p$	0.1385 W/m-K
Thermal conductivity of the eps foam for the experiment	$\lambda_e$	0.03509 W/m-K
Total heat transfer through the construction element	$Q_{HB}$	62.19 W
Air temperature of the hot chamber of the hot box	$\theta_{\!H}$	22.08 °C
Air temperature of the cold chamber of the hot box	$\theta_{C}$	2.01 °C
Baffle temperature of the hot chamber of the hotbox	$\theta_{\!BH}$	21.66 °C
Baffle temperature of the cold chamber of the hotbox	$\theta_{\!BC}$	2.06 °C

# 11.1.3. Thermophysical Properties of the Test Cell Envelope

The mean envelope temperatures for the construction elements are shown in Table 11.6. The thermophysical properties evaluated at these mean envelope temperatures are contained in Tables 11.7a to 11.7c.

Table 11.6. Mean envelope temperatures for experiment.

Construction element	Mean temperature, °C
Ceiling, east, west, and north walls	22.75
Floor	22.98
South wall	22.04

Table 11.7a. Ceiling, north, east and west wall constructions evaluated at 22.75°C.

Layer number	Material	Thickness mm	Thermal conductivity W/m-K	Density kg/m <sup>3</sup>	Specific heat J/kg-K
1	Sheet steel	0.7	53.62	7837	460.8
2	PU foam	139	0.02237	30	1800
3	Sheet steel	0.7	53.62	7837	460.8

Table 11.7b. Floor construction evaluated at 22.98°C.

Layer number	Material	Thickness mm	Thermal conductivity W/m-K	Density kg/m <sup>3</sup>	Specific heat J/kg-K
1	Sheet steel	0.7	53.62	7837	460.8
2	PU foam	140	0.02237	30	1800
3	PU foam (higher density)	20	0.070	45	1800
4	Sheet steel with surface Structure	2.5	53.62	7837	460.8

Table 11.7c. South wall construction elements evaluated at 22.04°C.

Layer number	Material	Thickness mm	Thermal conductivity W/m-K	Density kg/m <sup>3</sup>	Specific heat J/kg-K
1	Plywood	10	0.1403	850	1605
2	EPS foam	130	0.03645	28	1460
3	Plywood	10	0.1403	850	1605

#### 11.2. Results

The empirical validation for this exercise focused on comparing cooling power. Plots for cooling power from HELIOS, EnergyPlus, and DOE-2.1E are shown in Figures 11.5a to 11.5c, respectively. Two plots are contained in each figure. Table 11.8 contains overall and 10 most influential input uncertainties that impacted the cooling power predictions taken from the n-way factorial analysis. A summary of the statistical comparisons is contained in Table 11.9.

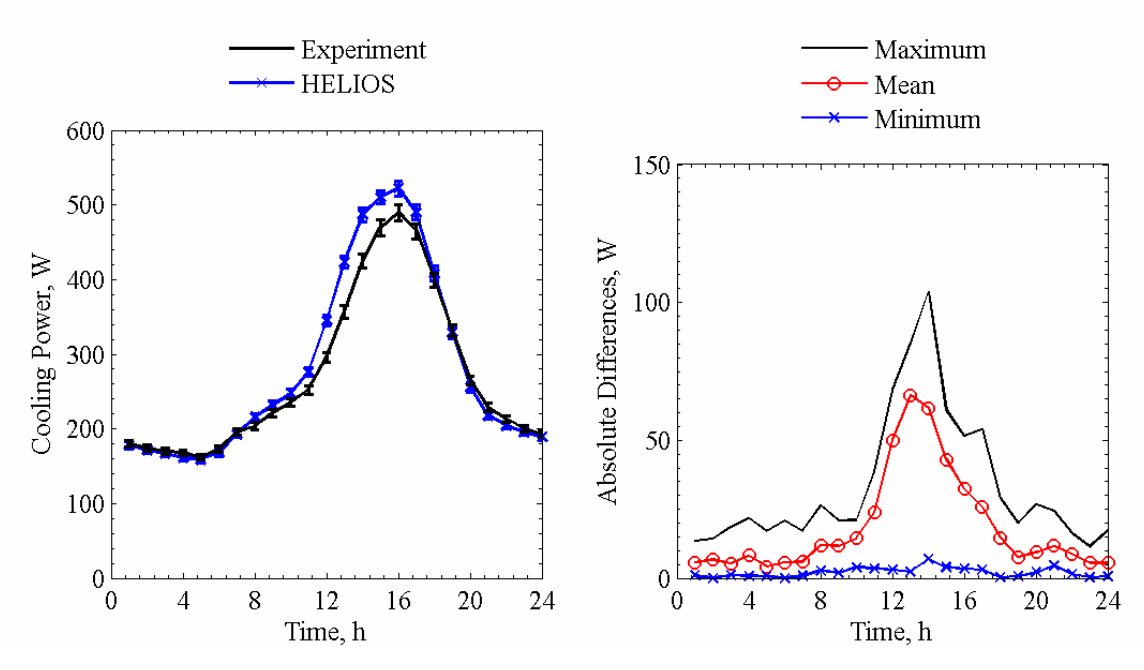


Figure 11.5a. Cooling power comparisons for HELIOS averaged over each given hour of the day (left) and absolute maximum, mean, and minimum differences for a given hour of the day (right).

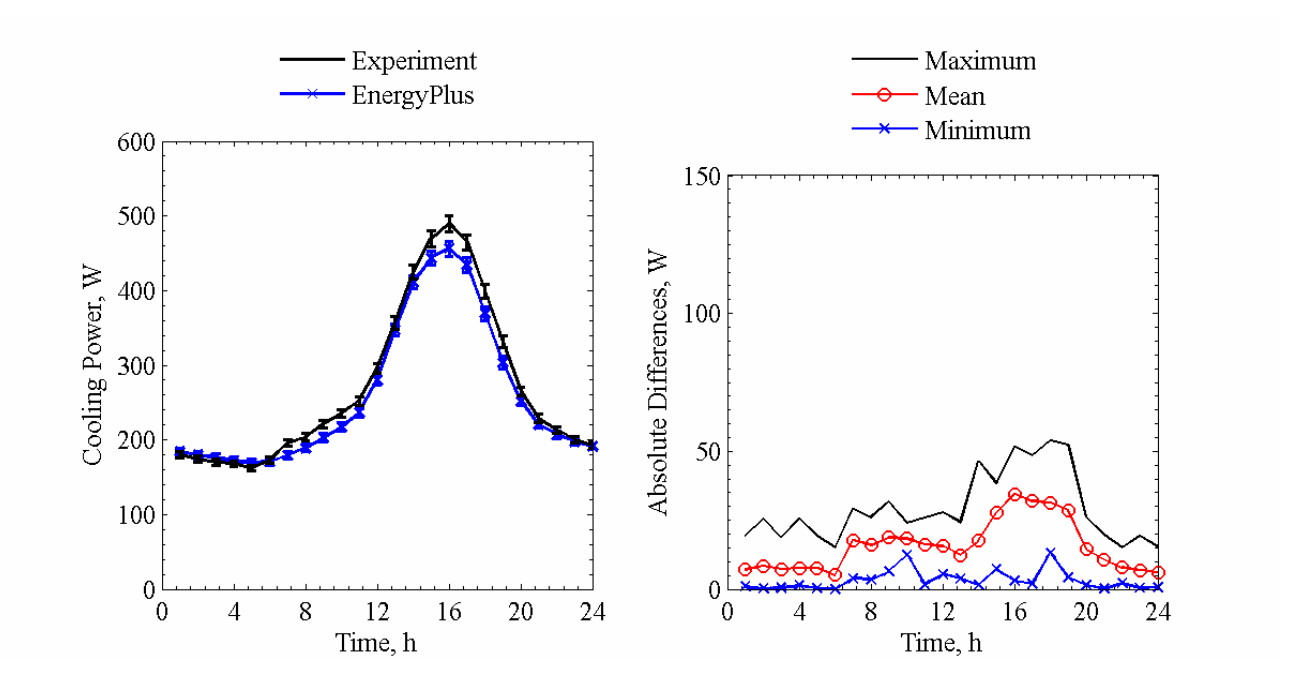


Figure 11.5b. Cooling power comparisons for EnergyPlus averaged over each given hour of the day (left) and absolute maximum, mean, and minimum differences for a given hour of the day (right).

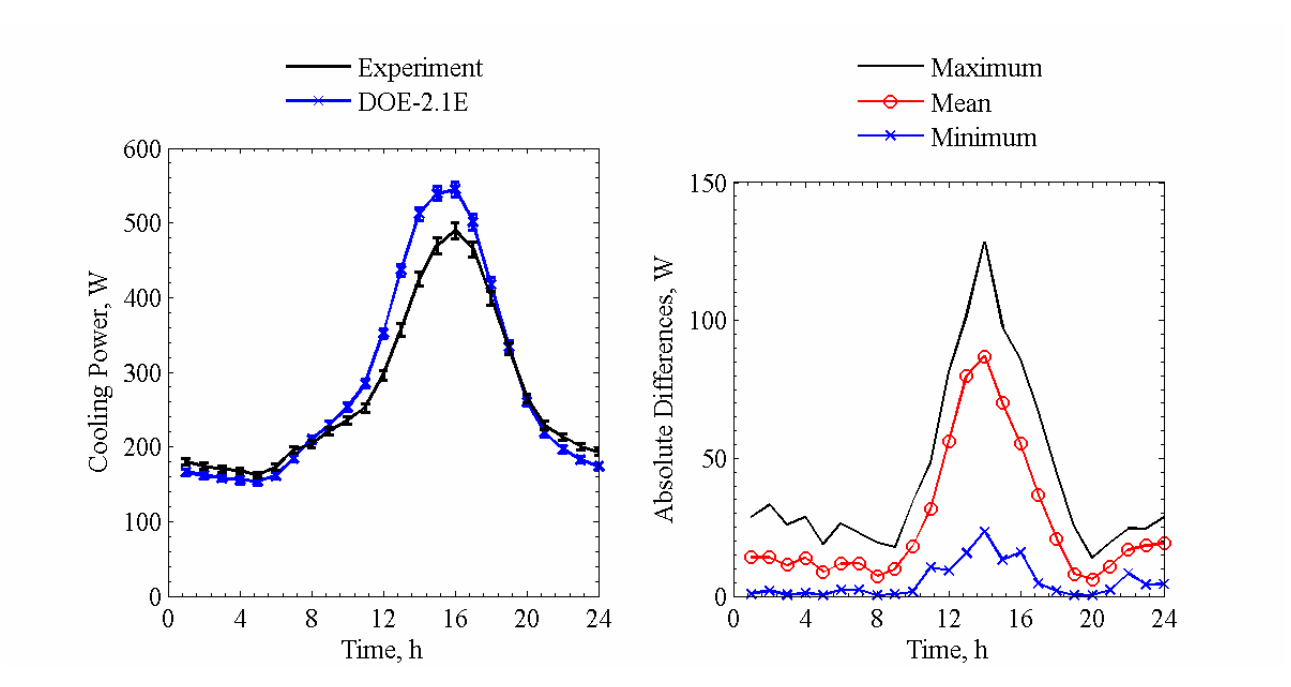


Figure 11.5c. Cooling power comparisons for DOE-2.1E averaged over each given hour of the day (left) and absolute maximum, mean, and minimum differences for a given hour of the day (right).

Table 11.8. Overall uncertainty and 10 most influential input parameters from the n-way factorial analyses in Watts.

Parameter	Forward	Backward
Overall uncertainty	3.39	3.40
Average air temperature	-1.88	1.88
Fan power	1.04	-1.04
West wall surface temperature	0.79	-0.79
Ceiling surface temperature	0.73	-0.73
North wall surface temperature	0.69	-0.69
East wall surface temperature	0.56	-0.56
Outside air temperature	0.56	-0.56
Direct-normal solar irradiance	0.55	-0.56
Diffuse horizontal solar irradiance	0.47	-0.50
Front reflectance of inner glass pane	-0.43	0.42

Table 11.9. Statistical comparisons for cooling power in Exercise 8.

Parameter	Experiment	HELIOS	EnergyPlus	DOE-2.1E
$\overline{x}$	269.5 W	281.2 W	257.8 W	282.8 W
S	112.8 W	130.8 W	101.4 W	141.5 W
$x_{max}$	576.2 W	614.4 W	524.5 W	637.0 W
$x_{min}$	133.1 W	145.3 W	158.0 W	143.0 W
$\overline{D}$	-	11.6 W	-11.7 W	13.3 W
$ \overline{D} $	-	18.6 W	15.7 W	26.6 W
$/D_{max}/$	-	103.9 W	54.0 W	128.4 W
$/D_{min}/$	-	0.0 W	0.0 W	0.2 W
$D_{rms}$	-	27.9 W	19.7 W	37.7 W
/D/ <sub>95%</sub>	-	69.7 W	40.8 W	88.0 W
$\overline{OU}$	6.1 W	-	6.3 W	-
$\overline{UR}$	-	1.3	1.2	1.9
$UR_{max}$	-	5.4	3.4	6.6
$UR_{min}$	-	0.0	0.0	0.0
$ \overline{D} /\overline{x} \times 100\%$	-	6.9%	5.8%	9.9%
$\overline{D}/\overline{x} \times 100\%$	-	4.3%	-4.3%	4.9%

Figure 11.6 contains a plot of the transmitted solar power for a given hour of the day through the glazing unit and interior shading screen for all programs.

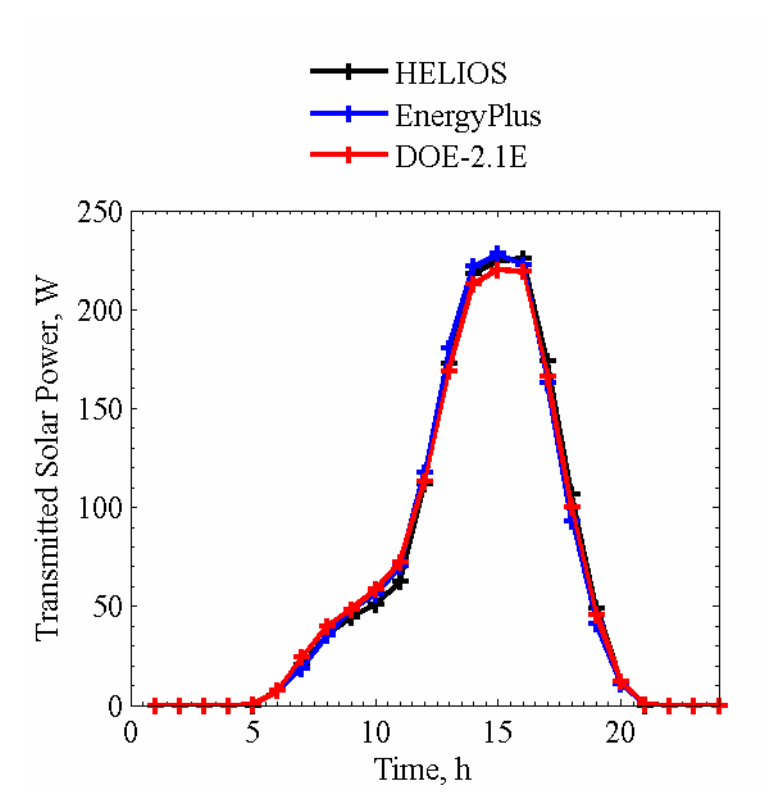


Figure 11.6. Transmitted solar power averaged over each given hour of the day.

Like in the glazing unit only exercise, the optical models used to simulating the glazing were very similar. Additional challenges were addressed in the building energy simulation programs concerning properly accounting for the thermal bridges due to the mounting, spacer, and window frame.

# **Chapter 12: Modeler's Reports**

For each exercise, the modelers performing the simulation were requested to provide a brief summary of methodology employed for modeling the experiments. During the course of the exercises, test specifications were and inputs were provided to modelers and results were submitted for blind exercise; the data were then provided to the participants to identify errors in program inputs. These errors and the associated changes are also documented by the modelers to provide guidance on common mishaps that can be made when simulating a building.

#### **12.1. HELIOS**

Name and Institution: Stephan Carl, Swiss Federal Laboratories for Material Testing and Research (EMPA), Laboratory for Building Technologies

Building Energy Simulation Software and Version: HELIOS XP

#### 12.1.1. General Information

HELIOS was developed at EMPA from 1982-1992 and is currently sold in Switzerland and Germany. A new initiative was started in 2004 to update software algorithms and develop a user-friendly interface for use with the Microsoft Windows operating system. The latest version of the program called HELIOS XP was released in November 2006. The software is now only available in German; however, an English version of the software is currently under development.

### 12.1.2. Transient Experiment Modeling (Exercise 1)

This exercise was simulated assuming constant convective heat transfer coefficients for each construction element as a function of surface orientation; these values were specified according to EN/ISO 6946 [18], and radiative heat transfer was neglected. For all simulations exercises, hourly outside surface temperatures and power input were scheduled into the program. The thermal bridges were accounted for with a fictitious wall of the same construction as the ceiling and interior walls and an equivalent area that corresponded to the overall thermal bridge conductance. The thermal mass inside the test cell was simulated as an internal construction element made of thin steel and appropriate dimensions were chosen to match the estimated thermal mass from specified in the experiments.

### 12.1.3. Evaluation of Irradiation Models on Tilted Surfaces (Exercise 2)

HELIOS uses a Perez 1987 model [19] to estimate radiation on a tilted facade. When implementing this model, the program accounted for elliptical orbit of the earth when computing extraterrestrial radiation. For this exercise and the subsequent solar gain exercises, global and diffuse horizontal solar irradiances were used as inputs to the program.

# 12.1.4. Glazing Only Experiment (Exercise 3)

A glazing unit was added to exterior wall in the model in Exercise 1. The external thermal bridge was then included with the linear thermal transmittance from the spacer. The emittance of glazing unit was adjusted in HELIOS to match the measured center-pane thermal transmittance. The solar normal transmittances and reflectances for each pane of glass and measured emittance were input into the program and an angular-dependent model described in the Window 4.1 manual [20] was employed to calculate optical properties of the glazing unit. Radiative heat transfer was accounted for in the test cell by using simulated average interior surface construction element temperatures and emittances to calculate a radiative heat transfer coefficient according to EN/ISO 6946. This

methodology linked the construction element surface temperatures to the interior test cell air node; convection was specified in the same manner as in Exercise 1.

No changes were made to the blind results.

### 12.1.5. Exterior and Interior Shading Screens (Exercises 4 and 5)

Exercises 4 and 5 used the same model as in Exercise 3 with the addition of shading screens. The exterior and interior shading screens were modeled as additional sheets of thin sheet of glass with inputs of normal solar reflectance and transmittance. The air gap calculations between the shading screens and the glazing unit were made according to an algorithm developed by Chauval and Millet [21]. The hemispherical emittances of the shading screens were estimated as 90%.

No changes were made to the blind results.

### 12.1.6. Exterior Venetian Blind and Internal Mini-Blind Assemblies (Exercises 6 and 7)

Exercises 6 and 7 used the same model as in Exercise 3 with the addition of interior and exterior blind assemblies. The blind model in HELIOS calculates two-dimension diffuse geometric view factors that account for curvature in the blind slat. The input optical properties were normal solar reflectance and hemispherical emittance. The underlying theory concerning the blind model is given by Simmler [22]. The air gaps between the blind assemblies and the glazing unit were modeled like in Exercises 4 and 5.

No changes were made to the blind results.

#### **12.1.7. Window (Exercise 8)**

Exercise 8 was simulated in the same manner as Exercise 3. The addition of the frame was accounted for by adding and additional thermal bridge that accounted for spacer, mounting, and window frame transmittances. In this version of HELIOS, energy absorbed by the window frame via longwave and/or solar radiation is neglected.

No changes were made to the blind results.

#### 12.1.8. Discussion of Results

HELIOS was used to simulate all exercises. For the eight exercises, the results for predicted cooling power were within 95% credible limits four times. HELIOS performed best for the glazing unit only and interior shading screen exercises.

#### 12.1.9. Validation Impact

Numerous changes to HELIOS were made as a result of this validation effort. The titled radiation model of the façade was changed from an Isotropic model to a Perez 1987 model and ground reflectance was made a user input. A new angular-dependent optical model was added for simulation of glazing units, and a blind assembly algorithm was implemented into the program. Changes were also implemented into the program to accommodate hourly schedules for internal loads and inside air and outer surface temperatures.

An error was discovered in the course of these validations in the thermal transmittance of the glazing unit. In the calculation, the thermal conductivities of the glass panes were neglected when computing the center-pane thermal transmittance.

## 12.2. EnergyPlus

Modeler and Institution: Peter Loutzenhiser, Swiss Federal Laboratories for Material Testing and Research (EMPA), Laboratory for Building Technologies

Building Energy Simulation Software and Versions:

Exercise 1: EnergyPlus Version 1.2.0.029 Exercise 2-3: EnergyPlus Version 1.2.2.030 Exercise 4-8: EnergyPlus Version 1.2.3.023

#### 12.2.1. General Information

The development of EnergyPlus began in 1996 as an initiative by the US Department of Energy; the first version of the software was released to the public in Spring 1998. Detailed information concerning the concept and development of the program is described in detail by Crawley et al. [23]

### 12.2.2. Transient Experiment Modeling (Exercise 1)

Exercise 1 was simulated using specifications and fixed thermophysical properties (as were subsequent exercises). Measured hourly outer surface temperatures and internal loads were used as program inputs. The thermal bridges were simulated in EnergyPlus by adding non-radiating surfaces to the back of the space with a constant outer cell surface temperature of 23.22 °C, which was the time-averaged outer cell surface temperature during the transient experiment. Because EnergyPlus calculates the radiative heat transfer using view factors and assuming gray and diffuse surfaces, six additional surfaces that faced each other were added to the model. The convective heat transfer coefficients for these surfaces were fixed and an equivalent area based on the thermophysical properties of the thermal bridge construction elements and was used to compute an equivalent area that accounted for total steady-state thermal bridge transmittance. For the other surfaces, a detailed approach was used to compute the convective heat transfer coefficient as a function of temperature difference between surface and cell air and surface orientation.

# 12.2.3. Evaluation of Irradiation Models on Tilted Facades (Exercise 2)

In EnergyPlus, a Perez 1990 model [24] was used to predict tilted surface solar irradiance using direct-normal and diffuse horizontal solar irradiances. The exercise was performed using weather data in 10 minute time intervals. In the EnergyPlus Perez 1990 algorithm, a constant averaged extra-terrestrial radiation is assumed for the whole year that does not account for the elliptical orbit of the earth around the sun.

### 12.2.4. Glazing Only Experiment (Exercise 3)

Exercise 3 was simulated by adding a glazing unit to the exterior façade of the model used in Exercise 1. Hourly internal loads, outer surface temperatures for the internal construction elements, and average air temperatures were scheduled into the program. For both panes of glass, reflectances and transmittances at near-normal incident angle in the wavelength interval between 250 and 2500 nm were used as inputs for EnergyPlus so that angular dependent calculations similar to those found in Window 5.2 could be made. The edge effects were modeled by modifying the "Ratio of Frame-Edge Glass Conductance" field. In EnergyPlus, the edge is defined as a 63.5 mm distance from the frame; therefore, an additional simulation was run in BISCO [13] software applying the same procedure described above to calculate a new center-of-glazing thermal transmittance using this definition. The impact of thermal bridges at the external wall edges was accounted for by adding additional thermal transmittance to the glazing edge calculation. Because EnergyPlus employs an algorithm for equivalent thermal conductivity of the glazing cavity that provides slightly higher values than those calculated above, the thermal conductivities of the glass

were reduced accordingly. A general overview for modeling windows in EnergyPlus is provided by Winkelmann [25]. Six hourly time steps were used with weather data at 10-minute intervals.

No changes were made from the blind to the non-blind exercise.

### 12.2.5. Exterior and Interior Shading Screen (Exercises 4 and 5)

The same model from Exercise 3 was used with the addition of exterior (Exercise 4) and interior (Exercise 5) shading screens. In the EnergyPlus optical model, all window layers such as glass panes and shading device(s), are assumed to be flat, parallel, and infinite. System reflectances and transmittances are computed based on a ray tracing technique. Spectral optical properties can be used for determining glazing reflectance and transmittance. The shading screen is, however, modeled using only a non-spectral method. The integral solar transmittances and reflectances of the screen based on measurements were used as program inputs. The ratios of the open sides as well as the openness factors of the shading devices were calculated and entered into the program. The screen thickness was assumed to be 0.5 mm and estimates for screen thermal conductivities (0.9 Wm<sup>-1</sup>K<sup>-1</sup>) were taken from ASHRAE Fundamentals [26]; these parameters were of very minor importance. The methodology employed to calculate the total heat transfer between the shade and the window in the program was taken from EN ISO 15099 [27], which factored in surface temperatures of the glazing and the screens to calculate the heat transfer through the air gap at each time step. According to a methodology proposed in [28], the emittances of the shading screens were assumed to be the product 0.9/(1-openness factor). The calculation performed in EnergyPlus assumed buoyancy driven flow. Weather data measured in 10 min intervals were input into the program as boundary conditions.

No changes were made from the blind to the non-blind exercises.

#### 12.2.6. Exterior Venetian Blind and Interior Mini-Blind Assemblies (Exercises 6 and 7)

The same model from Exercise 3 was used with the addition of exterior (Exercise 6) and interior (Exercise 7) shading screens. In the EnergyPlus optical model EnergyPlus contains a blind model that assumes flat diffuse slats [28] similar to the model proposed in prEN 13363-2 [29]. The slat's normal solar reflectance, hemispherical emittance, width, thickness, distance from the outer pane of glass (measured from the center of the blind slats), and distance between individual slats were entered into the program. The heat transfer between the window and the shading devices was calculated using ISO 15099 [27] assuming natural buoyancy; this was performed as an iterative procedure in the program.

No changes were made from the blind to the non-blind exercises.

#### **12.2.7. Window (Exercise 8)**

A window was specified in the exterior façade using the model from Exercise 1. Measured reflectances and transmittances for each pane of glass from 250 nm or 2500 nm were input in EnergyPlus as well as emittance. The thermal conductivities of the glass panes were reduced to match the thermal conductance measured from the hotbox due to the same constraints discussed in Exercise 3. The linear thermal transmittance due to the mounting was included in the overall window frame conductance as well as the external wall thermal bridge. The spacer effects were computed using the definition of edge-effects (Section 12.2.4) for EnergyPlus.

No changes were made from the blind to non-blind exercises.

#### 12.2.8. Discussion of Results

EnergyPlus was used to simulate every exercise. For this suit of experiments, EnergyPlus was within the overlapping 95% credible limits described by the uncertainty ratio for Exercises 1,4,6,

and 7 and outside 95% credible limits for the other exercises. The program performed best when simulating blind assemblies (both interior and exterior).

# 12.2.9. Validation Impact

During these validation exercises, it was discovered that input blind schedule inputs to specify the blind slat angle, the input was expected in radians but prescribed in degrees; this problem was fixed in Version 1.2.3.023.

#### 12.3. DOE-2.1E

Modeler and Institution: Peter Loutzenhiser, Swiss Federal Laboratories for Material Testing and Research, Laboratory for Building Technologies

Building Energy Simulation Software and Version: DOE-2.1E Version-119

#### 12.3.1. General Information

The original version of DOE-2.1E was released in November 1993 from Lawrence Berkley National Laboratories. DOE-2 was developed by Lawrence Berkeley National Laboratory, Hirsch & Associates, Consultants Computation Bureau, Los Alamos National Laboratory, Argonne National Laboratory and University of Paris. Major support was provided by the U.S. Department of Energy; additional support was provided by the Gas Research Institute, Pacific Gas & Electric Company, Southern California Edison Company, Electric Power Research Institute, California Energy Commission and others [30].

## 12.3.2. Transient Experiment Modeling (Exercise 1)

Exercise 1 was simulated using specifications and fixed thermophysical properties (as were subsequent exercises). To use the outer surface temperatures as boundary conditions, adjacent zones were created with a single zone air conditioner for each test cell surface. The zone temperature was scheduled as the outer cell surface temperature. The inside film resistance for these zones was specified as zero, thus making the adjacent zone temperature and the outer cell surface temperature equal. Because the inside surface temperatures of the construction elements were nearly the same the effect of radiative heat transfer between the surfaces was neglected. The inside film coefficients for the walls, ceiling and floor were specified according to EN ISO 6946 [18] considering only convective heat transfer. The thermal mass inside the cell was modeled as a steel sheet.

### 12.3.3. Evaluation of Irradiation Models on Tilted Facades (Exercise 2)

In DOE-2.1E, a Perez 1990 model [19] was used predict tilted surface solar irradiance using direct-normal and global horizontal solar irradiances. The exercise was performed using weather data in one hour time intervals. In the DOE-2.1E Perez 1990 algorithm, a constant averaged extraterrestrial radiation is assumed for the whole year that does not account for the elliptical orbit of the earth around the sun.

# 12.3.4. Glazing Only Experiment (Exercise 3)

Exercise 3 was simulated by adding a glazing unit to the exterior façade of the model used in Exercise 1. For DOE-2.1E, the glazing unit was modeled using Window 5.2 [31] coupled with wavelength-dependent near-normal optical measurements from a custom database file from Optics5 (Rubin et al. [32]). Background information for this type of modeling is provided by Reilly et al. [33]. Because there was no quantitative input for edge effects in DOE-2.1E (there were spacer types), a 3.0 cm window frame was modeled with an equivalent thermal conductivity to account for

the edge effects, exterior thermal bridges, one-dimensional heat transfer of the construction displaced by the frame, and two-dimensional heat transfer. The thermal transmittance from the Window 5.2/DOE-2 output file was modified to reflect the center-of-glazing thermal transmittance calculated above with adjustments made to account for different heat transfer coefficients. Hourly weather data were put into TMY2 weather format and read into the program; the outputs were verified with the measured data. In TMY2 weather format, the horizontal infrared irradiance is not explicitly described; therefore, the opaque sky cover quantity from the weather inputs (including the infrared irradiance) was calculated by reversing the algorithm used to calculate infrared irradiance in the program (Walton [34]; Clark and Allen [35]). Measured direct-normal and global horizontal solar irradiance were used as inputs for the calculations of the global vertical solar irradiance on the external façades. Combined constant heat transfer coefficients that factored in the impact of radiation and convection as a function of surface orientation using design standards were taken from 2001 ASHRAE Handbook—Fundamentals [26].

No changes were made from the blind to the non-blind exercise.

### 12.3.5. Exterior and Interior Shading Screen (Exercises 4 and 5)

The same model for Exercise 3 was used for these experiments with the addition of shading devices. The optical model of DOE-2.1E is much simpler than the EnergyPlus model. The transmitted solar energy through the glazing unit is reduced by the integral solar transmittance of the shading screen (i.e., no solar radiation reflected from the glazing and then back-reflected into the room is taken into account). Because the outer surface temperature of the glazing unit and the screen were not known, a less robust method was used to account for the heat transfer in the gap between the shade and the window. The amount of additional heat transfer through the gap between the glazing and the shading screen was calculated assuming the same screen properties used for EnergyPlus and the thermal resistance for a well-ventilated air layer using EN ISO 6946 [18].

No changes were made from the blind to the non-blind exercises.

#### **12.3.6. Window (Exercise 8)**

A window was specified in the exterior façade using the model from Exercise 1. Measured reflectances and transmittances for each pane of glass from 250 nm or 2500 nm were input in DOE-2.1E using Optics and Window 5.2 output file. The linear thermal transmittances due to the spacer and mounting and the external wall thermal bridge were included in the overall window frame conductance.

No changes were made from the blind to non-blind exercises.

#### 12.3.7. Discussion of Results

DOE-2.1 was used to simulate Exercises 1-5 and 8. Currently, DOE-2.1E or subsidiary software do not contain algorithms necessary for simulated complex window shading devices like Venetian blinds and mini-blinds. For this suit of experiments, DOE-2.1E was within the overlapping 95% credible limits described by the uncertainty ratio for Exercises 1 and 4 and outside 95% credible limits for the other exercises; however, the results were comparable with other programs with more advanced shading and heat transfer algorithms.

# **12.4. IDA-ICE**

Name and Institution: Sven Moosberger, University of Applied Science of Central Switzerland (HTAL), Forschungsbereich Architektur+Technologie (A+T)

Building Energy Simulation Software and Version: IDA-ICE 3.0 Build 14

#### 12.4.1. General Information

IDA is a simulation environment developed at the Royal Institute of Technology (KTH) in Stockholm, Sweden. Today it is maintained and supported commercially by EQUA SA in Stockholm. One application of IDA is IDA-ICE designed for thermal building simulations. IDA-ICE dynamically simulates room air temperatures, mean radiant temperatures at any point in a room, air humidity, and CO<sub>2</sub> concentrations and employs an adaptive time step. The distribution of incoming solar and longwave radiation to all room surfaces are calculated using a view factor method. Both IDA simulation environments and IDA-ICE employ various user levels which include:

- IDA room level for very simple simulations that are restricted to one room (web based freeware)
- IDA-ICE standard level with a graphical user interface for multiple zone buildings with HVAC System
- IDA-ICE advanced level for detailed model building, free variable linking, and reporting
- IDA-ICE modeler level for simple model changes

In the next version of IDA-ICE, a new detailed window model is planned. This model, called "Detwind", is under development and was used for Exercise 3 of this empirical validation.

## 12.4.2. Transient Experiment Modeling (Exercise 1)

The thermal bridges inputs were modeled at the standard level and linked in the advanced level to the outer floor surface temperature. Hourly outer surface temperatures and internal loads were scheduled into the program at the advanced level. The longwave radiative heat transfer was simulated using view factors. A dynamic convective heat transfer coefficient algorithm that accounted the construction element length, orientation, and air and surface temperature differences was used. The thermal mass inside the test cell was modeled by increasing the volume of the air.

# 12.4.3. Evaluation of Irradiation Models on Tilted Facades (Exercise 2)

IDA-ICE currently has three models used for predicting tilted surface radiation, including: ASHRAE [36], Kondratjev [37], and Perez 1990 [24]. From this exercise, the Perez 1990 model was chosen to model subsequent solar gain experiments because the results corresponded best with measured global vertical irradiance on the southwest façade. Hourly direct-normal and diffuse horizontal solar irradiances were the inputs into the program. A model called the "climate processor" was used to calculate the sun position; these pre-calculations were then used in conjunction with the selected diffuse tilted surface radiation model.

# **12.4.4.** Glazing Only Experiment (Exercise 3)

The model from Exercise 1 was used with the addition of a glazing unit in the external construction element. The thermophysical properties were modified to account for changing mean building element temperatures; these modifications were also made in all subsequent exercises as well.

Three window models were used to simulate the glazing only experiment. The existing model in IDA-ICE can take inputs that include: solar heat gain coefficient and solar transmittance and compute shading coefficients; however for this exercise the center-pane thermal transmittance, and inner and outer emittance were inputs and the shading coefficients for radiation (Sc) and solar radiation (Ssc) were computed using two different methods, including: 1) a manual calculation performed using SIA rules and 2) in a subsidiary software called PARASOL [38]. The computed Sc and Ssc using SIA rules were 0.5336 and 0.4730, respectively, and from PARASOL were 0.5563 and 0.4931, respectively. The program then adjusted the shading coefficients to account for angular dependent optical properties of the glazing unit. The new Detwind model used ISO 15099 [27] to compute radiative heat transfer and all window parameters.

For the glazing only experiment and subsequent solar gain experiments with the glazing unit, the thermal bridge between the test cell and the guarded zones was set at 4.526 W/K, and the thermal bridge to the outside was 0.5010 W/K. The outside thermal bridge included: the linear thermal transmittance of the glazing and the external thermal bridges.

To maintain the air temperature in the test cell, a terminal heating/cooling unit was added to the model to that supplied and exhausted conditioned air to and from the space. The mass flow rate of the supply air was fixed at 1 kg/s and the supply air temperature was controlled by a PI controller; the fan for the unit was always turned off, and hourly test cell air temperatures were scheduled into the program.

No changes were made to the model from the blind to the non-blind exercise.

## 12.4.5. Exterior and Interior Shading Screens (Exercises 4 and 5)

The same model was used as in Exercise 3 with the addition of exterior and interior shading screens. The Detwind window model currently does not support window shading devices so these exercises were performed using the existing model and the SIA rules. The SIA rules generated for the Sc and Ssc values were 0.255 and 0.238, respectively, for the exterior shading screen and were 0.655 and 0.337, respectively, for the interior shading screen. No changes were made in the software to account for the additional thermal resistant of the shading screen and the air gap.

No changes were made in the models from the blind to the non-blind exercises.

#### 12.4.6. Discussion of Results

All simulation results corresponded well with the experimental data. The existing IDA-ICE model was limited in accuracy while the new Detwind model required detailed knowledge of the window composition. Both models still cannot simulate blind assemblies. Current plans include the implementation of a blind assembly algorithm into the Detwind model.

### 12.4.7. Validation Impact

The accuracy of the existing window model was quantified. For most of the simulation cases, the accuracies were within the uncertainties of the window parameters. The new Detwind model provides better simulation performance in cases where there is detailed knowledge of the window parameters requiring access to an extensive window database. Plans are now in place for the development and refinement of a detailed window model (Detwind). An additional change that was made in IDA-ICE because of this validation exercise was that Perez 1990 model was made the default tilted surface radiation model in IDA-ICE.

# **Chapter 13: Discussion and Conclusions**

Empirical validations of building energy simulation programs are intensive undertakings that require well-instrumented facilities, experienced staff, and extensive collaboration between the people designing and running the experiments and the modelers. While programs are being continually improved to better simulate reality, the experimental design and data sets from these studies are available for evaluating and improving building energy simulation programs and algorithms and can be a lasting contribution for continued improvements in the area of building energy simulation.

The focus of empirical validations was to evaluate the performance within the constraints of the programs. Therefore, it was impossible to use an occupied building with changing internal loads, infiltration between zone, changing shading conditions, and other parameters that are varied by occupants. In such cases, the uncertainties associated with these predictions would make it impossible to assess the performance of programs. For this research, nearly every facet of the experiments was controlled.

Particular emphasis was placed on ensuring that the inputs to the building energy simulation programs were well-described.

### 13.1. Experiments

For the series of experiments performed, the optical properties of the glass panes, shading devices and interior surfaces over the entire solar spectrum, thermal conductivities of the construction materials, two and three-dimensional heat transfer simulation programs, and well-described boundary conditions (outside surface temperatures for construction elements adjacent to the guarded zone, measured internal loads, and accurate weather inputs) were measured or simulated for use in evaluating building energy simulation programs. While this level of detail could not be attained in actual practice, the precise determination in the study allowed for careful assessments and comparisons; in many cases, quantifying the input properties, particularly the thermal bridges, required calorimetric hotbox experiments and software calculations, were much more computationally intensive than what is currently found in building energy simulation programs. However from these comparisons, conclusions were drawn concerning heat transfer coefficients, transmitted solar energy, radiative heat exchange, heat transfer in the air gap between shading devices and window panes, tilted radiation models, and many more topics.

The order of experiments from simple to complex provided clear levels for identifying specific problems within the various models. This step-by-step methodology allowed for accurate diagnosis of potential deviations and a determination of the how the discrepancies in the models propagated through the various experiments. The list below identifies some of these items:

- The transient characterization experiment provided evidence that the thermophysical properties and thermal bridges within the test cell were well-described and could accurately characterize the test cell in the programs for subsequent experiments.
- An evaluation of tilted surface radiation models prior to evaluating solar gains through the glazing unit revealed differences associated with incident radiation on the exterior wall and glazing unit, which impacted the solar gain models. This study also identified differences between the components or irradiance (direct-normal, diffuse horizontal, and global horizontal). The predictions were compared and the most reliable tilted surface radiation model for this region was used for remaining experiments.
- The glazing unit experiment provided reliable information concerning the quantifying and modeling the thermal bridges associated with the glazing unit spacer and mounting. The experiment also offered insight into the performance of algorithms for modeling angular dependent window properties.
- Diffuse interior and exterior shading screens were the simplest of all shading devices used in this study. The two experiments revealed discrepancies and shortcomings in

- various programs' abilities to account for transmissions through the screens and model the heat transfer in the air gap between the shading device and the glazing unit.
- The outside Venetian blind and inside mini-blind assemblies were much more complicated shading device that could not be simulated by all building energy simulation programs. But the study revealed that there were models specifically designed to address these issues and implemented in EnergyPlus and HELIOS.
- The window experiment revealed the complexities associated the mounting, frame, and spacer; however, when these quantities were properly specified by combining hotbox measurements with two-dimensional simulations resulting in accurate simulation of the test cell in the building energy simulation programs.

In some instances, some of the effects in the glazing unit experiment did not affect the shading experiments. For example, the magnitude of the transmitted solar power to the test cell impacted the convective heat transfer coefficient algorithms which altered the time constant of the test cell in some programs; this was somewhat mitigated in several building energy simulation programs by the installation of shading devices where mostly diffuse radiation entered the test cell.

However for all the planning and preparation that went into the experiments, there were some issues that could not be addressed within this study and will be discussed.

#### 13.2. Overall Assessments

Many things can be taken from this study and used in future empirical validation efforts. The reasons for the relative success of the project was due to careful examination of the literature prior to initiating the endeavor, thoughtful design of the experimental setup using simulation tools, vigilant monitoring of the data, emphasis on thoroughly quantifying input parameters, careful consideration of uncertainties, collaboration with IEA Task 34/Annex 43 Subtask C, and a cohesive set of statistical parameters used for assessing the performance of the programs. While in retrospect, it is always possible to improve the experiments, this study was the one of most detailed empirical validations for building energy simulation programs ever performed.

# References

- [1] Judkoff RD. Validation of Building Energy Analysis Simulation Programs at the Solar Energy Research Institute, Energy and Buildings, 10, 1998, 221-239
- [2] Loutzenhiser PG, H Manz, C Felsmann, PA Strachan, T Frank, and GM Maxwell. Empirical validation of models to compute solar irradiance on inclined surfaces for building energy simulation. Solar Energy, In press
- [3] Strachan P, Model Validation using the PASSYS Test Cells, Building and Environment 28, 1993, 153-165
- [4] Moinard S and G Guyon. Empirical Validation of EDF ETNA and GENEC Test-Cell Models, A Report of Task 22, Project A.3 Empirical Validation, International Energy Agency, 1999
- [5] TRISCO Version 10.0w. A computer program to calculate 3D steady-state heat transfer, Physibel, Heirweg 21, B-9990 Maldegem, Belgium
- [6] prEN ISO 10077 2 Thermal performance of windows, doors and shutters -Calculation of thermal transmittance Part 2: Numerical method for frames (Final Draft), European Committee for Standardization, Brussels, 2003
- [7] European Standard EN 410. Glass in building Determination of luminous and solar characteristics of glazing. European Committee for Standardization, Brussels, Belgium, 1998
- [8] GLAD Software. Swiss Federal Laboratories for Materials Testing and Research (EMPA). Duebendorf, Switzerland, 2002
- [9] Duffie, JA and WA Beckman. Solar Engineering and Thermal Processes 2<sup>nd</sup> Edition, John Wiley and Sons Inc., New York, Chichester, Brisbane, Toronto, Singapore, 1991
- [10] Modest M. Radiative Heat Transfer 2<sup>nd</sup> Edition, Academic Press, Amsterdam, Boston, London, New York, Oxford, Paris, San Diego, San Francisco, Singapore, Sydney, Tokyo, 2003
- [11] Klein, SA. Engineering Equation Solver (EES) Software, Department of Mechanical Engineering, University of Wisconsin—Madison, 2004
- [12] Manz H, P Loutzenhiser, T Frank, PA Strachan, R Bundi, and G Maxwell. 2006. Series of experiments for empirical validation of solar gain modeling in building energy simulation codes—Experimental setup, test cell characterization, specifications and uncertainty analysis. Building and Environment Vol. 41, Issue 12: 1784-1797, 2006
- [13] BISCO Version 7.0w. A computer program to calculate 2D steady-state heat transfer, Physibel, Heirweg 21, B-9990 Maldegem, Belgium
- [14] Nussbaumer T and T Frank. Bestimmung des Wärmedurchgangskoeffizien-ten Ug einer 2-fach Isolierverglasung, Nr. 880'097, STS-Nr. 086, EMPA, Duebendorf, Switzerland, Nov. 30, 2004, (In German)
- [15] Loutzenhiser PG, H Manz, PA Strachan, C Felsmann, T Frank, GM Maxwell, and P Oelhafen. An empirical validation of modeling solar gains through a glazing unit using building energy simulation programs. HVAC & R Research Vol. 12 No. 4: 1097-1116, 2006
- [16] Loutzenhiser PG, H Manz, C Felsmann, PA Strachan, and GM Maxwell. An empirical validation of modeling solar gain through a glazing unit with external and internal shading screens. Applied Thermal Engineering 27: 528-538, 2007
- [17] Carl S, and H Simmler. Bestimmung des Wärmedurchgangskoeffizien-ten U<sub>w</sub>, Nr. 880'097, STS-Nr. 086, EMPA, Duebendorf, Switzerland, March 6, 2006, (In German)

- [18] EN ISO 6945, Building components and building elements—Thermal resistance and thermal transmittance—Calculation methods, Draft Revision, ISO, 2004
- [19] Perez, R, R Seals, P Ineichen, R Stewart, D Menicucci. A new simplified version of the Perez diffuse irradiance model for tilted surfaces. Solar Energy 39 (3), 221–232.1987
- [20] Finelayson, EU, DK Arasteh, C Huizenga, MD Rubin, MS Reilly. Window 4.0: Documentation of Calculation Procedures, Lawrence Berkley Laboratory Report LBL-33946 University of California Report UC-350, July 1993
- [21] Chauvel P and J Millet. L'appreciation des caracteristiques des pretections solaires des bais, Centre Scientifique et Technique du Batiment, Department de l'Energetique et de la Productique GEC/DAC-90.115R, October 1991
- [22] Simmler H and B Binder. Testing and modelling of angular-dependent solar heat gain of glazing with venetian shading DYNASTEE Conference 2005, 12-14. October 2005, Athens
- [23] Crawey DB, LK Lawrie, FC Winkelmann, WF Buhl, YJ Huang, CO Pedersen, RK Strand, R.J. Liesen, DE Fisher, MJ Witte, and J Glazer. EnergyPlus: creating a new-generation building energy simulation program, Energy and Buildings 33: 319-331, 2001
- [24] Perez R, P Ineichen, R Seals, J Michalsky, and R Stewart. Modeling daylight availability and irradiance components from direct and global irradiance. Solar Energy Vol. 44 No.5, 271-289, 1990
- [25] Winkelmann FC. Modeling windows in EnergyPlus. Proceedings IBPSA Building Simulation 2001, Rio de Janeiro (listed as LBNL Report 47972), 2001
- [26] ASHRAE. ASHRAE Fundamentals 2001 SI Edition, American Society of Heating, Refrigeration and Air-Condition Engineers, Inc, Atlanta, GA. 2001
- [27] ISO/FDIS 15099: 2003(E), Thermal performances of windows, doors, and shading devices—Detailed calculations, 2003
- [28] EnergyPlus, Input Output Reference, Board of Trustees of University of Illinois and the University of California through Orlando Lawrence Berkley Laboratories, October 11, 2005
- [29] prEN 13363-2 (Final Draft), Solar protection devices combined with glazing Calculation of total solar energy transmittance and light transmittance Part 2: Detailed calculation method (English Version), October 2004
- [30] DOE-2.1E Documentation. http://gundog.lbl.gov, 2006
- [31] Windows 5.2 Version 5.2.17a.. Code to calculate window properties, LBL, <a href="http://windows.lbl.gov/software/window/window.html">http://windows.lbl.gov/software/window/window.html</a>, 2005
- [32] Rubin M., K Von Rottkay, and R Powles. 1998. Window Optics. Solar Energy Vol.65 No. 3:149-161, 1998
- [33] Reilly MS, FC Winkelmann, DK Arasteh, and WL Carrol. Modeling windows in DOE-2.1E. Energy and Buildings 22:59-66, 1995
- [34] Walton GN. Thermal Analysis Research Program Reference Manual. NBSIR 83-2655, March 1983, 21, 1983
- [35] Clark G and Allen C. The Estimation of Atmospheric Radiation for Clear and Cloudy Skies. Proc. 2nd National Passive Solar Conference (AS/ISES), 675-678, 1978
- [36] ASHRAE. ASHRAE Fundamentals 1997 SI Edition, American Society of Heating, Refrigeration and Air-Condition Engineers, Inc., Atlanta, GA. 1997
- [37] Kondratjev K. Radiation Regime of Inclined Surfaces. WMO Technical Note 152. Geneva. 1977
- [38] Parasol Software Version 2.2. A window simulation program. www.parasol.se, 2006

# **Appendix A: Description of Associated Files**

For the exercises performed at the EMPA facility, measurements necessary for simulation and comparisons of the various parameters were collected and put into Excel files. The first two exercises were non-blind exercises and so the results were provided along with the input data. Subsequent experiments were blind exercises; for the first iteration of simulations; for the next iteration, the results were provided to the participants. A compact disc contains all the files necessary for simulating and comparing output; with these files, it is possible to repeat the exercises described in the report and make comparisons. This section contains a list of files and tables that describe the file headers. Table A.1 contains a list of file names and the corresponding Excel files associated with each exercise.

Table A 1 Exercises and associated files

Exercise	Associated File(s)
Exercise 1	Experiment 2.xls
Exercise 2	Experiment 3 Weather Data.xls
	Experiment 3.xls
Exercise 3	Experiment 3 Subhourly Data.xls
	Experiment 3 Validations.xls
	Experiment 4.xls
Exercise 4	Experiment 4 Subhourly Data.xls
	Experiment 4 Validations.xls
	Experiment 5.xls
Exercise 5	Experiment 5 Subhourly Data.xls
	Experiment 5 Validations.xls
	Experiment 6.xls
Exercise 6	Experiment 6 Subhourly Data.xls
Exercise 0	Experiment 6a Validations.xls
	Experiment 6b Validations.xls
	Experiment 7a.xls
	Experiment 7b.xls
Exercise 7	Experiment 7a Subhourly Data.xls
Exercise /	Experiment 7b Subhourly Data.xls
	Experiment 7a Validations.xls
	Experiment 7b Validations.xls
	Experiment 8.xls
Exercise 8	Experiment 8 Subhourly Data.xls
	Experiment 8 Validations.xls

#### A.1. Exercise 1

All the input information necessary for simulating Exercise 1 is contained in an Excel file entitled "Experiment 2.xls". Table A.2 contains a list and description of column headers in the file. The measurements for this experiment were averaged over one hour increments. During this experiment, none of the construction elements were exposed to the outside environment; therefore, measured weather data were not required.

Table A.2. Description of column header from the "Experiment 2.xls" workbook.

Colun	nn Header Names	Description
	Time	Specific time of the experiment in h
	Internal Load	Measured internal heat load in W
	T_floor_out	Average outer surface temperature of the floor in °C
0 0	T_ceiling_out	Average outer surface temperature of the ceiling in °C
sid	T_south_out	Average outer surface temperature of the south wall in °C
Outside Surface	T_west_out	Average outer surface temperature of the west wall in °C
	T_north_out	Average outer surface temperature of the north wall in °C
	T_east_out	Average outer surface temperature of the east wall in °C
လ ဖွ	T_floor_in	Average inner surface temperature of the floor in °C
Inside Surface Temperatures	T_ceiling_in	Average inner surface temperature of the ceiling in °C
Sur	T_south_in	Average inner surface temperature of the south wall in °C
de npe	T_west_in	Average inner surface temperature of the west wall in °C
nsi Fen	T_north_in	Average inner surface temperature of the north wall in °C
	T_east_in	Average inner surface temperature of the east wall in °C
	T_mean_cell_air	Average air temperature inside the test cell in °C
	T mean cell air unc	Average air temperature 95% credible limits from the
es	1_mean_cen_an_ane	experiment in K
Zone Air Temperatures	T_mean_cell_air_unc_MCA	Average air temperature 95% credible limits from the MCA
era		in K
du	T_cell_air_1	Air temperature measured at Thermocouple 1 in °C
Tel	T_cell_air_2	Air temperature measured at Thermocouple 2 in °C
\ir	T_cell_air_3	Air temperature measured at Thermocouple 3 in °C
e /	T_cell_air_4	Air temperature measured at Thermocouple 4 in °C
Con	T_cell_air_5	Air temperature measured at Thermocouple 5 in °C
. 7	T_cell_air_6	Air temperature measured at Thermocouple 6 in °C
	T_cell_air_7	Air temperature measured at Thermocouple 7 in °C
	T_cell_air_8	Air temperature measured at Thermocouple 8 in °C

### A.2. Exercise 2

All the information required for simulating Exercise 2 is contained in an Excel file entitled "Experiment 3 Weather Data.xls". This file contains two Excel worksheets. The first worksheet entitled "Weather" contains weather data for the experiment and second worksheet entitled "Artificial Turf" contains measured reflectance of the artificial turf as a function of wavelength. The headers for the "Weather" and "Artificial Turf" worksheets are contained in Tables A.3 and A.4, respectively.

Table A.3. Description of column header from the "Weather" worksheet.

Column	Header Names	Description
	Date and Time	Time and date of the experiment for the central European time zone (GMT+1) average over the previous hour (note: 01:00 corresponds to 00:01 to 01:00)
	Outside Air Temperature	Measured outside air temperature in °C
	Relative Humidity	Measured outdoor relative humidity in %
ıer	Barometric Pressure	Measured atmospheric pressure in hPa
Weather	Dew Point Temperature	Computed dew point temperature using EES in °C
W	Horizontal Wind Speed	Measured horizontal wind speed in m/s
	Vertical Wind Speed	Measured vertical wind speed in m/s
	Horizontal Wind Direction	Measured horizontal wind direction in degrees
	Global Horizontal Irradiance	Measured global horizontal solar irradiance in W/m <sup>2</sup>
0	Global Vertical Irradiance (29° West of South)	Measured global vertical solar irradiance on the exterior façade in W/m <sup>2</sup>
Solar Irradiance	Global Vertical Irradiance Experimental Uncertainty	Computed global vertical solar irradiance 95% credible limits from the experiment on the exterior façade in W/m <sup>2</sup>
Solar I.	Global Vertical Irradiance MCA Uncertainty	Computed global vertical solar irradiance 95% credible limits from the MCA on the exterior façade in W/m <sup>2</sup>
	Direct-Normal Irradiance	Measured direct-normal solar irradiance in W/m <sup>2</sup>
	Diffuse Horizontal Irradiance	Measured diffuse horizontal solar irradiance in W/m <sup>2</sup>
ed ince	Global Horizontal Infrared Irradiance	Measured global horizontal infrared irradiance in $\ensuremath{W/m^2}$
Infrared Irradiance	Global Vertical Infrared Irradiance (29° West of South)	Measured global vertical infrared irradiance on the exterior façade in W/m <sup>2</sup>
Solar Angle	Elevation or Solar Altitude	Computed solar altitude in degrees
So.	Azimuth	Computed solar azimuth in degrees

Table A.4. Description of column header from the "Artificial Turf" worksheet.

Column Header Names	Description
Wavelength	Wavelength in nm
Direct-Hemispherical Reflectance	Measured direct to hemispherical reflectance of the
	artificial turf in nm

Because some building energy simulation programs can use weather data in subhourly timesteps. Weather data were made available in 6, 10, and 12 minute intervals. These data are contained in an Excel file entitled "Experiment 3 Subhourly Data.xls". Table A.5 contains a list of column header names for all the worksheets contained in "Experiment 3 Subhourly Data.xls".

Table A.5. Description of the column headers in the "Experiment 3 Subhourly Data.xls" workbook.

Column Header Names	Description
Date and Time	Time and date of the experiment for the central European time zone (GMT+1) average over the previous hour time period
Drybulb Temperature	Measured outside air temperature in °C
Relative Humidity	Measured outdoor relative humidity in %
Pressure	Measured atmospheric pressure in hPa
Dew Point Temperature	Computed dew point temperature using EES in °C
Wind Speed	Measured wind speed in m/s
Wind Direction	Measured wind direction in degrees
Global Horizontal Irradiance	Measured global horizontal solar irradiance in W/m <sup>2</sup>
Direct-Normal Irradiance	Measured direct-normal solar irradiance in W/m <sup>2</sup>
Diffuse Horizontal Irradiance	Measured diffuse horizontal solar irradiance in W/m <sup>2</sup>
Global Vertical Irradiance (29° W of S)	Measured global vertical solar irradiance on the outside façade in W/m <sup>2</sup>
Global Horizontal Infrared Irradiance	Measured global horizontal infrared irradiance in W/m <sup>2</sup>
Global Vertical Infrared Irradiance	Measured global vertical infrared irradiance on the exterior façade in W/m <sup>2</sup>

### A.3. Exercise 3

All the inputs required for simulating Exercise 3 is contained in an Excel file entitled "Experiment 3.xls". The workbook consists of four worksheets that contain various measurements required for input including: "Weather", "Temp BC and Internal Load", "Glazing Measurements", and "Individual Cell Air Temps". Table A.6 contains column header for the worksheet entitled "Weather".

Table A.6. Description of column header from the "Weather" worksheet.

Table A.o. Description of column header from the weather worksheet.		
Column Header Names		Description
	Date and Time	Time and date of the experiment for the central European time zone (GMT+1) average over the previous hour (note: 01:00 corresponds to 00:01 to 01:00)
	Outside Temperature	Measured outside air temperature in °C
	Relative Humidity	Measured relative humidity in °C
	Barometric Pressure	Measured atmospheric pressure in hPa
Weather	Dew Point Temperature	Computed dew point temperature with EES in °C
×	Horizontal Wind Speed	Measured horizontal wind speed in m/s
	Vertical Wind Speed	Measured vertical wind speed in m/s
	Horizontal Wind Direction	Measured horizontal wind direction in degrees
93	Global Horizontal Irradiance	Measured global horizontal solar irradiance in W/m <sup>2</sup>
adian	Global Vertical Irradiance (29° West of South)	Measured global vertical solar irradiance on the exterior façade in W/m <sup>2</sup>
Solar Irradiance	Direct-Normal Irradiance	Measured direct-normal solar irradiance in W/m <sup>2</sup>
So	Diffuse Horizontal Irradiance	Measured diffuse horizontal solar irradiance in W/m <sup>2</sup>
Infrared Irradiance	Global Horizontal Infrared Irradiance	Measured global horizontal infrared irradiance in W/m <sup>2</sup>
	Global Vertical Infrared Irradiance (29° West of South)	Measured global vertical irradiance on the exterior façade in W/m <sup>2</sup>
ır es	Elevation or Solar Altitude	Computed solar altitude in degrees
Solar Angles	Azimuth	Computed solar azimuth of the exterior façade in degrees

The boundary conditions for the experiment included hourly outer surface temperatures of all construction elements adjacent to guarded zones, average test cell air temperatures, and internal loads. This information is contained in a worksheet entitled "Temp BC and Internal Load"; the column headers for this worksheet are given in Table A.7. An additional worksheet entitled "Individual Cell Air Temps" contains a drawing and individual hourly measured air temperatures shown in Table A.8. Table A.9 contains a description of the column headers from the "Angular Dependent Measurements".

Table A.7. Column headers for the "Temp BC and Internal Load" worksheet.

Column Header Names		Description
	Date and Time	Time and date of the experiment for the central European time zone (GMT+1) average over the previous hour (note: 01:00 corresponds to 00:01 to 01:00)
Cell Air	Average Temp	Average air temperature of the test cell in °C
Average Outside Surface Temperatures	Floor Temp	Average outside surface temperature of the floor in °C
	Ceiling Temp	Average outside surface temperature of the ceiling in °C
	West Wall Temp	Average outside surface temperature of the west wall in °C
	North Wall Temp	Average outside surface temperature of the north wall in °C
	East Wall Temp	Average outside surface temperature of the north wall in °C
	Internal Heat Gains	Measured internal gains inside the test cell in W

Table A.8. Column headers for the "Glazing Measurements" worksheet.

Column Header Names		Description
	Wavelength	Wavelength in nm
Outer Pane	Transmittance	Measured transmittance of the outer glazing in %
	Reflectance (front)	Measured front reflectance of the outer glazing in %
	Reflectance (back)	Measured back reflectance of the outer glazing in %
Inner	Transmittance	Measured transmittance of the inner glazing in %
	Reflectance (front)	Measured front reflectance of the inner glazing in %
	Reflectance (back)	Measured back reflectance of the outer glazing in %

Table A.9. Column headers for the "Angular Dependent Measurements" worksheet.

Column Header Names		Description
Wavelength		Wavelength in nm
	0°	Measured transmittance at a 0° angle of incident in %
75	15°	Measured transmittance at a 15° angle of incident in %
stec	30°	Measured transmittance at a 30° angle of incident in %
ss s	45°	Measured transmittance at a 45° angle of incident in %
t se	50°	Measured transmittance at a 50° angle of incident in %
smittance at sele incident angles	55°	Measured transmittance at a 55° angle of incident in %
anc	60°	Measured transmittance at a 60° angle of incident in %
nitt Icid	65°	Measured transmittance at a 65° angle of incident in %
nsu ir	67.5°	Measured transmittance at a 67.5° angle of incident in %
Transmittance at selected incident angles	70°	Measured transmittance at a 70° angle of incident in %
	72.5°	Measured transmittance at a 72.5° angle of incident in %
	75°	Measured transmittance at a 75° angle of incident in %
SI	15°	Measured reflectance (front) at a 15° angle of incident in %
joi	30°	Measured reflectance (front) at a 30° angle of incident in %
var	45°	Measured reflectance (front) at a 45° angle of incident in %
at les	50°	Measured reflectance (front) at a 50° angle of incident in %
Reflectance (Front) at various incident angles	55°	Measured reflectance (front) at a 55° angle of incident in %
Fro nt a	60°	Measured reflectance (front) at a 60° angle of incident in %
e (	65°	Measured reflectance (front) at a 65° angle of incident in %
anc	67.5°	Measured reflectance (front) at a 67.5° angle of incident in %
ect	70°	Measured reflectance (front) at a 70° angle of incident in %
eff	72.5°	Measured reflectance (front) at a 72.5° angle of incident in %
R	75°	Measured reflectance (front) at a 75° angle of incident in %
S	15°	Measured reflectance (back) at a 15° angle of incident in %
ion	30°	Measured reflectance (back) at a 30° angle of incident in %
var	45°	Measured reflectance (back) at a 45° angle of incident in %
at at	50°	Measured reflectance (back) at a 50° angle of incident in %
ck) ang	55°	Measured reflectance (back) at a 55° angle of incident in %
ance (back) at vincident angles	60°	Measured reflectance (back) at a 60° angle of incident in %
Se (	65°	Measured reflectance (back) at a 65° angle of incident in %
anc	67.5°	Measured reflectance (back) at a 67.5° angle of incident in %
ect	70°	Measured reflectance (back) at a 70° angle of incident in %
Reflectance (back) at various incident angles	72.5°	Measured reflectance (back) at a 72.5° angle of incident in %
× -	75°	Measured reflectance (back) at a 75° angle of incident in %

Due to the preconditioning phase, the first 120 h of the experiment were used as a warm-up period for all of the simulations; therefore comparisons with experimental data were only made with the last 480 h of the experiment. The measured data from the experiment used for comparison is provided in an Excel file entitled "Experiment 3 Validations.xls". Two worksheets are contained in this file: 1) "Experiment" and 2) "Uncertainties". The column headers for these worksheets are contained in Tables A.10 and A.11, respectively.

Table A.10. Column headers for the "Experiment" worksheet.

Column Header Names		Description
	Date and Time	Time and date of the experiment for the central European time zone (GMT+1) average over the previous hour (note: 01:00 corresponds to 00:01 to 01:00)
	Cooling Power	Measured cooling power in W
Surface Temperatures	Outer Glazing Unit	Average outer surface temperature of the glazing unit in °C
	Inside Glazing Unit	Average inner surface temperature of the glazing unit in °C
	West Inside Wall	Average inner surface temperature of the west wall in °C
	North Inside Wall	Average inner surface temperature of the north wall in °C
	East Inside Wall	Average inner surface temperature of the east wall in °C
	Ceiling Inside	Average inner surface temperature of the ceiling in °C
	Floor Inside	Average inner surface temperature of the floor in °C

Table A.11. Column headers for the "Uncertainties" worksheet.

Column Header Names De		Description
	Date and Time	Time and date of the experiment for the central European time zone (GMT+1) average over the previous hour (note: 01:00 corresponds to 00:01 to 01:00)
e Limits of Power	Experiment	Computed 95% credible limits for the measured cooling power in W
95% Credible Limits of Cooling Power	Monte Carlo Analysis	Computed 95% credible limits from MCA for the cooling power in W

#### A.4. Exercises 4 and 5

Files with the same worksheets and column headers were produced for Exercises 4 and 5; one exception is that the worksheet entitled "Glazing Measurements" from "Experiment 3.xls" was replaced in "Experiment 4.xls" and "Experiment 5.xls" workbooks with worksheets named "Shade Properties"; a description of the column headers for this worksheet is contained Table A.12. Excel workbooks similar to the "Experiment 3 Validation.xls" were made for Exercises 4 and 5 entitled "Experiment 4 Validation.xls" and "Experiment 5 Validation.xls", respectively.

Table A.12. Column headers for the "Shade Properties" worksheet.

Column Header Names	Description
Wavelength	The wavelength in nm
Transmittance	Measured transmittance as a function of wavelength in %.
Reflectance	Measured reflectance as a function of wavelength in %.

# A.5. Exercises 6 and 7

Files with the same worksheets and column headers as in Exercise 4 were produced for Exercises 6 and 7; one exceptions is that the worksheet entitled "Shade Properties" was replaced by worksheets called "Blind Slat Properties"; a description of the column headers is shown in Table A.13. For the blind assembly experiments, results from two blind slat positions were assessed. In Exercise 6, the second experiment was performed immediately after the first experiment (i.e. there is only one input file and two output files). For the two output files, the horizontally and 45° downward tilting experiments were differentiated with "a" and "b", respectively. For Exercise 7, the experiments were run and different times of the year and therefore there are two input and output files using the same distinction for blind slat positions as in Exercise 6. Excel workbooks

similar to the "Experiment 3 Validation.xls" were made for Exercises 6 and 7 entitled "Experiment 6 Validation.xls", respectively.

Table A.13. Column headers for the "Blind Slat Properties" worksheet.

Column Header Names	Description
Wavelength	The wavelength in nm
Reflectance	Measured reflectance as a function of wavelength in %.

#### A.6. Exercises 8

For Exercise 8, input and output files were generated that contain the same headers as in Exercise 3. An Excel workbook similar to the "Experiment 3 Validation.xls" was made for Exercises 8 entitled "Experiment 8 Validation.xls".